ELECTRIC SPRINGS: A NEW APPROACH TO DEMAND SIDE MANAGEMENT

BY

EMAD FUAD NAIM AREED

A Thesis Presented to the
DEANSHIP OF GRADUATE STUDIES

KING FAHD UNIVERSITY OF PETROLEUM & MINERALS

DHAHRAN, SAUDI ARABIA

In Partial Fulfillment of the
Requirements for the Degree of

MASTER OF SCIENCE

In

ELECTRICAL ENGINEERING

MAY 2015

KING FAHD UNIVERSITY OF PETROLEUM & MINERALS

DHAHRAN- 31261, SAUDI ARABIA

DEANSHIP OF GRADUATE STUDIES

This thesis, written by **EMAD FUAD AREED** under the direction his thesis advisor and approved by his thesis committee, has been presented and accepted by the Dean of Graduate Studies, in partial fulfillment of the requirements for the degree of **MASTER OF SCIENCE IN ELECTRICAL ENGINEERING**

Dr. MOHAMED ALI ABIDO
(Advisor)

Dr. ALI AHMAD AL-SHAIKHI
Department Chairman

Dr. IBRAHIM MOHAMMAD EL-AMIN
(Member)

Dr. Salam A. Zummo
Dean of Graduate Studies

Dr. IBRAHIM HABIBALLAH
(Member)

2/6/15
Date

Dedicated to

My beloved father and mother, for their prayers, love, support, and encouragement, which brought to me all the success and progress in my life.

My great appreciation to my brothers, sisters, and all my family for their kind care and happiness for my success.

God bless you and reward you all the best

ACKNOWLEDGMENTS

"In the name of Allah, The Most Gracious and The Most Merciful"

All praise belongs to Allah (S.W.T.) for bestowing me with courage and perseverance to carry out this work sincerely. I thank Almighty Allah for providing me opportunity to do my M.S. successfully at King Fahd University of Petroleum and Minerals, Dhahran.

I would like to express my deepest gratitude to King Fahd University of Petroleum and Minerals for providing me good academic platform and financial support during my M.S. My deepest gratitude and appreciation goes to my thesis advisor and mentor **Dr. Mohamed Abido** for his continuous guidance, motivation and support during the course of my studies. His valuable suggestions broadened my horizon in the field of power engineering and made this work interesting and challenging for me. Without his invaluable support and help, it would not have been possible for me to complete this work successfully

I would like to send a special thanks to the Electrical Engineering Department represented by the chairman **Dr. Ali A. Al-Shaikhi**. I would also like to thank the committee members, **Prof. Ibrahim M. El-Amin** and **Dr. Ibrahim HabibAllah** for their suggestions and interest in my work.

Last of all, I would like to express my adoration to my family and friends for always standing by my side and being there. I am indebted to them for all the hardships they had to go through in order for me to succeed. I would never have reached to where I am without their prayers and their help.

Contents

LIST OF TABLES

LIST OF FIGURES

LIST OF ABBREVIATIONS

DSM	:	Demand Side Management
ES	:	Electric Spring
ILC	:	Interruptible Load Control
RTP	:	Real Time Pricing
FACTS	:	Flexible AC Transmission Systems
SSSC	:	Static Synchronous Series Compensator
UPFC	:	Unified Power Flow Controller
VSC	:	Voltage Source Converter
PWM	:	Pulse Width Modeulation
RCGA	:	Real Coding Genetic Algorithm
PSO	:	Particle Swarm Optimization
RTDS	:	Real Time Digital Simulator
GPC	:	Gigabyte Processor Card
3PC	:	Triple Processor Card
DSP	:	Digital Signal Processing
PMU	:	Phasor Measurement Unit

WIF	:	Workstation Interface
DS1103	:	dSPACE Controller
GTAI	:	Giagabit Transceiver Analogue Input
GTAO	:	Giagabit Transceiver Analogue Ouput
PV	:	Photovoltaic
MPPT	:	Maximum Power Point Tracking
P & O	:	Perturb and Observe
RSCAD	:	RTDS Software
RTI	:	Real Time Interface
PLL	:	Phased Locked Loop
PI	:	Proportional-Integral Controller
HIL	:	Hardware in the Loop

NOMENCLATURE AND SYMPOLS

V_{es}	:	Electric Spring Voltage (V)
V_C, V_{nc}	:	Critical and Non-Critical Load Voltage (V)
I_c, I_{nc}	:	Critical and Non-Critical Load Current (I)
R_c, R_{nc}	:	Critical and Non-Critical Load Resistance (Ω)
L_c, L_{nc}	:	Critical and Non-Critical Load Inductance (H)
Z_c, Z_{nc}	:	Critical and Non-Critical Load Impedance (Ω)
P_c, P_{nc}	:	Critical and Non-Critical Load Real Power (W)
P_r	:	Renewable Energy Source Real Power (W)
P_g	:	Grid Real Power (W)
R_f, L_f, C_f	:	Filter Resistance (Ω), Inductance (H),and Capacitance (F)
C_{dc}	:	Electric Spring dc Side Capacitor (F)
P_{sl}, Q_{sl}	:	Smart Load Real and Reactive Power (W, VAR)
Q_{es}	:	Electric Spring Reactive Power (VAR)
V_l, V_s	:	Load and Source Voltage (V)
S_s, S_l, S_{es}	:	Complex Power of Voltage Source, Load, and Electric Spring (VAR)

Q_s, Q_l, Q_{es}	:	Reactive Power of Voltage Source, Load, and Electric Spring (VAR)
P_s, P_l, P_{es}	:	Real Power of Voltage Source, Load, and Electric Spring (W)
V_g	:	Grid Voltage (V)
Z_{int}	:	Internal Impedance of Power Grid (Ω)
Z_{f1}, Z_{f1}	:	Distribution Feeder Impedance (Ω)
I_r	:	Renewable Energy Source Current (A)
D	:	Candidate Solution
G_{max}	:	Maximum Number of Iteration
N_{Pop}	:	Population Size
C_i^1, C_i^2	:	Candidate Parents
C_{inew}^1, C_{inew}^2	:	Candidate Offsprings
I_{inj}	:	Electric Spring Injected Current (A)
T_s	:	Switching period (s)
d	:	Duty Ratio
$x_{j,k}^*, x_{j,k}^{**}$	:	Individual and Global Best Position
C_1, C_2	:	Acceleration Constant

C_{factor}	:	Constriction Factor $v_{j,k}$
$v_{j,k}$	:	Iteration Velocity

ABSTRACT

Full Name : Emad Fuad Naim Areed

Thesis Title : Electric Spring: A New Approach To Demand Side Management In Smart Grid Area

Major Field : Electrical Engineering-Power

Date of Degree : MAY-2015

Demand side management (DSM) is an approach of consumer demand modification for energy consumption. Various programs such as real time pricing and interruptible load control are considered to meet DSM goals. It aims at encouraging the consumer to use less energy during the peak demand hours or shift the time of energy use to off-peak demand time. DSM is popular for various issues. It is beneficial for cost reduction, environmental and social improvement, increasing the reliability of network through reducing demand, and improving the electricity markets.

The objective of this thesis is to design, integrate and analyze the electric spring (ES) with the power system as a novel approach to DSM. It has the capability to regulate the main voltage and allow the loads to follow the power generation. ES is developed using switched and averaged models. Switching model accurately describes the steady-state and dynamic behavior of the converter. It can calculate the instantaneous values of the current and voltage variables. For this model, Real Coded Genetic Algorithm (RCGA) is employed to identify the optimal values of dc and ac control parameters using non-linear time domain simulations. ES with the proposed controller is implemented on MATLAB/SIMULINK and the proposed MATLAB results are compared with those results coming from the experimental setup. Real Time Digital Simulation (RTDS)

integrated with an external dSPACE 1103 controller is considered as a hardware in the loop (HIL) physical implementation.

To describe the ES dynamics as a function of modulating signal, the ES averaged model is developed. It is concerned with the averaged values of the variables instead of the instantaneous values as in a switching model. This model is simple and accurate for simulation. It takes less time to be simulated under several disturbances. It gives the simulation specialist the confidence to incorporate this model in large-scale power system simulation studies because it is effective for collective operation. It is suitable to simulate a large number of ES specially when the physical inverters are not available in the labs. An efficient well-known intelligent optimization technique particle swarm optimization (PSO) is considered to optimize the parameters of the ac controller. To validate the averaged model, multiple simulations have been carried out with different kinds of disturbances and load variations. In addition, the averaged model is considered to investigate the ES characteristics and for performance analysis.

The results show the effectiveness of the ES switching and averaged models under different kinds of disturbances and load variations.

ملخص الرسالة

الاسم الكامل: عماد فؤاد نعيم عريض

عنوان الرسالة: النوابض الكهربائية : المنهجية الجديدة في ادارة الطلب على الطاقة في الشبكات الذكية

التخصص: الهندسة الكهربائية

تاريخ الدرجة العلمية: مايو/ 2015

ادارة الطلب على الطاقة هي تعديل استهلاك الطاقة بالنسبة للمستهلك عن طريق الأخذ بعين الاعتبار مجموعة من البرامج مثل برنامج التسعير بالزمن الحقيقي وبرنامج التحكم بانقطاع الحمل لتحقيق أهداف ادارة الطلب على الطاقة. هذه البرامج تهدف الى تشجيع المستهلك على أن يستهلك طاقة أقل خلال ساعات الذروة أو استهلاكها بوقت لا تكون فيه قمة الطلب على الطاقة. ادارة الطلب على الطاقة شائعة لمثل هذه المسائل، فهي مفيدة لتقليل الأسعار، وللتحسن البيئي والاجتماعي، وتزيد من موثوقية الشبكة من خلال تقليل الأحمال وتحسين سوق الكهرباء.

تهدف هذه الرسالة الى تصميم، وتكامل، والى تحليل النوابض الكهربائية مع شبكات القدرة الكهربائية كونها المنهجية الجديدة لادارة الطلب على الطاقة. النوابض الكهربائية لها المقدرة على تنظيم فولتية الأحمال بالاضافة للسماح للأحمال بتتبع الطاقة المولدة. تم تطوير النوابض الكهربائية باستخدام النموذج التبديلي والمتوسط. النموذج التبديلي يصف الاستجابة الديناميكية و الحالة المستقرة للمحول. هذا النموذج له القدرة على حساب القيم اللحظية لمتغيرات الفولتية والتيار. لمثل هذا النوع من النماذج، تم ايعاز الخوارزمية الجينية ذات الترميز الحقيقي (RCGA) لايجاد القيم المثلى لقيم متحكمات التيار المباشر والتيار المتردد باسخدام المعادلات ذات النطاق غير الخطي. هذه النوابض الكهربائية والمتحكمات تم محاكاتها باستخدام الماتلاب ومقارنتها بالتجارب العملية المنبثقة عن تطبيقها على جهازي المعامل الرقمي في الزمن الحقيقي (RTDS) و المتحكمات العملية الخارجية (dSPAC E1103) كتجربة متكاملة ذات حلقة مقفلة (HIL) .

أما بالنسبة لوصف ديناميكية النوابض الكهربائية كاقتران بدلالة الاشارة التعديلية فتم استخدام النموذج المتوسط . هذا النموذج يهتم بالقيم المتوسطة للمتغيرات بدلا عن تلك القيم اللحظية في حالة النموذج التبديلي. النموذج المتوسط هو نموذج بسيط ودقيق في عملية المحاكاة، وهو ياخذ وقتا أقل في عملية المحاكاة خصوصا عند تعرض النظام لمجموعة من الاضطرابات المفاجئة. يعطي هذا النموذج الثقة لمختصي عملية المحاكاة لدمج هذا النموذج في دراسة محاكاة أنظمة الطاقة ذات النطاق الكبير لأن هاذا النموذج ذو فعالية في التشغيل التجميعي. هذا النموذج مناسب في عملية المحاكاة خصوصا عندما لا يكون هناك عدد كاف من قلابات الجهد في المختبر. تم استخدام أحد الخوارزميات الفعالة الأخرى مع هذا النموذج وهي خوارزمية سرب الجسيمات الأمثل (PSO). للتأكد من من هذا النموذج، تم تطبيق مجموعة من الاضطرابات المختلفة بالاضافة الى تغير الأحمال

المفاجئ. بالاضافة الى ذلك، تم أخذ النموذج المتوسط بعين الاعتبار للتحقق من خصائص النوابض الكهربائية وتحليل ادائها.
تظهر النتائج فعالية النموذج التبديلي والمتوسط للنوابض الكهربائية عند تعرضها لمجموعة من الاضطرابات المختلفة بالاضافة الى تغير الأحمال المفاجئ.

CHAPTER 1

INTRODUCTION

1.1 Background

A microgrid is a collection of distributed generators, loads and energy storage systems which are recently expected to be installed massively. A microgrid is connected to the local generating units and also to the national grid to increase the security and reliability of the power system. Installing a microgrid involves several benefits such as: it is more environmentally friendly because it uses the renewable resources with low or zero emission generators, it aims at reducing the number of failure of the utility grid during the peak load demand, it increases the overall energy efficiency of the power system being the users close to the renewable sources, it lends some financial benefits whilst it generates some or all of energy requirements for its users.

On the other hand, modern electric power systems with new distributed renewable power sources such as wind power and solar power have seen significant penetration of intermittent renewable energy sources. The recently developed technology related to the concept of smart grid in power systems also contributes to make the system more complex. The increasing use of renewable energy sources contributes further to the arising power quality problems like voltage and frequency that must be controlled to an acceptable standard and also, to maintain an energy balance between supply and demand.

There are other shortcomings related to microgrid protection, implementation, maintenance, energy storage system spaces and resynchronization with the utility grid. That is becoming more and more serious problem, and has been a great threat to the security of electric power systems and the national economy as a whole. A serious action must be considered to mitigate these shortcomings and improve the power quality being supplied to the customers and relief more transmission capacity.

One of the emerging, innovative, and new technologies in smart grid area is the electric springs (ES). Since 1660s, when the British scientist Robert Hooke described the principle of the mechanical spring, there were no serious attempts during these three centuries to extend the principle of the mechanical spring to an electrical concept. Electric spring is a power inverter connected in series with a non-critical load. It has great potential in stabilizing the future smart grid by regulating the main voltage despite the fluctuation of the output power of the intermittent renewable energy sources. It can be integrated with home appliances allowing the load to follow the intermittent generation of renewable energy sources. This is unlike the previous idea that depends on generating enough energy to cover the load demand either completely or partially.

One of the applications of using the electric spring in the smart grid is to decrease the required capacity of energy storage in the power system. ES extension usage gives a new vision of the power system stability that will not depend in any way on communication technology. ES relies on a local voltage controller to regulate the main voltage bus instead of using communication tools to receive the required commands to do the action.

1.2 Thesis Motivation

The price of fuels is increasing over time, so renewable energy sources are getting more popular rapidly. Many isolated or remote areas already depend mainly on renewable energy to generate their requirement of electricity. Renewable energy is affected by weather conditions and diurnal variations which make them interruptible power sources. For this reason, it will not be easy to deal with such variable sources. This imbalance of power between the energy sources and the load demand leads to instability of the power system which is considered as one of the important issues in the power system either grid connected or remote systems. Different techniques of demand side management have been proposed to create the balance. Some of these techniques cannot follow the generation instantaneously in real time and the others such as energy storage systems have limited capacity and could be very expensive.

Recently, a new technology that has come to the horizon in power system area is electric springs. It can be utilized in smart grid or microgrid. An electric spring can be considered as a controlled voltage source connected in series with non-critical load to form a new combination of smart load. This smart load is connected in parallel with the critical load where power and voltage should remain constant. ES operation is similar to that of a mechanical spring, hence three different operations of ES can be analogous to these three cases of mechanical spring, neutral, mechanical push and mechanical pull situations.

ES is a series reactive power compensator such as FACTS devices. It can generate and consume reactive power. But, there are some differences as compared to FACTS

devices such as SSSC and UPFC. The ES is used for input-feedback and input-voltage control while FACTSs devices are usually used for output-feedback and output-voltage control. ES has also a major advantage over FACTS devices as it causes the load to follow the power generation by automatically changes the applied voltage across the non-critical load. Therefore, it is capable of offering smart solutions for some shortcomings of the renewable energy sources. It has great potential in stabilizing the future smart grid by regulating the main voltage despite the fluctuation of the output power of the intermittent renewable energy sources. It allows the load to follow the intermittent generation of renewable energy sources, reduces three phase imbalance load current, and improves the power factor. Also, it is used for real and reactive power compensation because it has a battery at dc side terminal, and decreases the required capacity of energy storage systems. Other benefits and applications haven't been explored yet.

1.3 Thesis Objectives

This thesis aims at implementing and applying a new approach based on electric springs for demand side management. It is also aimed at building real time energy management strategy to achieve electric network with higher power quality, more efficient, and highly reliable. First of all, this electric spring embedded in power system will be modeled and simulated using a dedicated software and implemented in laboratory scale prototype using advanced hardware. The thesis entails eight main specific objectives as follows:

1- Developing an ES switching model that is robust enough to be simulated under different disturbances and load variations.

2- Designing and implementing of intelligent control strategies for a power system including electric spring using an efficient heuristic technique (RCGA) to optimally design an ES voltage controller.
3- Developing a linearized model of the power system equipped with the ES and voltage control.
4- Developing an averaged model of the ES integrated with the power system with different load types.
5- Using a particle swarm optimization (PSO) as an efficient intelligent technique to optimize the control parameters of the ES.
6- Identifying the performance characteristics of the ES with different modes and operations.
7- Building a laboratory setup for real-time demand side management with the proposed ES.

1.4 Thesis Contribution

The contributions of this thesis are as follows:

- Developing a detailed ES switching model and integrate it with the power system to verify the capability of this model in both simulation and experimental work.
- Optimizing the ES controller using a RCGA technique to enhance the behavior of the ES using time-domain based objective function.
- Linearizing the power system including the power components and control.
- Developing an averaged model of the ES integrated with the power system especially when the smart load is either resistive or inductive load.

- Using a PSO to optimize the controller parameters using a time-domain based objective function and getting the solution using a RungeKutta solver.
- Finding the operating limits of the electric spring with different types of disturbances such as renewable current source variations, non-critical load variations, modulation index variations and finally with different power factor variations.
- Implementing the ES in real time using RTDS and dSPACE controller as a Hardware-in-the loop implementation to investigate the effectiveness of the ES.
- Validating the simulation results with the experimental ones.

1.5 Thesis Organization

This thesis is organized in eight chapters as follows:

Chapter one contains a background of microgrid benefits and shortcomings. It introduces electric spring as an emerging and promising technology in smart grid area. Thesis motivation and objectives are also included. In chapter two, a comprehensive literature review of various techniques of demand side management is presented while in chapter three an intensive theoretical background of ES principles, operating conditions and applications are demonstrated. In chapter four, a detailed switching model of ES has been developed and the ES controller is optimized to enhance the ES behavior in the power system. Chapter five consists of a full derivation of the power system equations including the power system grid, transmission lines, ES, single phase PLL, and controllers. An averaged model of ES is developed and investigated in different cases. ES performance are discussed in chapter six. A setup of real time implementation is demonstrated and the

results are compared in chapter seven. Finally, conclusions of this thesis work and future direction for research are discussed in chapter eight.

CHAPTER 2

LITERATURE REVIEW

It is a well-known fact that a smart grid has become a future trend of power system because of its ability for delivering and processing power in a more efficient way. Since increasing use of distributed generators, smart grid has attracted a lot of attention since it depends on new integrated technologies such as control strategies, data acquisition and communication technology. This will enhance the security and reliability of the power system and make it more intelligent [1-5].

By comparing smart grid to existing grid characteristics, smart grid is digital and use two way communication while existing grid is electromechanical and depends on one-way communication. Smart grid is a distributed generation using renewable energy sources. Furthermore, smart grid has sensors throughout. Therefore, it is self-monitoring. On the contrary, conventional grid has few sensors throughout the grid, monitoring and restoration is manually [6].

The utility may have to incorporate demand side management (DSM) programs in their future planning. The existence of uncertainty in future power demand, uncertainty of fuel and construction costs, competition between the utilities and spread of distributed generators may lead to create a major problem for power utility [7-10]. So, different DSM programs are implemented by the utility such as load management program, conservation and energy efficiency programs, fuel substitution programs and other dedicated programs to improve the power system and increase its efficiency [7,11-12].

Several benefits for using DSM on smart grid functionalities such as: reshaping the profile of load demand curve, increasing the capability to control and manage the electricity market. Moreover, it has a significant effect on the capacity of electrical equipments of the power system such as power plants, transformers, and ac power lines. Also, it reduces the peak load demand, total energy cost, and the carbon emission levels. [1,7,13]

Different approaches for demand side management have been presented in literature as follows:

2.1 Interruptible Load Control

One type of demand side management is interruptible load control (IL). It causes interruption of the electricity within constraints to improve the security of the power system, improve the reliability, reduce the peak demand, and provide some ancillary services like voltage and frequency regulation. Those interrupted loads consist of residential, commercial and industrial loads. Residential loads aim to reduce the electricity bills cost and industrial loads have their own backup generators and capable to reschedule their production schemes in case of a power outage [11,14-15].

New and powerful tools for the analysis and operation of power systems, as well as for DSM are currently available. The new tools of interest are those of artificial intelligence (AI) which called heuristic methods, as well. The use of AI techniques in electric power has received extensive attention from researchers in the electric power area and the literature on these applications has become rather large in volume [11,16-2]. Artificial Intelligence has been realized as a suitable tool for the analysis of DSM problems.

A binary particle swarm optimization technique (BPSO) is proposed in [11] to minimize the total payment and total interruption of the electricity for customers over 16 hours using two objective functions. Sometimes the load is to be interrupted continuously or at different intervals of time depending on the agreement of the customers. BPSO is a robust and an effective technique for this type of problem in which the constraints are non-linear and non-continuous. The customers will have some benefits with respect to the tariff cost [16-17].

An optimal power flow technique is presented in [18] to support the scheme of the interruptible load management. This leads to optimal selection of the interruptible loads by taking different factors in consideration. Some of these factors are network configuration, power factor of the interruptible load and its period. Lagrange relaxation is used as an optimization technique in [19] to choose an optimal interruptible load in an electricity market.

The effect of interruptible loads on the power system reliability and marginal cost problem is formulated as a mixed integer linear programming. The model was programmed on GAMS software and solved by MIP solver CPLEX 8.0.

Two stages have been given in [21] to carry out the demand subscription services. The iterative dynamic programming (IDP) to create day-ahead schedule and decrease the peak load of the substation, and the heuristic inference rule (HIR) to overcome the problem of uncertainties of the practical load on the IDP results. HIR has the ability to adjust the schedule of the interruptible load in real time which is considered as an advantage for its usage.

Other techniques based on merit order method, fuzzy dynamic programming and priority-based heuristic inference rules are proposed in [22-23].

In general, one of the interruptible load control advantage is that the utility shed some loads to prevent the breakdown of the electrical network. However, it has some disadvantages as it is not able to balance the power generation and load demand in real time. Also, it may cause disturbances for the customers

2.2 Real Time Electricity Pricing

Another approach to satisfy the demand side management is the real time electricity pricing (RTP) [24-27]. Several problems can occur in an electricity utility when the utility is unable to cover the load during peak demand or when the load demand is less than the generation capacity. So, it is indispensable to maintain a less difference between power generation and load demand. Thus, the generation should be planned in a better way. A better way is using a demand response (DR) which is defined as a tariff or program such as time-of-use (TOU). However, TOU is an approach that a utility can follow to influence the behavior of the customers and is widely discussed in recent years. RTP cost is changed daily or per few hours where the day-ahead RTP is considered as one of its typical type that the customer is informed the prices for next 24 hours [24,28-29].

Many authors used the game theoretic approach in power system especially for demand side management [30-34]. Game theory is used to optimize the TOU pricing strategies (GT-TOU) [35] in which different cost models for companies and users response have been proposed. Authors proposed [35] single-user-type scenario and

multiple type of users whom behaviors for real time pricing vary for each one. This method proved its effectiveness in TOU optimization, decreased the costs for the utility and increased the benefits for the users. A Nash equilibrium strategy is used for this problem [36].

Price prediction technique helps users to shape their load properly [37]. Each residential customer has smart meter which contains two units. Energy scheduling unit to decide on the energy consumption of the home and price predictor unit which predict the upcoming prices. Furthermore, energy management controllers [38] is used to help users to manage their power usage. Thus, [35] is practically implemented easier than [37-38]. It can inform the customer earlier the price of the electricity. This price is relatively constant as long as no significant change in both the characteristic of the load demand or the generation cost.

The benefits of TOU for both the utility company and customers have been experimentally proved [39]. Authors proposed a new optimal real-time pricing [40] which is based on utility maximization. RTP depends on interaction between utility company and each user individually. The new algorithm depends on the interactions between the smart meters (among users via message exchange) and the utility to maximize the benefit of the users and minimize the energy cost production of the company while maintaining a reserve capacity in the generators.

One of the efficient models is described in [41] such that the day is divided in four periods with three levels of prices to minimize the operating costs of the facilities. This technique may have some important drawbacks as follows: it is difficult for the users to

manually respond to prices that are changing hourly [42]. Moreover, it is not able to balance the power generation and load demand in real time. However, this technique may lead to load synchronization problem where the significant amount of load is shifted from the peak demand to the same period of non-peak demand. In other words, the peak to average ratio is still high [43].

2.3 Energy Storage Systems

Energy storage is also used as one of the choices for demand side management. Different control strategies of energy storages have been proposed in [44-45]. H_∞ design [44] is used to adjust the state of the energy storage economically according to electricity price. Therefore, energy storage is in charging mode when the electricity price is low and in discharging mode when the electricity price is high. The game theory has been presented in [45] to reduce the peak-to-average ratio using the energy storage in such a way that it is charged and discharged according to the electricity pricing.

Other optimal control techniques of energy storage have been utilized [46-50], an optimal control of end -user energy storage was proposed [46] to organize the process of purchasing the energy storage to minimize the long-term energy costs under variable demands and prices. Levels of charging and discharging have been determined.

The work also concentrates on when to consume energy from battery or grid. The problem has been modeled using Markov decision process. The performance of energy storage control is investigated in data center [47] and extended to multiple data centers [48] such that each of them has its own time-varying prices. Linear programming

technique is proposed in [49-50] in which the prices are known in advance in a finite horizon setting.

The energy storage is considered as an effective solution for real time balance between power generation and load demand. However, it is very expensive, not suitable for some geographic areas and causes pollution.

2.4 Electric Spring

The new approach and technology of distributed voltage control and demand side management is to use electric spring made of single phase or three phase inverter. The traditional DSM approaches have some drawbacks as follows:

1. Interruptible load control technique is not able to balance the power generation and load demand in real time. Also, it is inconvenient for the customers.
2. The cost of electricity is updated hourly in real time pricing technique. So, the response of the customer is expected to be ineffective. Also, the load synchronization may happen when the customers shift their load from high peak load demand to the same low peak demand period.
3. Energy storage technique is very expensive. It is not suitable for some geographic areas and also causes pollution.

ES technology offers viable solution to these problems as a new technology in smart grid. The electric spring technology principles, model, modes of operation, limitations and applications have been described for the first time in [51-53]. Simple and accurate averaged dynamic model for ES have been developed in [52] which can be incorporated in large scale of power system for simulation studies. In this model, the

dynamic of dc link voltage is ignored and considered as a constant voltage. Comparing the experimental and simulation results shows the validation of this model for collective operation when it is distributed in power system. In addition, the results show the effectiveness of the dynamic model for different load power factor and different proportions of critical and non-critical loads.

Three practical experiments have been carried out in [51] to investigate the performance and the capability of the ES to perform voltage regulation to the main voltage and allow the load demand to follow the power generation. However, in the first experiment, the ES is connected in series with the non-critical load and fed by a standard ac power supply to test the ES performance in neutral, capacitive and inductive modes by measuring its voltage and current. In the second experiment, the critical and non-critical resistive loads are fed by an unstable ac power supply like wind turbines simulator and power plant taking into consideration two cases when the ES is enabled and disabled in the power system. Electric spring is programmed to perform voltage boosting function only to regulate the main voltage and allow the non-critical load to follow the generation. In the third experiment, ES is connected in power distribution system and the cable impedance is also considered in this case. ES works for voltage boosting and voltage reduction.

Different scenarios for electric spring have been described in [54] where ES is connected with different types of loads such as resistive, capacitive, inductive and constant power loads. The models of the load characterization are derived mathematically and verified by practical experiments.

Several applications of ES have been discussed in [55- 62]. General steady-state analysis is performed to investigate the ability of the ES for real and reactive power compensation [55]. ES voltage can be controlled by changing the modulation index value. Consequently, the voltage of the series connected load is dynamically changed. So, the amount of the current flowing in the circuit changes. As a result, the amount of power delivery to grid varies and the ES takes part in power compensation. Practical Experiments are performed using different types of loads to verify the derived models of steady-state analysis. These experiments have been carried out for two cases. In the first case, the grid delivers only real power and both the resistive and inductive or capacitive loads in series with ES are connected to the grid. The ES is responsible for reactive power compensation either by generating reactive power in case of an inductive load or absorbing the reactive power in case of a capacitive load. In the second case, both of the grid and the ES supply positive or negative complex power to the load.

Droop control scheme has been used to control ES for parallel operation in power distribution network [56]. It has a feature that the voltage reference of the ES is automatically adjusted according to the location of the ES in the distribution system. A distribution transmission line has been simulated with traditional ac generator and intermittent renewable energy source at three different locations of ES. Electrical loads are connected to investigate the behavior of the ES as voltage regulator and power compensator with and without droop control scheme. Each experiment is divided into three sections: without ES, ES with traditional controller and ES with droop control. According to the results, the main voltage of the feeder remains stable in both cases with and without droop control, but the ES doesn’t operate in a coordinated manner without

droop control. This can be explained as follows: 1- One electric spring works in inductive mode to suppress the main voltage while the other works in capacitive mode to improve the voltage and the third one operates between both of these modes. 2- Modulation indices of all the three ES exhibit different behavior from each other. 3- The power consumed by the non-critical load is poorly shared. However, the droop control scheme has the capability to solve of these issues.

It was reported that the ES can reduce the storage capacity requirements in the power system in future smart grid [57]. The charging and discharging rates of the battery with ES is much less than those without ES. In [58], the hardware implementation of the ES with its digital controller is described in details. For power quality improvement, a new control scheme has been proposed to improve the power quality of the power system [59-60]. The new controller scheme contains multiple resonant controller and second order generalized integrator to improve the power quality by enabling the ES and eliminating the transmission line harmonics [59]. When the dc link capacitor is replaced by a battery, ES can work in eight different modes. These modes are inductive and capacitive modes, resistive and negative-resistive modes, inductive plus resistive and capacitive plus resistive modes, and inductive plus negative-resistive and capacitive plus negative-resistive modes. The input current controller is designed for ES with a battery. Hence, the ES is capable of working as a power factor corrector for different RL and RC loads [60].

Distribution voltage control (ES) and single point voltage control (STATCOM) have been compared with respect to the total voltage regulation and also, total requirement of reactive power capacity [61]. ES and STATCOM models are

implemented in MATLAB/SIMULINK using controllable voltage source. The only difference is that the ES is connected in series with the non-critical load. Simple case study is implemented using an ES and a STATCOM at a time. This study is extended for both IEEE 13-bus test feeder and on a part of distribution network of Hong Kong [61]. The results show that the effectiveness of ES for total voltage regulation along the transmission line is better than the STATCOM. In addition, ES requires less reactive power capacity than STATCOM. The capability of the ES depends mainly on the ratio of the critical and non-critical load.

Power imbalance reduction of three phase power system in the buildings is a new potential of ES [62]. The second generation of distribution voltage control which include a battery at the dc terminal of the ES is used. This may lead to some ES limitations that the maximum output voltage of the inverter (ES) is the maximum voltage value of a battery. In this case, the phase angle varies within $0^{\circ} - 360^{\circ}$. Imbalance current of the transmission line can be reduced when the ES re-distribute the power of non-critical loads. Practical and simulation study verified the capability of ES to reduce the power imbalance in the buildings making it adaptive to any internal load changes and also regulate the external main voltage for any disturbances [62].

Several advanced control schemes to the instantaneous output voltage of single phase inverter were introduced in the literature. Some of these controllers are current and voltage controllers, repetitive controllers, deadbeat controllers, d-q controllers, in addition to, fuzzy logic controllers [63-66]. These controllers aim at improving the dynamic response and zero steady-state error performance of the power system.

Full detailed switching model of ES isn't considered in literature to simulate the power system. Switching model gives more details regarding ES switching variables such as voltage and current. Switching model is considered to simulate the power inverter response as in the reality. There is no heuristic techniques is used to optimize the controller parameters in literature. One of the heuristic technique RCGA is considered to optimally design the parameters of the ac and dc controllers. To investigate the ES experimentally, MATLAB simulation results are compared with those results of RTDS and dSPACE controller which are connected as a hardware-in-the-loop (HIL) implementation. Also, Averaged model is developed when the critical and non-critical loads are resistive and inductive respectively. PSO technique is considered for controller parameters optimization. Several disturbances are conducted in this case. Another contribution in this work is a full linearization of power system and control. ES performance is analyzed to investigate the operational constrains and limitations of the ES under several situations.

CHAPTER 3

ELECTRIC SPRING THEORY AND OPERATION

3.1 Basic Principles

ES operation is similar to a mechanical spring in many applications. Mechanical springs are mainly used to provide a mechanical support, store energy and damp the mechanical oscillations while the electric springs aim to support voltage, damp electrical oscillation and also can store the electrical energy. We can notice the analogy in terms of equations between the mechanical and electrical spring. The implemented force on the realistic mechanical spring is:

$$F = -k * x \tag{3.1}$$

Where:

' k ' represents the spring constant and' x 'is the displacement. While for the electric spring,

$$q = -C * V_{es} \tag{3.2}$$

Where:

' q ' is the charge stored in the capacitor with capacitance 'C ' and ' V_{es} ' is the voltage at the terminal of the electric spring.

There is also similarity in stored energy equation where the energy stored in the mechanical spring is:

$$E = \frac{1}{2} * k * x^2 \tag{3.3}$$

Where:

' E ' is the amount of energy stored, ' k ' is the material constant and ' x ' is the displacement. While in the electric spring the energy stored is:

$$E = \frac{1}{2} * C * {V_{es}}^2 \tag{3.4}$$

Where:

' C ' is the capacitance and ' V_{es} ' is the terminal voltage. [9]

Generally, there are three situations for the mechanical spring according to the spring position: neutral position such that no force is applied on the spring, compressed and stretched positions when the mechanical spring is exposed to any force. In the same way, three different operations of ES can be analogous to those cases of mechanical spring as in Figure 3-1.

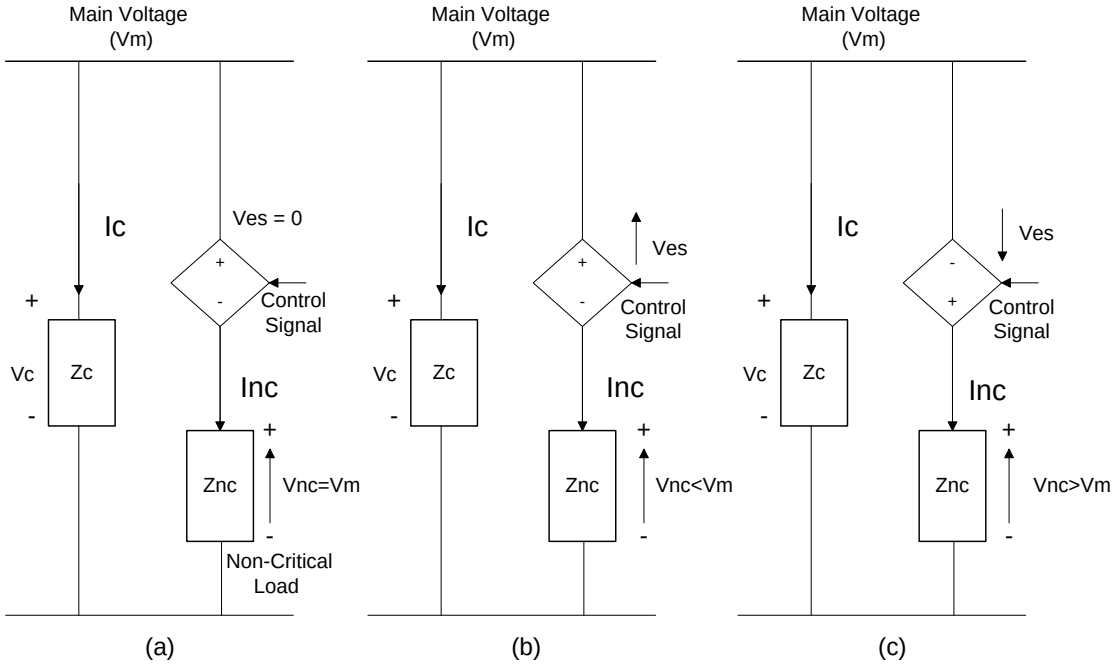

Figure 3-1 ES in three different modes (a) Neutral mode (b) Inductive mode (c) Capacitive mode

Where:

Z_c & Z_{nc}: critical and non-critical loads respectively.

V_m: main voltage of the load bus.

V_{es}: voltage at the electric spring terminals.

V_c & V_{nc}: voltage of critical and non-critical loads respectively.

I_c & I_{nc}:current of critical and non-critical loads respectively.

There are two different types of loads which are named critical loads where the voltage and power consumption should remain constant and non-critical loads where the voltage can be fluctuated within a certain range, as a result, the power consumption of non-critical load is affected. Electric spring connected in series with non-critical load to form a new combination of smart load such as home appliances.

In Figure 3-1, the electric spring can be considered as a controlled voltage source. The neutral position case of mechanical spring implies that the force applied on mechanical spring equals to zero. Similarly, the neutral position of ES means that its voltage ' V_{es} ' is zero and the main voltage ' V_m ' is at its nominal value as shown in Figure 3-1 (a). This means that the renewable energy sources is delivering sufficient amount of required power.

In the second case shown in Figure 3-1 (b) when the main voltage is less than the nominal value and the amount of generated power is not enough to cover the load. The electric spring works in the capacitive mode as a voltage boosting function to regulate the

mains voltage to its nominal value and decrease the applied voltage across the series connected non-critical load to consume less real power.

In the third case shown in Figure 3-1 (c) when the main voltage is greater than the nominal value and the generated power is higher than the load demand, it is necessary to decrease the mains voltage to its nominal value. In this case, the electric spring operates in the inductive mode as a voltage reduction function. The voltage of the series connected non-critical load is decreased and the consumed real power is also decreased accordingly. This voltage reduction of non-critical load in case of capacitive mode is considered as a limitation when resistive load is integrated in series with the ES. If the non-critical load is inductive, the voltage of non-critical load is reduced when the ES operates in inductive mode and boosted if it operates in capacitive mode. Inductive and capacitive modes of the electric spring are two different modes similar to the mechanical spring that can change the displacement in either direction by applying a mechanical force. Non-critical load voltage is increased or decreased within a certain limit regarding device specifications. This variation shouldn't affect the users convenience. Electric spring can have different forms as shown in Figure 3-2.

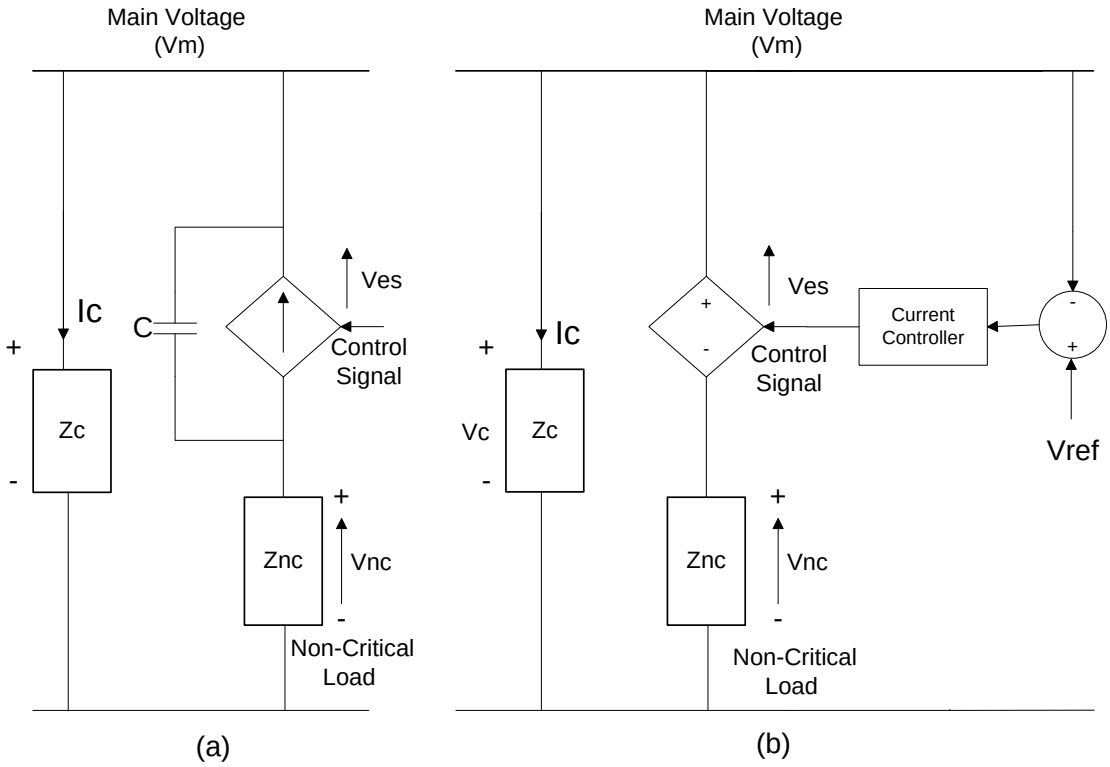

Figure 3-2 Different forms of the electrical springs (a) current source model (b) voltage source model

In Figure 3-2 (a), the electric springs is considered as a capacitor in parallel with a controlled current source or electric spring is modeled as a controlled voltage source connected in series with a dissipative load as in Figure 3-2 (b) The general schematic diagram of the smart grid with electric spring is shown in Figure 3-3.

Figure 3-3, shows the combination of ES in series with the non-critical load to form a smart load. The smart load is then connected in parallel with the critical load.

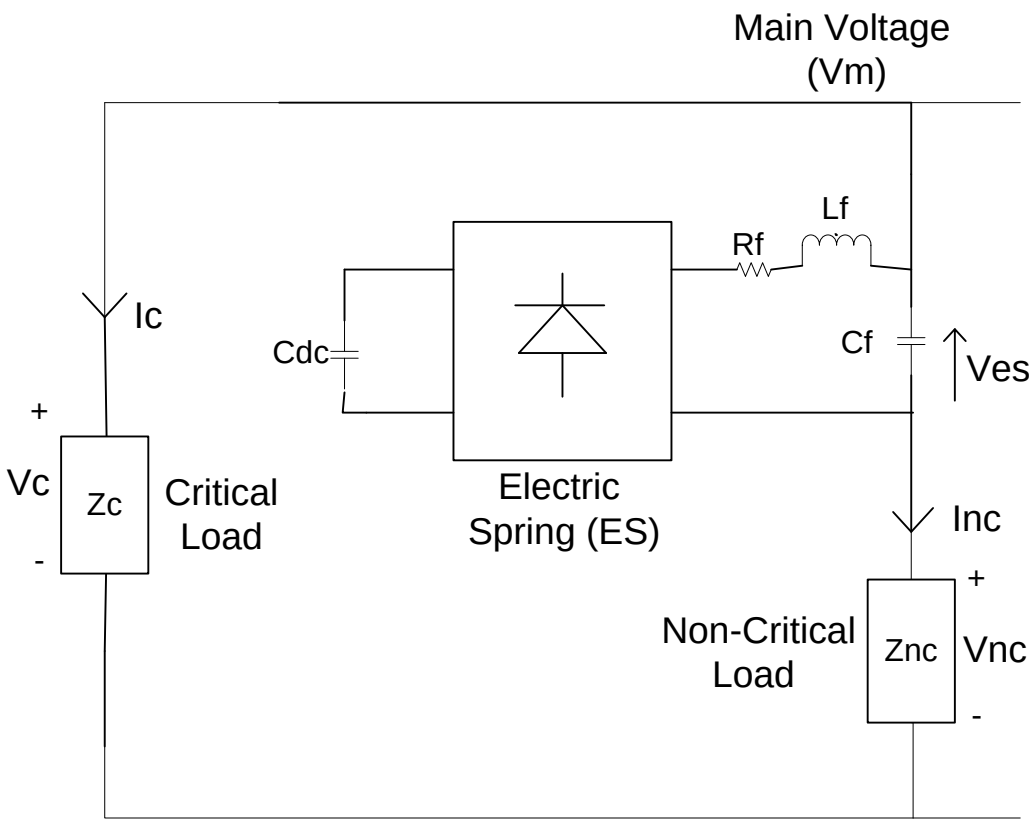

Figure 3-3 Electric spring connection with critical and non-critical load

Where :

R_f, L_f, C_f: resistance, inductance and capacitance of a low pass filter

C_{dc}: capacitor of the dc side of the electric spring

ES voltage changes dynamically in such a way to regulate the main voltage of the power system at the point of connection while non-critical load voltage is affected depending on the variation of the ES voltage as these components are connected together in series. The Loads of smart grid or even the loads of microgrid are mainly fed by intermittent renewable energy sources like wind turbines and PV systems.

Electric spring is useful for different applications like: main voltage regulation, load demand following the power generation, real and reactive power compensation,

reduction the capacity of the energy storage, reduction the imbalance in 3- Ø system, reduction of frequency instability, improving power quality and power factor.

ES is defined as a series reactive power compensator. ES is used for input voltage control while FACTSs devices such as SSSC, and UPFC are usually used for output voltage control. ES has also a major advantage over FACTS devices that it causes the load to follow the power generation.

3.2 Non-critical Load Classifications

The concept of ES operation (either single or three phase power inverter) is described as a new form of smart load that is connected in series with a single or group of non-critical loads. This new combination is an innovative idea that proved its capability to handle the voltage fluctuation of the distribution system and energy generation of different traditional and renewable energy sources in smart grid area. It also opens the doors for more research and comparison between different available techniques in demand side management.

As different non-critical loads are available, ES is connected with different types of loads such as resistive, inductive and capacitive. The ES response represented by phasor diagrams of the smart loads and full derivations of ES model in different cases can be described as follows [54]:

3.2.1 Inductive and Capacitive Loads

ES operates in two different modes, inductive mode and capacitive mode. In inductive mode, it suppresses the excessive voltage above the nominal value of the main bus by consuming sufficient amount of reactive power. In capacitive mode, it supports

the main bus voltage by delivering more reactive power to the network system. The phasor diagrams of ES operates in inductive and capacitive modes with inductive non-critical load are depicted in Figure 3-4.

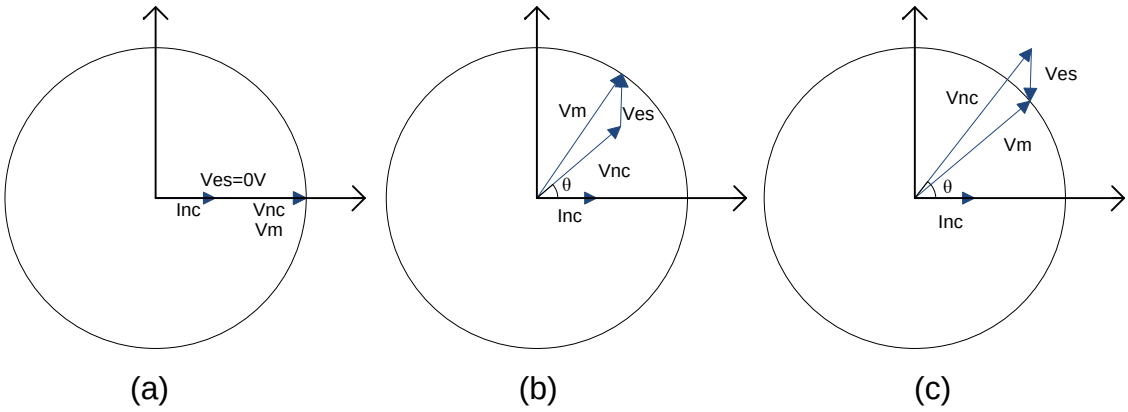

Figure 3-4 Phasor diagrams of ES to maintain main bus voltage constant in different modes for an inductive non-critical load a) Neutral mode b) Inductive mode c) Capacitive mode

In Figure 3-4, the angle difference between electric spring voltage V_{es} and non-critical load current I_{nc} is either +90 (inductive mode) or -90 (capacitive mode) while θ represents the phase angle of the non-critical load. Therefore, the voltage expression can be written as:

$$\vec{V}_m = \vec{V}_{es} + \vec{V}_{nc} \tag{3.5}$$

The relation between these three voltages can be expressed mathematically as follows:

$$V_m{}^2 = (V_{nc}\cos(\theta))^2 + (V_{nc}\sin(\theta) \pm V_{es})^2 \tag{3.6}$$

Solving Eq. (3.6) to get positive root of V_{nc} yields:

$$V_{nc} = -V_{es}\sin\theta + \sqrt{(V_{es}\sin\theta)^2 - \left(V_{es}{}^2 - V_m{}^2\right)} \tag{3.7}$$

Accordingly, the expressions of the output current (I_{nc}), real and reactive power of the smart load (P_{sl}) and (Q_{sl}) are as follows:

$$I_{nc} = \frac{V_{nc}}{Z_{nc}} = \frac{V_{nc}}{\sqrt{{R_{nc}}^2 + {X_{nc}}^2}} \tag{3.8}$$

$$P_{sl} = V_{nc}\, I_{nc} \cos\theta = \frac{{V_{nc}}^2 \cos\theta}{Z_{nc}} \tag{3.9}$$

$$Q_{sl} = V_{nc}\, I_{nc} \sin\theta + V_{es}\, I_{nc} = \frac{{V_{nc}}^2 \sin\theta + V_{nc}V_{es}}{Z_{nc}} \tag{3.10}$$

Where Z_{nc}, R_{nc}, X_{nc} represent the non-critical load impedance, resistance, and reactance respectively.

Eq.(3.8), Eq. (3.9) and Eq. (3.10) are used for both inductive and capacitive load where $\sin\theta$ term is positive in case of inductive load while it has a negative sign in case of capacitive load.

3.2.2 Resistive Loads

When the phase angle of non-critical load is zero with a pure resistive load, i.e., $\sin\theta = 0$, this leads to modify the phasor diagrams of Figure 3-4 to be as shown in Figure 3-5.

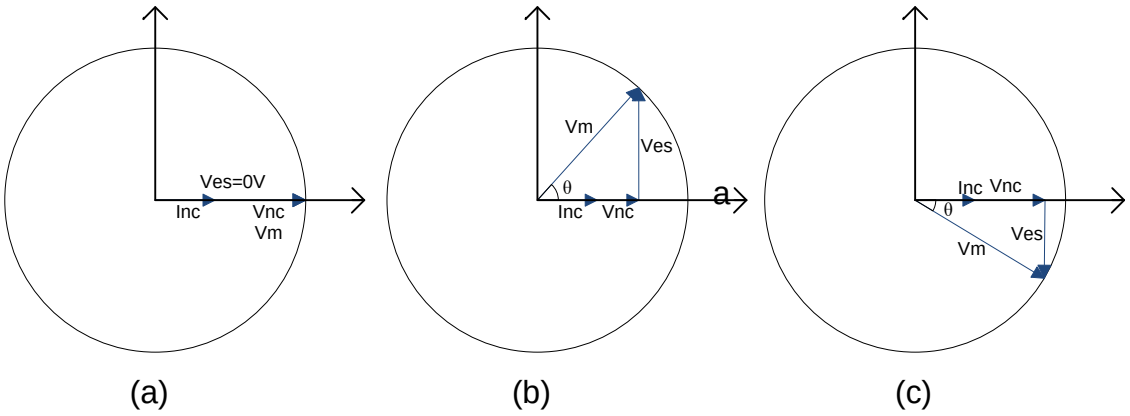

Figure 3-5 Phasor diagrams of ES to maintain main bus voltage constant in different modes for a resistive non-critical load a) Neutral mode b) Inductive mode c) Capacitive mode

Subsequently, after substituting unity power factor in Eq. (3.7), non-critical load voltage expression becomes as given in Eq. (3.11)

$$V_{nc} = \sqrt{\left({V_{es}}^2 - {V_m}^2\right)} \tag{3.11}$$

Other related smart load real and reactive power expressions can be expressed as follows:

$$I_{nc} = \frac{V_{nc}}{R_{nc}} \tag{3.12}$$

$$P_{sl} = \frac{{V_{nc}}^2}{R_{nc}} \tag{3.13}$$

$$Q_{sl} = V_{es} I_{nc} \tag{3.14}$$

Where I_{nc} and R_{nc} are ES current (ES current is same as non-critical load current since ES and Non-critical loads are connected in series) and non-critical load resistance respectively.

This leads to conclude that the reactive power of smart load equals the reactive power consumption or generation by the electric spring. In addition, the resistive load

represents the simple case to study the ES behavior in different modes under different types of disturbances.

3.3 Electric Spring Versions

Two versions of ES are developed and validated in research papers. The first version is initially implemented when the dc side of ES are represented by a dc capacitor and regulated by a controller. This version aims to generate a sinusoidal compensation voltage at the ac terminal of ES normal to the non-critical load current. So, it is considered simply as a reactive power controller like TCSC and UPFC that can generate or consume sufficient amount of pure reactive power to regulate the main voltage.

The second version of ES is able to handle a real power exchange between the ES and power system to extend its usage for more applications. This includes power system stability improvement and imbalance reduction. This version consists of a battery connected at the dc side of ES instead of the capacitor or connected in parallel with this capacitor. It provides a free angle difference control ($0^o - 360^o$) between ES voltage and non-critical load current. This extends the number of ES active modes to be eight modes instead of two as shown in Figure 3-6.

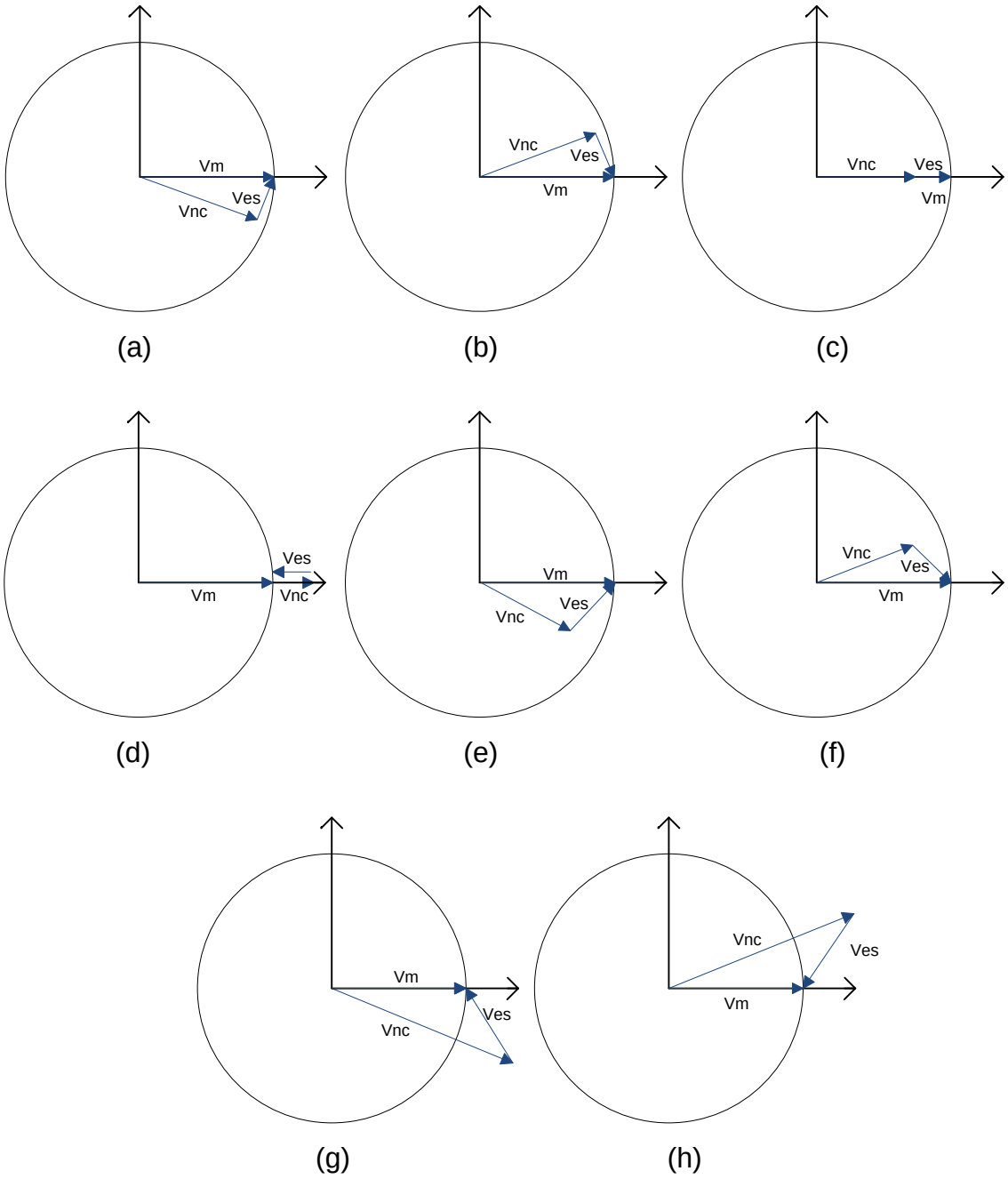

Figure 3-6 Phasor diagrams of ES in eight different modes with batteries a) inductive mode b) capacitive mode c) resistive mode d) negative-resistive mode e) inductive plus resistive mode f) capacitive plus resistive mode g) inductive plus negative-resistive h) capacitive plus negative-resistive

Generally, the operating mode of ES is specified by the phasor relationship (phase angle) between V_{es} and I_{nc}. I_{nc} and V_{nc} are in phase. In case of capacitor, there are two modes when V_{es} and I_{nc} are perpendicular ($+Q_{es}$,- Q_{es}). However, in the second version,

ES has four primary modes, the first two modes are when V_{es} and I_{nc} are perpendicular (version one) and the last two modes namely resistive mode when V_{es} and I_{nc} phasors are in phase (ES consumes real power by charging the battery) or negative-resistive mode when the phasors are in an opposite direction (ES generates real power by discharging the battery). Other four secondary modes are inductive plus resistive mode, capacitive plus resistive mode, inductive plus negative-resistive mode and finally, capacitive plus negative-resistive mode. The secondary modes are considered as a combination of the primary modes.

It is noted that the inductive and inductive plus resistive phasor diagrams are nearly similar. In case of inductive mode, the non-critical load voltage amplitude V_{nc} is taller as compared to inductive plus resistive case. The reason is the angle difference between V_{es} and V_{nc} (I_{nc} is in phase with V_{nc}) in case of inductive mode should be perpendicular to keep the main bus V_m constant. Also, there should be a small deviation in angle for inductive plus resistive case to consume real power. The situation is repeated for capacitive and capacitive plus resistive case.

It is important to note that five of these modes inductive, capacitive, resistive, inductive plus resistive, capacitive plus resistive modes operate as a load shading function by automatically adjusting the applied voltage on non-critical load to force this load to follow the profile of power generation. On the other hand, negative-resistive, inductive plus negative-resistive, capacitive plus negative-resistive modes have the capability to boost the voltage of non-critical load and consequently increase the power consumption.

3.4 Electric Spring Compensation

In this section, a general ES steady-state analysis for different real and reactive power compensation is described and full mathematical model is derived in details. Different typical loads compensated partially or completely by ES are discussed. At the end, a numerical example shows how the ES is controlled in such a way to achieve a certain range of power sharing for compensation purposes between ES and power grid for different loads.

3.4.1 Overview of Electric Spring Compensation Principle

The amplitude of the load voltage and angle displacement changes automatically when the power electronic (ES) injects a sinusoidal voltage profile at its ac terminal as a voltage compensator. This voltage and angle variation will contribute basically to control the power flowing to the load since it is connected in series as seen in Figure 3-7

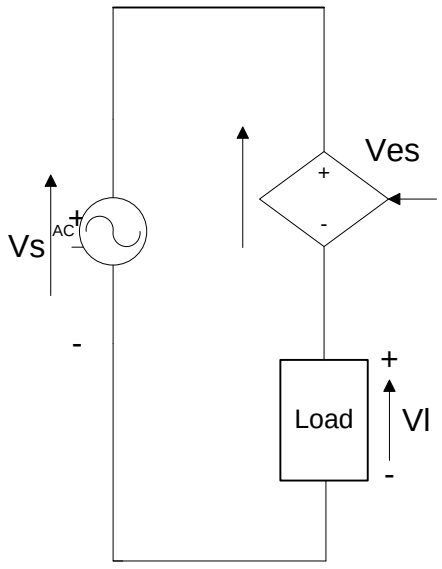

Figure 3-7 Power system including power source, load and ES

where V_s represents the voltage source of the power system which may be considered a strong or a weak power source where the instantaneous voltage expression of the system is expressed in Eq. (3.15) or in Eq. (3.16). The System voltage is ac sinusoidally time varying signal.

$$v_s\,(t) \;=\; v_l\,(t) \;+\; v_{es}\,(t) \tag{3.15}$$

$$|V_s|\,sin(\omega t) \;=\; |V_l\,|\,sin(\omega t \;+\; \theta_V\,) \;+\; |V_{es}\,|sin(\omega t \;+\; \varphi_V\,) \tag{3.16}$$

where $|V_s|$, $|V_l\,|$ and $|V_{es}\,|$ are root mean square values of the ac sinusoidal time varying voltage signals for source, load and ES respectively. ωt is the angular frequency, θ_V and φ_V are the angle displacement of load and ES voltage respectively.

Different characteristics of load connected with ES allow the displacement angles to be allocated in different values as specified below.

- When the connected load is inductive:

$$0 \;<\; \theta_V \;< +\frac{\pi}{2}, -\frac{\pi}{2} < \varphi_V < 0 \tag{3.17}$$

- When the connected load is capacitive:

$$-\frac{\pi}{2} < \theta_V < 0, 0 \;<\; \varphi_V \;< +\frac{\pi}{2} \tag{3.18}$$

- When the connected load and ES are resistive:

$$\theta_V = 0, \varphi_V = 0 \tag{3.19}$$

- When the connected load is resistive and ES is negative resistive:

$$\theta_V = 0, \varphi_V = -\pi \tag{3.20}$$

- When the connected load is negative resistive and ES is resistive:

$$\theta_V = -\pi, \varphi_V = 0 \tag{3.21}$$

- When the connected load and ES are resistive:

$$\theta_V = -\pi, \varphi_V = -\pi \tag{3.22}$$

The current displacement angle θ_s referred to voltage grid $|V_s|\angle 0^o$ is given as:

- When the voltage source is inductive:

$$-\frac{\pi}{2} < \theta_s < 0 \tag{3.23}$$

- When the voltage source is capacitive:

$$0 < \theta_s < +\frac{\pi}{2} \tag{3.24}$$

- When the voltage source is resistive:

$$\theta_s = 0 \tag{3.25}$$

- When the voltage source is negative resistive:

$$\theta_s = -\pi \tag{3.26}$$

Steady-state complex power can be represented in phasor form as:

$$|S_s|\angle\phi_S = |S_l|\angle\theta_S + |S_{es}|\angle\varphi_S \tag{3.27}$$

Where $|S_s|$, $|S_l|$ & $|S_{es}|$ are the magnitudes of the complex powers of the source, load and ES respectively. ϕ_S, θ_S & φ_S are the corresponding angles of the previous combination. Other equations can be considered to represent the steady-state complex power using voltages and currents as:

$$\left|S_s\right|\angle\phi_S = |V_s|\angle 0^o . |I_s|\angle -\theta_s = |V_s|\left|I_s\right|\angle -\theta_s \tag{3.28}$$

$$\left|S_l\right|\angle\,\theta_S = |V_l|\angle\theta_V . |I_s|\angle -\theta_s = |V_l|\left|I_s\right|\angle(-\theta_V - \theta_s) \tag{3.29}$$

$$\left|S_{es}\right|\angle\,\varphi_S = |V_{es}|\angle\varphi_V . |I_s|\angle -\theta_s = |V_{es}|\left|I_s\right|\angle(-\varphi_V - \theta_s) \tag{3.30}$$

Each of these complex power can be analyzed into their power components:

$$|S_s|\angle \phi_S = \pm P_s \pm jQ_s \tag{3.31}$$

$$|S_l|\angle \theta_S = \pm P_l \pm jQ_l \tag{3.32}$$

$$|S_{es}|\angle \varphi_S = \pm P_{es} \pm jQ_{es} \tag{3.33}$$

$$\pm P_s = \pm P_l \pm P_{es} \tag{3.34}$$

$$\pm Q_s = \pm Q_l \pm Q_{es} \tag{3.35}$$

ES power compensation can be classified into eight categories as mentioned in the following points (two categories for each point):

- Inductive and capacitive power compensation($+jQ_{es}, -jQ_{es}$).
- Positive and negative real power compensation($+P_{es}, -P_{es}$).
- Inductive plus positive or negative real power compensation ($+jQ_{es} + P_{es}, +jQ_{es} - P_{es}$).
- Capacitive plus positive or negative real power compensation ($-jQ_{es} + P_{es}, -jQ_{es} - P_{es}$).

These points indicate clearly how the ES behaves in different situations especially when it is required to perform a certain compensation function in the power system. It emulates inductor or capacitor element connected in the power system.

3.4.2 Complex Power Compensations

As mentioned previously in Figure 3-7 , the power system consists of three electric components which are connected in series. According to Figure 3-7, the same ac

current flows through the power system. This connection or topology gives the ES capability to control the current flow and consequently the power sharing among these elements. The load can be represented in terms of R & X as:

$$|Z|\angle\theta_Z = R + jX \tag{3.36}$$

The total load real and reactive power can be expressed as:

$$P_l = \frac{[|V_l|cos(\theta_V)]^2}{R} \tag{3.37}$$

$$Q_l = \frac{[|V_l|sin(\theta_V)]^2}{X} \tag{3.38}$$

By substituting$|V_s|\angle 0^o = |V_l|\angle\theta_V + |V_{es}|\angle\varphi_v$

$$P_l = \frac{[||\,|V_s|\angle 0^o - |V_{es}|\angle\varphi_V||\,cos(\theta_V)]^2}{R} \tag{3.39}$$

$$Q_l = \frac{[||\,|V_s|\angle 0^o - |V_{es}|\angle\varphi_V||\,sin(\theta_V)]^2}{X} \tag{3.40}$$

Eq. (3.39) and Eq. (3.40) show that the load real and reactive power can be varied by controlling the voltage and angle displacement of the ES. This variation will also change the power sharing of ES as given in Eq. (3.41) & Eq. (3.42)

$$P_{es} = |V_{es}||I_s|\cos(\varphi_V - \theta_I) \tag{3.41}$$

$$Q_{es} = |V_{es}||I_s|\sin(\varphi_V - \theta_I) \tag{3.42}$$

Thus, the real and reactive power compensation from the power grid side are also changed based on the variation of ES voltage amplitude and angle displacement as:

$$P_s = |V_s||I_s|\cos(-\theta_I) = |V_l||I_s|\cos(\theta_V - \theta_I) + |V_{es}||I_s|\cos(\varphi_V - \theta_I) \tag{3.43}$$

$$Q_s = |V_s||I_s|\sin(-\theta_I) = |V_l||I_s|\sin(\theta_V - \theta_I) + |V_{es}||I_s|\sin(\varphi_V - \theta_I) \tag{3.44}$$

However, connected load real power can be represented using an attractive mathematical expression as:

$$P_l = |V_l||I_s|\cos(\theta_V - \theta_I) = |V_s||I_s|\cos(-\theta_I) - |V_{es}||I_s|\cos(\varphi_V - \theta_I) \quad (3.45)$$

where

$$P_l > P_s \ if \ \cos(\varphi_V - \theta_I) = -ve; i.e., \frac{\pi}{2} < |\varphi_V - \theta_I| \leq \pi \quad (3.46)$$

$$P_l < P_s \ if \ \cos(\varphi_V - \theta_I) = +ve; i.e., 0 < |\varphi_V - \theta_I| \leq \frac{\pi}{2} \quad (3.47)$$

$$P_l = P_s \ if \ \cos(\varphi_V - \theta_I) = 0; i.e., |\varphi_V - \theta_I| = \frac{\pi}{2} \quad (3.48)$$

At the same time, reactive power can be represented as:

$$Q_l = |V_l||I_s|\sin(\theta_V - \theta_I) = |V_s||I_s|\sin(-\theta_I) - |V_{es}||I_s|\sin(\varphi_V - \theta_I) \quad (3.49)$$

where

$$Q_l > Q_s \ if \ \sin(\varphi_V - \theta_I) = -ve; i.e., -\pi < \varphi_V - \theta_I < 0 \quad (3.50)$$

$$Q_l < Q_s \ if \ \sin(\varphi_V - \theta_I) = +ve; i.e., 0 < \varphi_V - \theta_I < \pi \quad (3.51)$$

$$Q_l = Q_s \ if \ \sin(\varphi_V - \theta_I) = 0; i.e., |\varphi_V - \theta_I| = 0 \ or \ \pi \quad (3.52)$$

3.4.3 Electric Spring Analysis

In this section, two cases are considered to demonstrate the capability of ES for real and reactive power compensation. ES analysis is conducted when the ES, load and voltage source are connected together as shown in Figure 3-7. These cases are:

Case 1: ES Real and Reactive Power Compensation in Case of Delivering Only a Real Power From the Grid

In this section, a power grid is only used for delivering a certain amount of real power to the system. In other words, the angle of ac current circulating in the system is in

phase with the voltage source. The reactive power compensation will be performed by ES to cover the reactive power of the load. ES will be able to deliver or consume reactive power to compensate the load requirements.

- Real Power Compensation (P)

As discussed previously, the grid will deliver a certain amount of real power through the network to cover the connected load. To do so, the angle difference of the power source voltage and current angles is zero. The load is considered a resistive load with $\theta_V = 0$. The expression which describe the ES power compensation is described as:

$$|V_s| = |V_l| + |V_{es}| \cos \varphi_V \; where \; \varphi_V = 0 \; or \; \pi \tag{3.53}$$

In case of $\varphi_V = 0$, Eq. (3.53) will be simplified as given in Eq. (3.54). ES will be handled as a resistive load (sink load) and the real power of the grid will be provided for both ES and resistive load. This distributed power between ES and load will be expressed mathematically based on voltage divider rule as:

$$|V_s| = |V_l| + |V_{es}| \tag{3.54}$$

$$\frac{P_{es}}{P_l} = \frac{|V_s|}{|V_l|} \tag{3.55}$$

However, ES voltage and current can be derived as:

$$|I_s| \angle \theta_I = \sqrt{\frac{P_l}{R}} \angle 0 \tag{3.56}$$

$$|V_{es}| \angle \varphi_V = |V_s| - |I_s| R \angle 0 \tag{3.57}$$

But, when $\varphi_V = \pi$, Eq. (3.53) will be simplified to

$$|\mathrm{V_l}| = |\mathrm{V_s}| + |\mathrm{V_{es}}| \tag{3.58}$$

The distributed power of the system and ES voltage and current are based on the power ratio described as:

$$\frac{P_{es}}{P_s} = \frac{|V_{es}|}{|V_s|} \tag{3.59}$$

$$|I_s|\angle\theta_I = \sqrt{\frac{P_l}{R}}\angle 0 \tag{3.60}$$

$$|V_{es}|\angle\,\varphi_V = |I_s|R - |V_s|\angle\pi \tag{3.61}$$

- Reactive Power Compensation (Q)

  When reactive power is completely compensated by the ES, then:

$$|V_s| = |V_l|\cos\theta_V + |V_{es}|\cos\varphi_V \tag{3.62}$$

$$|V_{es}|\sin\varphi_V = -|V_l|\sin\theta_V \tag{3.63}$$

In this case, ES is capable to generate or consume reactive power by shifting the angle $\varphi_V\ to\ \pm\frac{\pi}{2}$ with respect to circulating current I_s. The second term in Eq. (3.41) indicates clearly how the load is fully compensated by the ES. This pure reactive power compensation doesn't allow any real power exchange between the ES and the power system as:

$$|V_{es}||I_s|\cos\pm\frac{\pi}{2} = 0 \tag{3.64}$$

ES voltage and current will be represented as:

$$|I_s|\angle\theta_I = \frac{|V_s|}{R}\angle 0 \tag{3.65}$$

$$|V_{es}|\angle\theta_V = X|I_s|\angle\frac{\pi}{2} \tag{3.66}$$

ES voltage and current expressions can be modified as:

$$|I_s|\angle\theta_I = \frac{\left(1-\frac{P_{es}}{P_l}\right)|V_s|}{R}\angle 0 \tag{3.67}$$

$$|V_{es}|\angle\theta_V = \frac{\left|\sqrt{{P_{es}}^2+{Q_{es}}^2}\right|}{|I_s|}\angle \arctan\left(\frac{Q_{es}}{P_{es}}\right) \tag{3.68}$$

Case 2: ES Real and Reactive Power Compensation in Case of Delivering or Absorbing a Complex Real and Reactive Power From the Grid

ES can be controlled in such a way to allow the voltage source to contribute simultaneously in compensation process either by generating or consuming real and reactive power components.

- Complex Power Compensation (S)

When the ES is activated in the power system, the grid real and reactive power represented by ($P_{s1,}\ Q_{s1,}$) change automatically to new values represented by ($P_{s2,}Q_{s2}$). In addition, current I_{s1} will vary from $|I_{s1}|\angle\theta_{I1}$ to $|I_{s2}|\angle\theta_{I2}$ by controlling the amplitude and angle (V_{es}, φ_V) values of the ES.

Before switching on the ES, the complex power and reactive power of the voltage source is equivalent to that of the load power as:

$$|S_{s1}|\angle(-\theta_{I1}) = |S_{l1}|\angle(\theta_{V1}-\theta_{I1}) \tag{3.69}$$

where

$$\left|P_{s1}\right| = |P_{l1}| = |V_{l1}|\left|I_{s1}\right|\cos(\theta_{V1} - \theta_{I1}) = |V_s||I_{s1}|\cos(-\theta_{I1}) \tag{3.70}$$

$$\left|Q_{s1}\right| = |Q_{l1}| = |V_{l1}|\left|I_{s1}\right|\sin(\theta_{V1} - \theta_{I1}) = |V_s||I_{s1}|\sin(-\theta_{I1}) \tag{3.71}$$

The load voltage, current and impedance are represented by complex power and voltage source as:

$$|V_{l1}|\angle\theta_{V1} = |V_s|\angle 0 \tag{3.72}$$

$$|I_{s1}|\angle\theta_{I1} = \frac{\sqrt{{P_{s1}}^2 + {Q_{s1}}^2}}{|V_s|}\angle - arc\left(\frac{Q_{s1}}{P_{s1}}\right) \tag{3.73}$$

$$|Z|\angle\theta_Z = \frac{|V_s|^2}{\sqrt{{P_{s1}}^2 + {Q_{s1}}^2}}\angle arc\left(\frac{Q_{s1}}{P_{s1}}\right) \tag{3.74}$$

The grid power and current are changed accordingly as:

$$S_{s\_new} = |S_{s2}|\angle(-\theta_{I2}) \tag{3.75}$$

$$|I_{s2}|\angle -\theta_{I2} = \frac{\sqrt{{P_{s2}}^2 + {Q_{s2}}^2}}{|V_s|}\angle - arc\left(\frac{Q_{s2}}{P_{s2}}\right) \tag{3.76}$$

Based on that, the complex power and load voltage are represented by

$$S_{l\_new} = |S_{l2}|\angle(\theta_{V2} - \theta_{I2}) \tag{3.77}$$

$$P_{l2} = |I_{s2}|^2|Z|\cos(\theta_Z) = \frac{{P_{s2}}^2 + {Q_{s2}}^2}{\sqrt{{P_{s1}}^2 + {Q_{s1}}^2}} cos\left[arctan\left(\frac{Q_{s1}}{P_{s1}}\right)\right] \quad (3.78)$$

$$Q_{l2} = |I_{s2}|^2|Z|\sin(\theta_Z) = \frac{{P_{s2}}^2 + {Q_{s2}}^2}{\sqrt{{P_{s1}}^2 + {Q_{s1}}^2}} sin\left[arctan\left(\frac{Q_{s1}}{P_{s1}}\right)\right] \quad (3.79)$$

$$|V_{l2}|\angle\theta_{V2} = \frac{|S_{l2}|}{|I_{l2}|}\angle(\theta_{V2} - \theta_{I2}) + \theta_{I2}$$

$$= |V_s|\left|\sqrt{\frac{{P_{s2}}^2 + {Q_{s2}}^2}{{P_{s1}}^2 + {Q_{s1}}^2}}\right|\angle\left[arctan\left(\frac{Q_{s1}}{P_{s1}}\right) - arctan\left(\frac{Q_{s2}}{P_{s2}}\right)\right] \quad (3.80)$$

This value of load voltage can be substituted in Eq. (3.80) to find the expected voltage and angle of the ES to make a necessary action of power compensation.

$$|V_{es}|\angle\varphi_V = |V_s|\angle 0 - |V_{l2}|\angle\theta_{V2} \quad (3.81)$$

- Real and Reactive Power Compensation (P & Q)

Two cases will be introduced, in the first case, the real power of the grid source when it is changed from P_{s1} to P_{s2} such as the reactive power of the power grid Q_{s1} is kept constant as shown in Eq. (3.82). Source current and load voltage expressions are given as:

$$Q_{s1} = Q_{s2} = Q_s \quad (3.82)$$

$$|I_{s2}|\angle\theta_{I2} = \frac{\sqrt{{P_{s2}}^2 + {Q_{s2}}^2}}{|V_s|}\angle - arctan\left(\frac{Q_s}{P_{s1}}\right) \quad (3.83)$$

$$|V_{l2}|\angle\theta_{V2} = |V_s|\sqrt{\frac{{P_{s2}}^2 + {Q_{s2}}^2}{{P_{s1}}^2 + {Q_{s1}}^2}}\angle\left[arctan\left(\frac{Q_s}{P_{s1}}\right) - arctan\left(\frac{Q_s}{P_{s2}}\right)\right] \quad (3.84)$$

In the second case, the reactive power of the voltage source is changed from Q_{s1} level to Q_{s2} while the real power P_{s1} is kept constant as shown in Eq. (3.85). Source current and load voltage expressions are:

$$P_{s1} = P_{s2} = P_s \quad (3.85)$$

$$|I_{s2}|\angle\theta_{I2} = \frac{\sqrt{{P_{s2}}^2 + {Q_{s2}}^2}}{|V_s|}\angle - arctan\left(\frac{Q_{s2}}{P_s}\right) \quad (3.86)$$

$$|V_{l2}|\angle\theta_{V2} = |V_s|\sqrt{\frac{{P_{s2}}^2 + {Q_{s2}}^2}{{P_{s1}}^2 + {Q_{s1}}^2}}\angle\left[arctan\left(\frac{Q_{s1}}{P_s}\right) - arctan\left(\frac{Q_{s2}}{P_s}\right)\right] \quad (3.87)$$

CHAPTER 4

ELECTRIC SPRING CONTROLLER DESIGN USING THE SWITCHING MODEL

4.1 Switching Model of Electric Spring

This section presents a dc to ac switching model of single phase full-bridge converter shown in Figure 4-1. Single phase full bridge inverter is better than the half bridge inverter with respect to harmonic analysis.

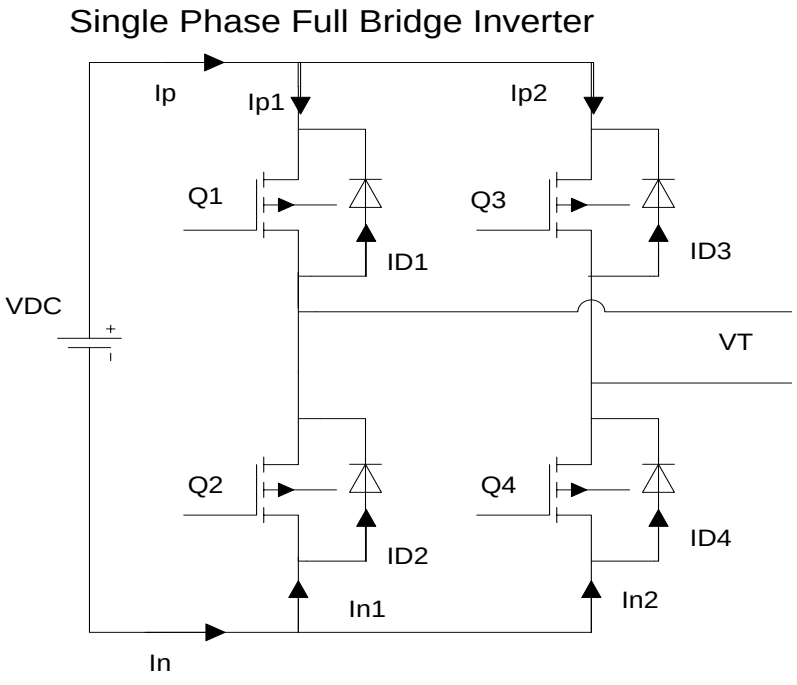

Figure 4-1 Single phase full bridge inverter

This figure consists of a four switch group numbered 1-4 with antiparallel connection of each controllable unidirectional switch like transistor, MOSFET or other power electronic switch and a single diode.

Each switch and diode in the bridge are named Q_i and D_i respectively, where i is the element number, $i = 1,2,3,4$.

In this work, MOSFET is utilized to present a voltage source converter (VSC) where the current flows from the source to drain while flows from anode to cathode in the diode. The main currents out of the battery through the upper and lower switches are called I_p and I_n respectively. The terminal voltages at the dc side are connected with a dc battery. It is denoted by V_p and V_n respectively. The currents are then distributed through the converter arms namely I_{p1}, I_{p2}, I_{n1} and I_{n2}. The ac terminal voltage is donated by V_t.

Accordingly, the relationship of the voltage source converter (VSC) currents can be expressed as follows:

$$I_{p1} = I_{Q1} - I_{D1} \tag{4.1}$$

$$I_{p2} = I_{Q3} - I_{D3} \tag{4.2}$$

$$I_{n1} = I_{D2} - I_{Q2} \tag{4.3}$$

$$I_{n2} = I_{D4} - I_{Q4} \tag{4.4}$$

Thus, the output power of dc side and the delivered power to the ac side of the converter are defined by P_{DC} and P_{AC} respectively. The converter is switched by comparing a carrier signal (Triangle signal with switching period T_s) and a modulation signal $m(t)$ through pulse width modulation (PWM) technique.

There are eight different operation modes for the converter taking into consideration the direction of the current. Four modes for each current direction when the ac current flows out the bridge (positive direction) or to the bridge (negative direction).

For positive direction, let Q_1 and Q_4 are conducted and Q_3 and Q_2 are blocked. Therefore, the current will flow through Q_1 and Q_4 and will not flow through the corresponding diodes D_1 and D_4 because the $i_{D1}$and i_{D4} can not be negative, thus $V_t = V_{DC}$. Also, when the switching signal sent to S3 and S2, the current will flow through the diodes D_2 and $D_3$and Q_2, Q_3 don't carry any current. Consequently, $V_t = -V_{DC}$. Last two modes are when Q_1 and Q_3 or Q_2 and Q_4 are on. The current will flow in D_3 and Q_1 in the first one and flow in Q_4 and D_2 in the last mode. In the last two cases, V_t will be zero.

Similarly, the same approach are applied when the ac side current is negative. The same results are concluded for current flowing through the opposite direction. i.e., positive current flow in Q_1 and Q_4 in the first mode and in D_1 and D_4 in the first negative current mode. Mathematical relationships of voltage, current and the switching of single phase full bridge inverter are described as follows:

$$s_1(t)s_4(t) + s_3(t)s_2(t) + s_1(t)s_3(t) + s_2(t)s_4(t) \equiv 1 \tag{4.5}$$

$$V_t(t) = (V_{DC})s_1(t)s_4(t) - (V_{DC})s_3(t)s_2(t) \tag{4.6}$$

For positive direction

$$i_p(t) = is_1(t)s_4(t) - is_3(t)s_2(t) \tag{4.7}$$

$$i_n(t) = -is_1(t)s_4(t) + is_3(t)s_2(t) \tag{4.8}$$

For negative direction

$$i_p(t) = is_3(t)s_2(t) - is_1(t)s_4(t) \tag{4.9}$$

$$i_n(t) = -is_3(t)s_2(t) + is_1(t)s_4(t) \tag{4.10}$$

Power at the ac and dc side are derived accordingly as:

$$P_t(t) = V_t(t)i = (V_{DC})[s_1(t)s_4(t) - s_3(t)s_2(t)]i \tag{4.11}$$

For positive direction

$$P_{DC1}(t) = V_{DC}\big(is_1(t)s_4(t)\big) - V_{DC}\big(is_3(t)s_2(t)\big) = V_{DC}i\big(s_1(t)s_4(t) - s_3(t)s_2(t)\big) \tag{4.12}$$

For negative direction

$$P_{DC2}(t) = V_{DC}\big(is_3(t)s_2(t)\big) - V_{DC}\big(is_1(t)s_4(t)\big) = V_{DC}i\big(s_3(t)s_2(t) - s_1(t)s_4(t)\big) \tag{4.13}$$

$$\text{So, } P_{DC}(t) = V_{DC}\big(s_1(t)s_4(t) - s_3(t)s_2(t)\big)i \tag{4.14}$$

The power loss of that converter is

$$P_l = P_{DC} - P_t \tag{4.15}$$

4.2 Power System Description

ES is integrated with a dissipative non-critical load (Z_{nc}) in the distribution system to represent a new form of smart load. The voltage amplitude and angle of the electric spring are controlled by modulation index (m) and angle ($\emptyset$). Distribution

system is fed by the power grid with voltage (V_g), internal impedance (Z_{int}) and renewable energy current source (I_r). Instead of integrating PV system in the smart grid, intermittent renewable energy source is represented by a current source. The effects of variable incident irradiance on the PV surfaces or the effect of partial shading phenomenon which occurs when clouds, dust, snow and buildings cover the PV panel [67-70] can be represented by injecting a variable current into the system. Energy is transferred through the distribution feeders (Z_{f1}) and (Z_{f2}) to the connected loads which are represented by critical and non-critical loads (Z_c) & (Z_{nc}) respectively. Electric spring voltage changes dynamically to regulate the main voltage and also allow the load consumption to follow the power generation. Renewable energy source is emulated using an intermittent current source such that the main voltage of the load bus is fluctuating around its nominal value. Schematic diagram of the network considered is shown in Figure 4-2.

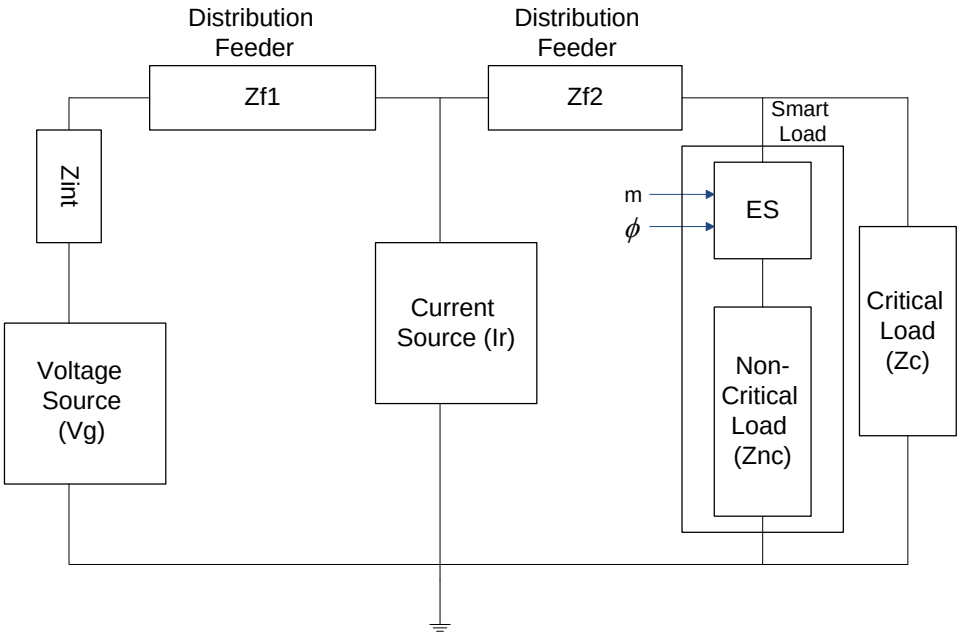

Figure 4-2 Schematic diagram of the power system

4.3 Problem Formulation

4.3.1 Controller Design

Controllers are designed to regulate the main voltage of ac load bus and dc capacitor voltage at the dc terminal of the power inverter as shown in Figure 4-3. It consists of ac and dc PI controllers. The dynamics of dc bus are taken into consideration, so the ES exchanges real and reactive power with the distribution network. The angle difference between V_{es} and I_{nc} load is $\pm 90^{o}$. The sign of angle depends mainly on electric spring modes (inductive or capacitive mode). However, this angle is slightly deviated because the electric spring absorbs small amount of real power to keep the dc voltage constant and due to the switching losses. The output of the ac controller loop is the modulation index that varies within ±1. Phased locked loop (PLL) block is used to track the current angle of the non-critical load.

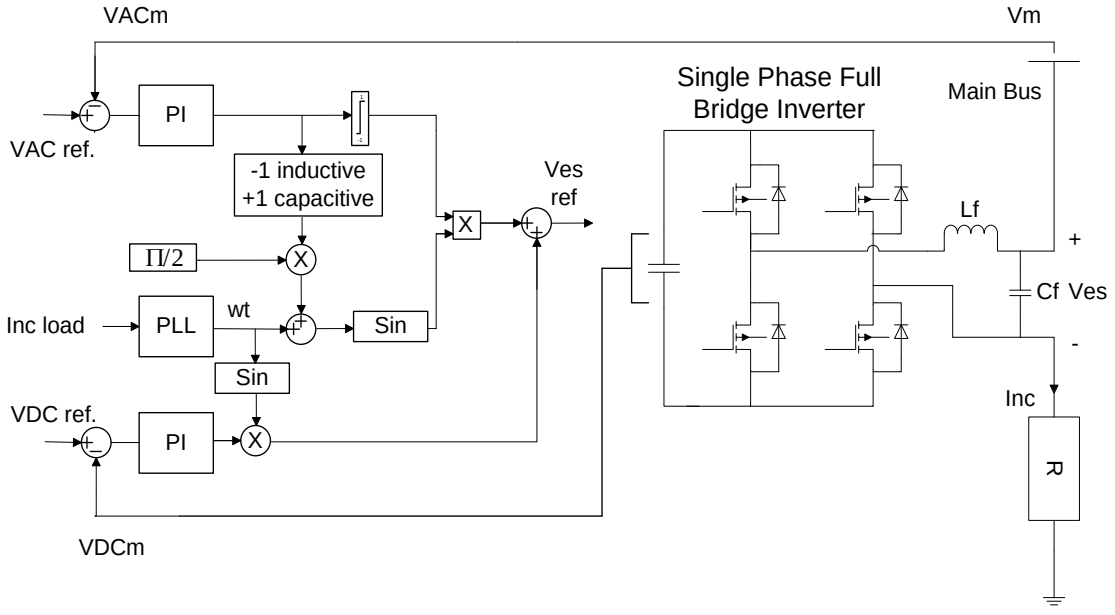

Figure 4-3 Control blocks for the electric spring (single phase full bridge inverter)

To enhance the dynamic performance of the electric spring, the controllers should be optimally designed. The design problem is formulated to optimize the objective function J subject to some inequality constrains. In this work, nonlinear time-domain based objective function is proposed to minimize the ac and dc voltage deviations weighted by the simulation time. This will reduce the overshoot and the settling time. The objective function can be expressed as:

$$\mathbf{J} = \left(\boldsymbol{\alpha} * \int \boldsymbol{t} \, |\Delta \boldsymbol{V_{ac}}| \, \boldsymbol{dt} + \int \boldsymbol{t} \, |\Delta \boldsymbol{V_{dc}}| \, \boldsymbol{dt} \right) \tag{4.16}$$

Subject to

$$\begin{cases} \boldsymbol{K_{p1}}^{\boldsymbol{min}} \leq \boldsymbol{K_{p1}} \leq \boldsymbol{K_{p1}}^{\boldsymbol{max}} \\ \boldsymbol{K_{i1}}^{\boldsymbol{min}} \leq \boldsymbol{K_{i1}} \leq \boldsymbol{K_{i1}}^{\boldsymbol{max}} \\ \boldsymbol{K_{p2}}^{\boldsymbol{min}} \leq \boldsymbol{K_{p2}} \leq \boldsymbol{K_{p2}}^{\boldsymbol{max}} \\ \boldsymbol{K_{i2}}^{\boldsymbol{min}} \leq \boldsymbol{K_{i2}} \leq \boldsymbol{K_{i2}}^{\boldsymbol{max}} \end{cases} \tag{4.17}$$

Where $\boldsymbol{t}$ is the simulation time, $\boldsymbol{\alpha}$ is a weighting factor, $\Delta \boldsymbol{V_{ac}}$ is the ac main voltage deviation, $\Delta \boldsymbol{V_{dc}}$ is dc voltage deviation, and $\mathbf{K_{p1}}$, $\mathbf{K_{i1}}$, $\mathbf{K_{p2}}$ and $\mathbf{K_{i2}}$ are the parameters of ac and dc PI voltage controllers.

Genetic algorithm optimization technique is selected to search for the optimal parameters of the given controllers in research space.

4.3.2 Real Coded Genetic Algorithm Optimization Technique (RCGA)

Genetic algorithm is one of the optimization techniques which belongs to evolutionary algorithms (EA). RCGA is a robust technique which can be used to deal with wide range of problems to find the optimal solutions. Moreover, RCGA has several advantages of being able to solve complex optimization problems effectively. It is a

reliable technique that can be easily interfaced with different simulations and models. RCGA principle is defined by utilizing natural evolution process such as selection, cross over and mutation [71]. The following steps describe the process of the genetic algorithm to solve the optimization problem:

1- For initialization, optimization process starts by defining some required parameters such as:

A) Number of control parameters per a candidate solution (D), In this work, K_{p1}, K_{i1}, K_{p2} and K_{i2} are the dc and ac control parameters.

B) Population size (N_{pop}).

C) Number of iterations (generations) (G_{max}).

D) Mutation and cross over probabilities within [0,1].

E) Control parameters equality and inequality constraints for each parameter $[X_{j,min}, X_{j,max}]$. Where j is the order of the optimized parameter.

Initial population is constructed by generating Np solution. Each solution consists of D parameters selected randomly within the parameters constraints. In order to generate the initial population, the following expression will be taken into consideration

$$X_{i,j} = X_{j,min} + rand\left(X_{j,max} - X_{j,min}\right), where\ i = 1 \ldots . Np; j = 1 \ldots . D \quad (4.18)$$

2- Each solution is evaluated by calculating the objective function defined in (4.16). The best solution is selected in each generation and updated throughout the generations. The proposed objective function is based on minimizing the error of

the measured voltage of ac and dc controllers by calculating the time weighted voltage deviation for both controllers.

3- Selection process begins by selecting randomly the parents. Tournament selection is used to select two pairs of solutions and the best one will be selected.

4- To improve the diversity of the solutions (individuals), Cross over operation is applied. Two parents will be randomly selected and the cross over will be applied as given in Eq. (4.19) and Eq. (4.20).

$$\boldsymbol{C_{new}^{1} = \lambda C_{i}^{1} + (1 - \lambda) C_{i}^{2}} \tag{4.19}$$

$$\boldsymbol{C_{new}^{2} = \lambda C_{i}^{2} + (1 - \lambda) C_{i}^{1}} \tag{4.20}$$

where:

$\boldsymbol{C_i^1, C_i^2}$ are the parents and $\boldsymbol{C_{new}^1, C_{new}^2}$ are the offsprings that represent the new control parameters of the ac and dc controllers respectively.

$\boldsymbol{\lambda}$ is a constant between 0 and 1. Cross over is applied with probability of 0.9, otherwise, the selected parents will be the same without any modifications and continue the process.

5- Mutation is utilized after cross over operation to increase the perturbation of the elements. The non-uniform mutation process is applied with probability of 0.15.

$$\boldsymbol{C_{inew}} = \begin{cases} \boldsymbol{C_i + \Delta\,(T, B_i - C_i)\ if\ \tau = 0} \\ \boldsymbol{C_i - \Delta\,(T, C_i - A_i)\ if\ \tau = 1} \end{cases} \tag{21}$$

$$\boldsymbol{\Delta(T, Y) = Y\left(1 - R^{\left(1 - \frac{T}{G_{max}}\right)^{B}}\right)} \tag{22}$$

where:

$\boldsymbol{B_i}$ and $\boldsymbol{A_i}$ represent the maximum and minimum values of the mutated control parameter respectively. Also, $\boldsymbol{R}$ is a random number between 0 and 1. $\boldsymbol{B}$ is a prespecified index selected by the user.

6- Genetic algorithm continues processing until the stopping criteria is met. Different criteria are adopted in intelligent techniques either when the maximum number of generations is reached or when the objective function is less than a certain tolerance value or when the optimal solution values doesn't change for a certain number of generations specified by the users. In this thesis, the first option has been used. Figure 4-4 shows the flowchart of RCGA algorithm implementing the previous steps.

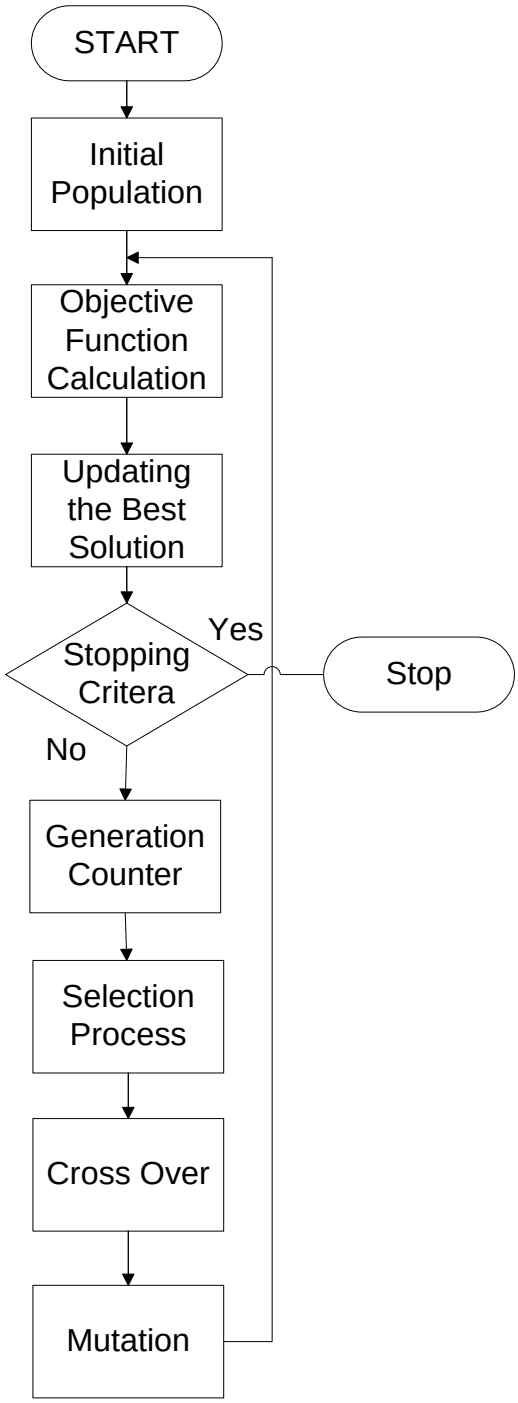

Figure 4-4 Flowchart for controller parameters optimization using RCGA technique

4.4 Simulation Results

4.4.1 Test System

Power system including electric spring as shown in Figure 4-2 is modeled in MATLAB/SIMULINK. It consists of a regulated weak power grid ($\boldsymbol{V_g}$). Power grid is modeled by voltage source with internal impedance ($\boldsymbol{Z_{int}}$). Renewable energy sources with variable output real power is represented by controllable current source ($\boldsymbol{I_r}$). The output current of the controllable current source is fluctuated from $\boldsymbol{0-11\ A}$. So, the load bus is fluctuating around its nominal value of $\boldsymbol{230V\ RMS}$.

The impedances of the transmission lines is represented by ($\boldsymbol{Z_{f1}}$) and ($\boldsymbol{Z_{f2}}$) respectively. The real power is transferred through the transmission network to the connected critical ($\boldsymbol{Z_c}$) and non-critical loads ($\boldsymbol{Z_{nc}}$). The dc capacitor ($\boldsymbol{C_{dc}}$) of the electric spring is regulated to $\boldsymbol{200V}$. Three different cases have been considered in this study. These are sudden change analysis case (inductive and capacitive modes), multiple disturbances and multiple load variations. Power system parameters are summarized in Table 1

Table 1 Parameters specifications of the test system

Description	Parameters	Nominal Values
Weak power grid	V_g	$240\ V\ RMS$
Grid internal impedance	Z_{int}	$0.51 + j6.145\ \Omega$
controllable current source	I_r	$0 - 11\ A$
transmission lines impedance	$Z_{f1}\ ,\ Z_{f2}$	$0.1 + j0.905\ \Omega$ $0.1 + j0.46\ \Omega$
Critical and non-critical load	$Z_c\ , Z_{nc}$	$50\ \Omega$
DC capacitor	C_{dc}	$3000\ \mu F$

4.4.2 Results and Discussions

Referring to Figure 4-2, three different cases are taken into consideration. These cases are:

1- Sudden change analysis.

2- ES response with multiple disturbances using renewable current source.

3- Multiple disturbances by inserting different loads to the system.

Case 1: Sudden Change Analysis

- Inductive mode (suppression mode)

In this case, renewable energy source generates $10\,A$ which leads to increase in the voltage of the load bus to $238V$. Electric spring will operate in inductive mode when the main voltage is greater than the nominal value ($230\,V$) and the generated power is higher than the load demand. Figure 4-5 to Figure 4-7 describe the sudden change behavior of the electric spring in inductive mode.

Figure 4-5 shows the angle difference response between electric spring terminal voltage and non-critical load current. Electric spring terminal voltage is leading the non-critical load current by 87.1^0 and the dc capacitor is charged to $200\,V$ according to the reference value of the dc voltage controller. In Figure 4-6, electric spring absorbs small amount of real power ($16.2\,W$) and sufficient amount of reactive power ($336.5\,VAR$) to regulate the voltages of dc capacitor and ac main load bus while Figure 4-7 shows the sudden change response of critical, non-critical loads and ES voltages respectively.

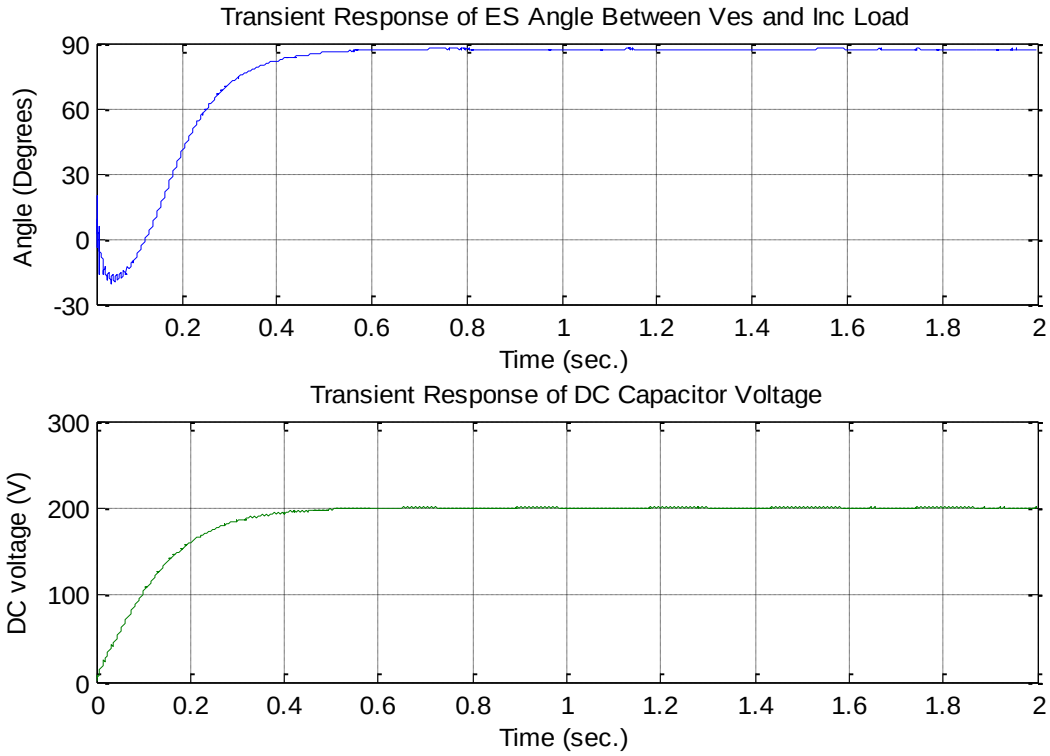

Figure 4-5 Sudden change response of ES angle and dc capacitor voltage in inductive mode

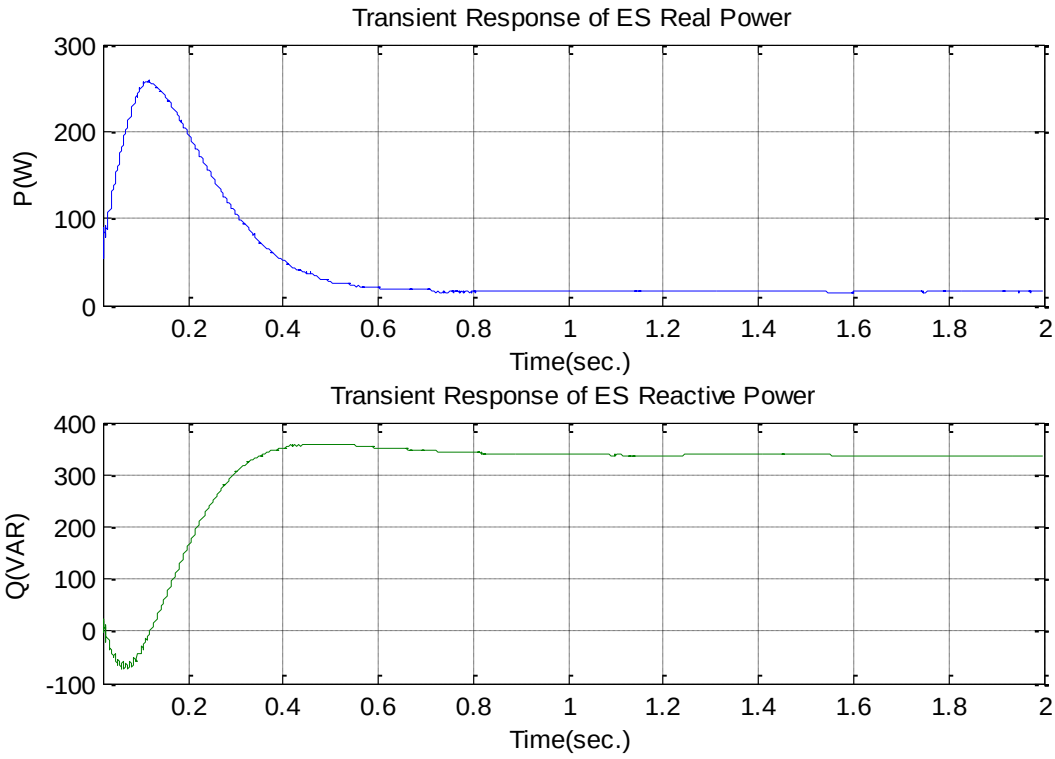

Figure 4-6 Sudden change response of ES real and reactive power in inductive mode

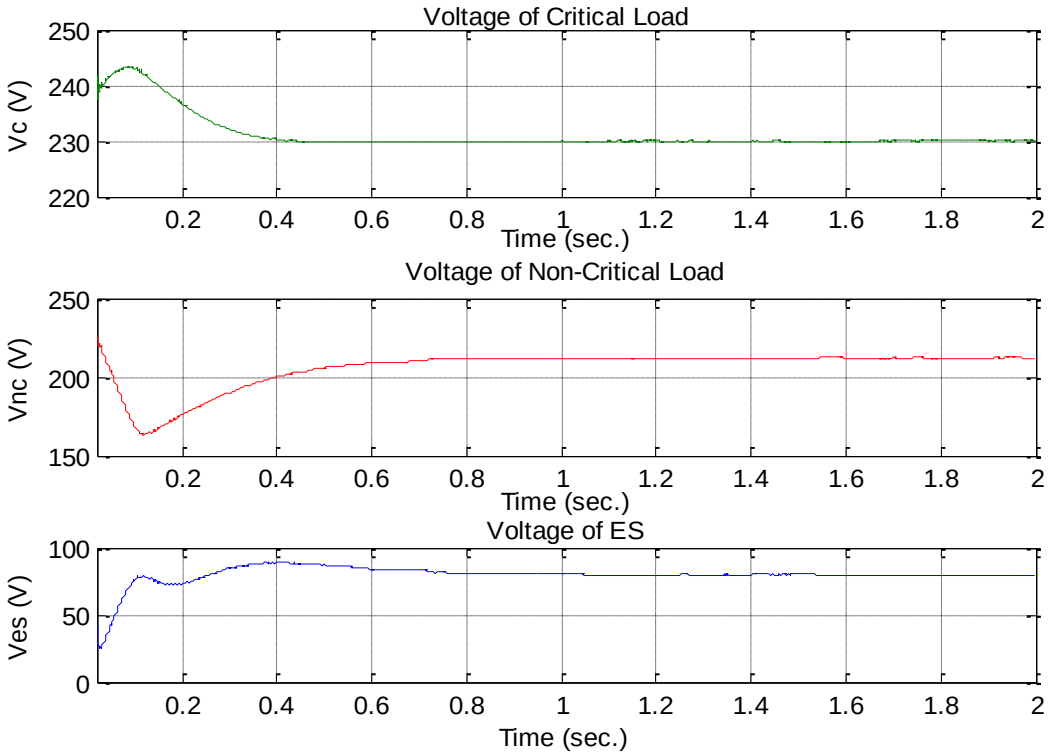

Figure 4-7 Sudden change response of critical, non-critical loads and ES voltages

- Capacitive mode (supportive mode)

In this case, renewable energy source generates $\mathbf{0}\ \boldsymbol{A}$ which leads to a drop in the nominal value of the load bus voltage to $\mathbf{224}\boldsymbol{V}$. Electric spring will operate in capacitive mode when the main voltage is less than the nominal value ($\mathbf{230}\ \boldsymbol{V}$) and the generated power is less than the load demand. Electric spring will support the main voltage to its nominal value by generating sufficient amount of reactive power. Figure 4-8 to Figure 4-10 describe the sudden change behavior of the electric spring in capacitive mode.

Electric spring terminal voltage is lagging the non-critical load current by $\mathbf{85.3^0}$ as shown in Figure 4-8. The dc capacitor is charged to $\mathbf{200}\ \boldsymbol{V}$ according to the reference value of the dc voltage controller. In Figure 4-9, electric spring absorbs small amount of real power ($\mathbf{15.6}\boldsymbol{W}$) and generate sufficient amount of reactive power ($-\mathbf{188.7}\ \boldsymbol{VAR}$) to

regulate the voltage of dc capacitor and ac main load bus. Finally, Figure 4-10 shows the sudden change response of critical, non-critical loads and ES voltages respectively.

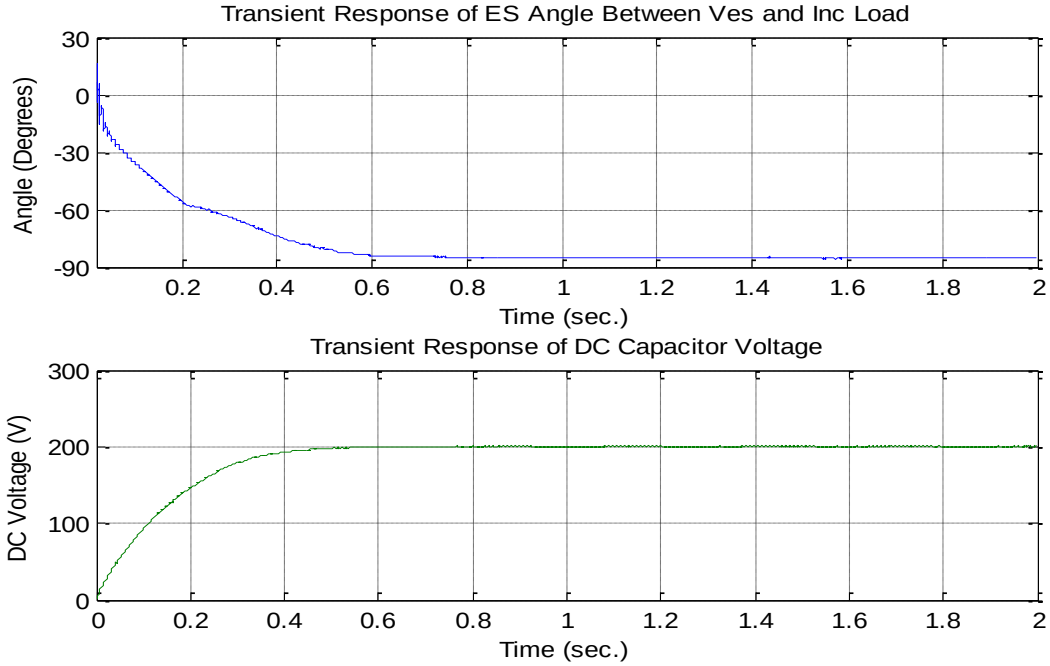

Figure 4-8 Sudden change response of ES angle and dc capacitor voltage in capacitive mode

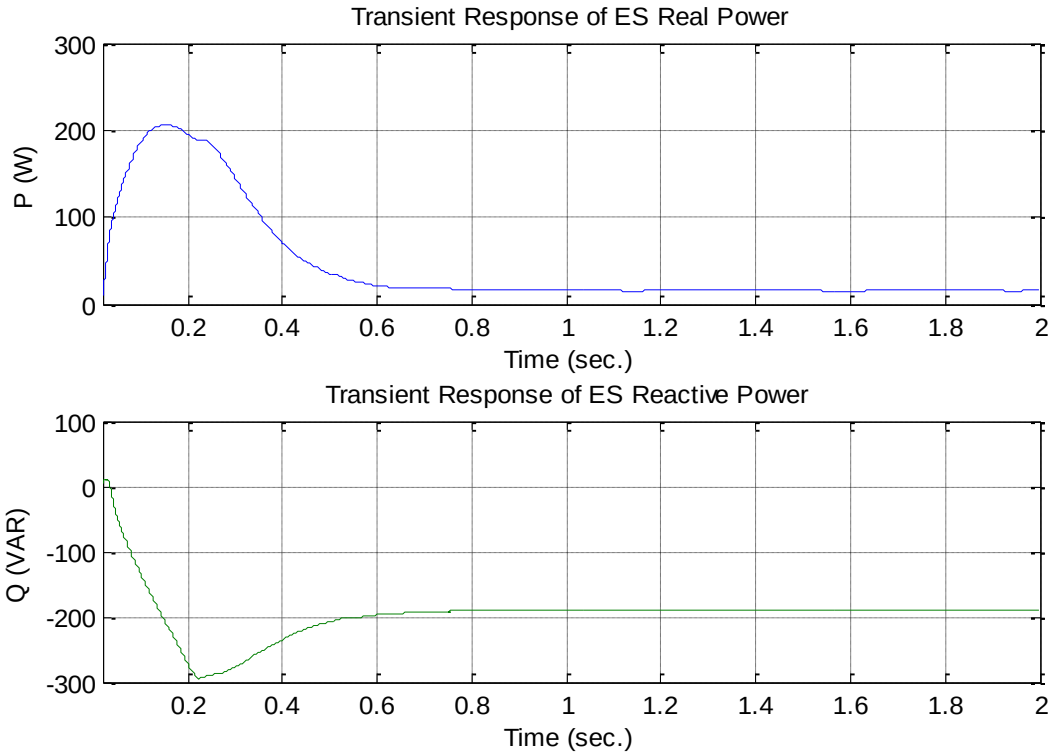

Figure 4-9 Sudden response of ES real and reactive power in capacitive mode

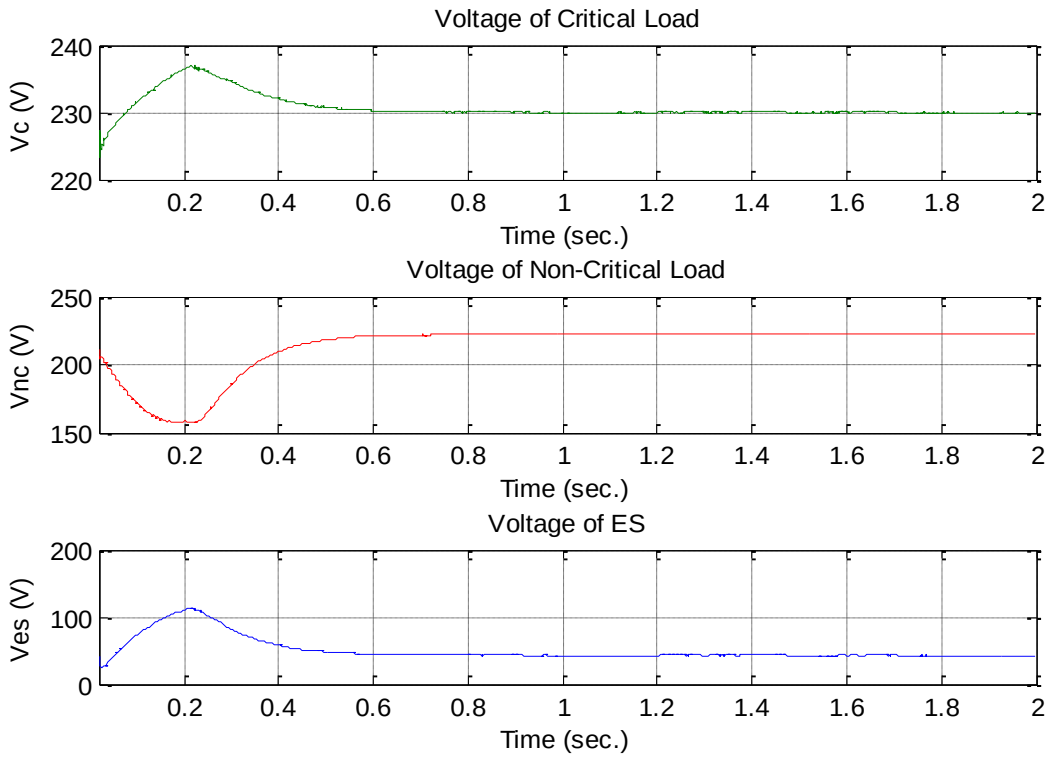

Figure 4-10 Sudden response of critical, non-critical loads and ES voltages

Case 2: ES response with multiple disturbances using renewable current source

Simulation of multiple disturbances is carried out for 7.5s to investigate the performance of the electric spring. This simulation is divided into three time periods. The first time period is of 1.5s when the renewable energy source and the electric spring are disabled. Electric spring is disabled by implementing short circuit on its terminal.

In the second period, the renewable energy source is activated for 3s which starts injecting variable amplitude of sinusoidal active current ($\boldsymbol{I_r}$) ($\mathbf{7.5, 0, 11}\ \boldsymbol{A}$ peak each for 1s). According to that, the main voltage is fluctuating around its nominal value of 230Vac from 233.8 V to 224 V and then to 240 V respectively. During this time period, the ES is

deactivated. The critical and non-critical load voltage ($\boldsymbol{V_c, V_{nc}}$) and power ($\boldsymbol{P_c, P_{nc}}$) are identical.

During the last time period, electric spring is enabled and current profile of the renewable energy source is repeated for 3s to show the effectiveness of the electric spring in regulating the main voltage by dynamically injecting sinusoidal voltage ($\boldsymbol{V_{es}}$). In this case, electric spring will operate in different operating conditions. The capability of the electric spring in regulating the main voltage is depicted in Figure 4-11. The output power of renewable energy source ($\boldsymbol{P_r}$), real power consumption by critical and non-critical load ($\boldsymbol{P_c, P_{nc}}$) and the generated power by the grid connected ($\boldsymbol{P_g}$) are depicted in Figure 4-12. The output current profile of renewable energy source is repeated again to show the responses of modulation index ($\boldsymbol{m}$), angle difference between electric spring voltage and the non-critical load current ($\boldsymbol{\theta}$) and the reactive power generation by the electric spring ($\boldsymbol{Q_{es}}$) in different modes as depicted in Figure 4-13. Figure 4-13 shows that the ES operates in different modes due to the fluctuated voltage of the main bus. In addition, the angle difference ($\boldsymbol{\theta}$) is close to $\boldsymbol{+90^o}$ or $\boldsymbol{-90^o}$ based on the electric spring modes. It is noted that the electric spring generates reactive power in the capacitive mode. On the other hand, it consumes reactive power in the inductive mode.

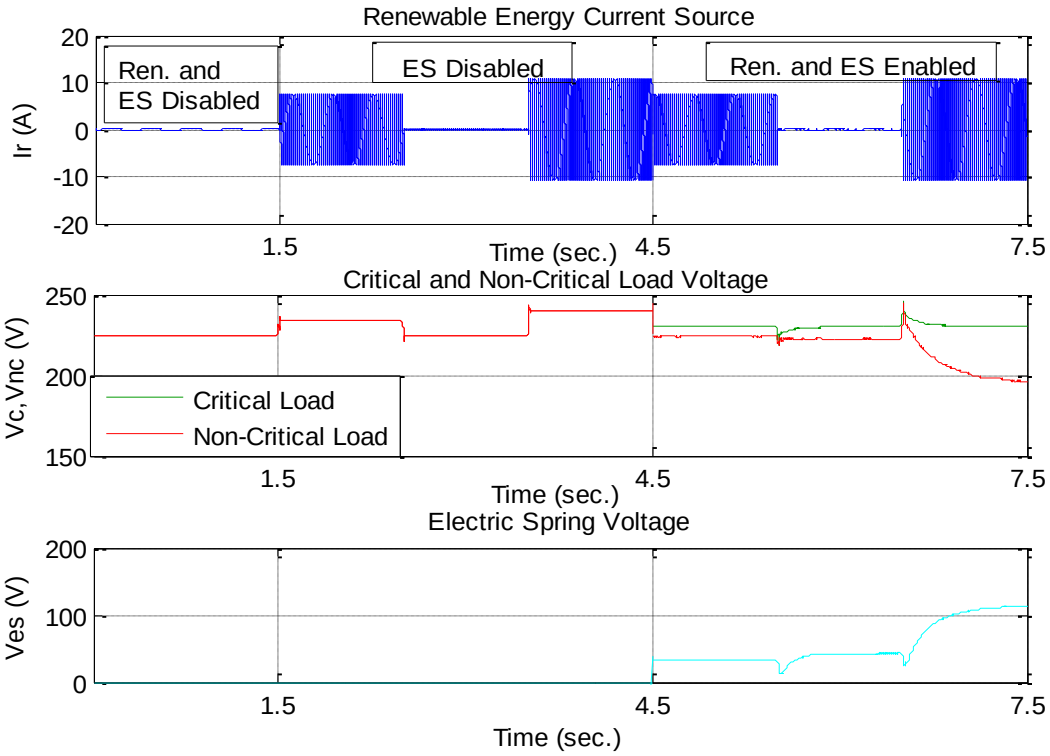

Figure 4-11 Voltage analysis of test system in different modes

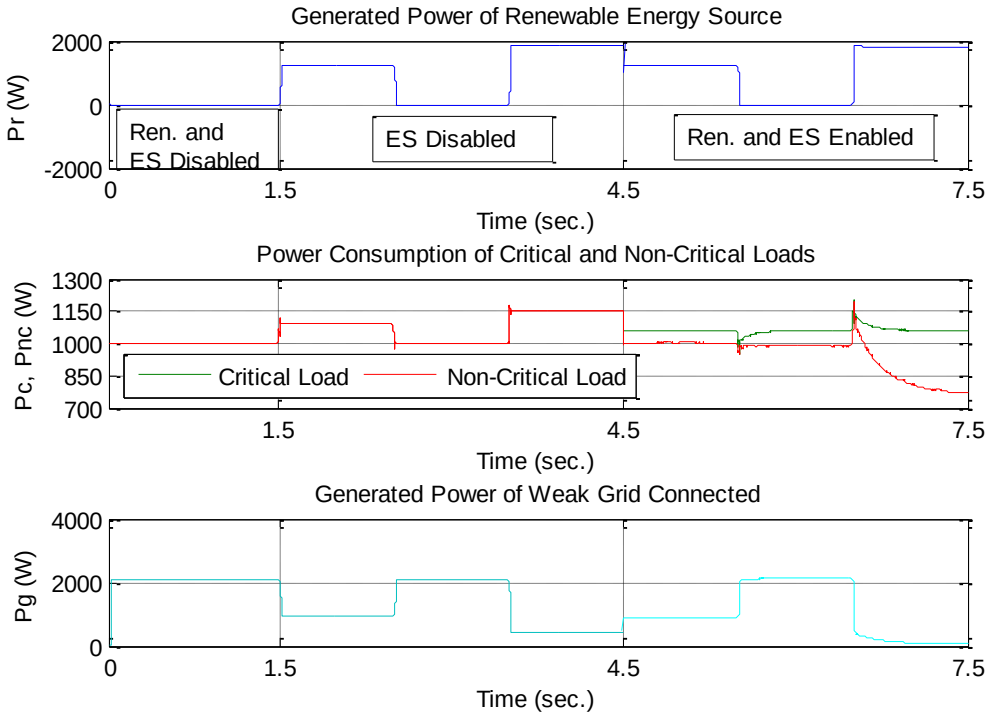

Figure 4-12 Power analysis of test system in different modes

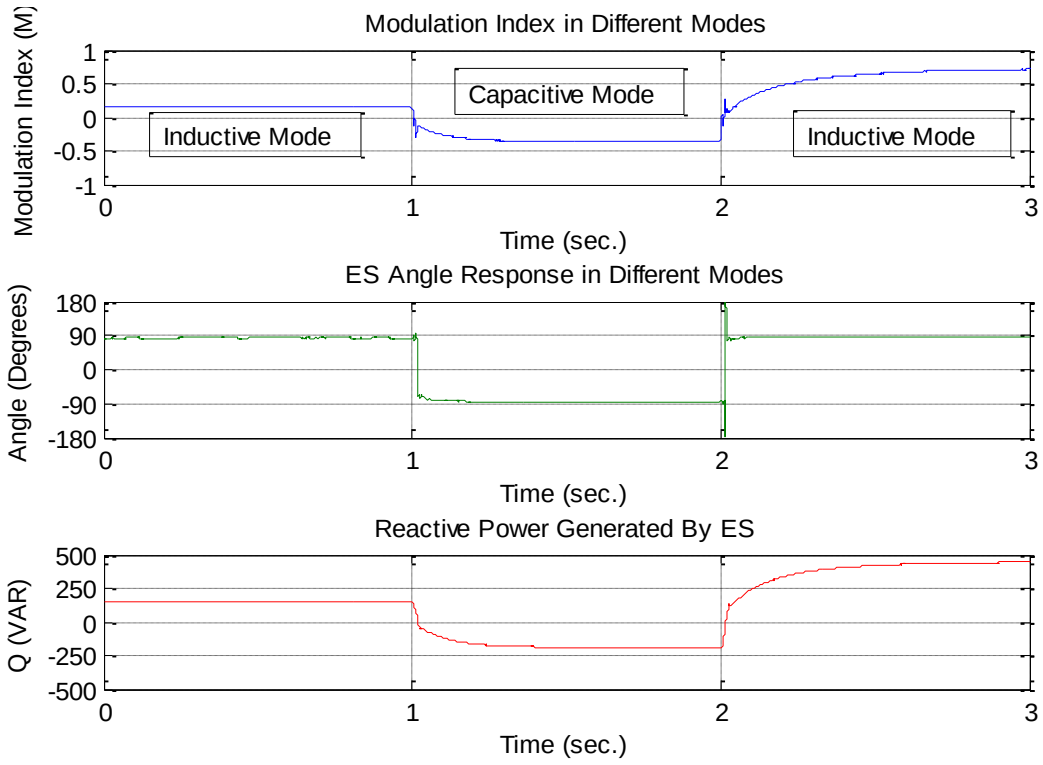

Figure 4-13 Modulation index, angle and reactive power responses in different modes.

Case 3: Multiple disturbances by inserting different loads to the system

- ES response analysis with inductive load disturbance (PF=0.9) to critical load

Different types of disturbances can be applied to investigate the performance of the ES to maintain the main voltage bus constant at its nominal value. To do so, the power system will be simulated for 2 s. The renewable current source is 10 A. The critical load impedance will be suddenly changed by inserting an inductive load of $\mathbf{50 + 24\,\Omega}$ ($\boldsymbol{P.F = 0.9}$) at t = 1 s. In this case, ES will automatically change the voltage of its terminal to maintain the main voltage bus constant as depicted in Figure 4-14.

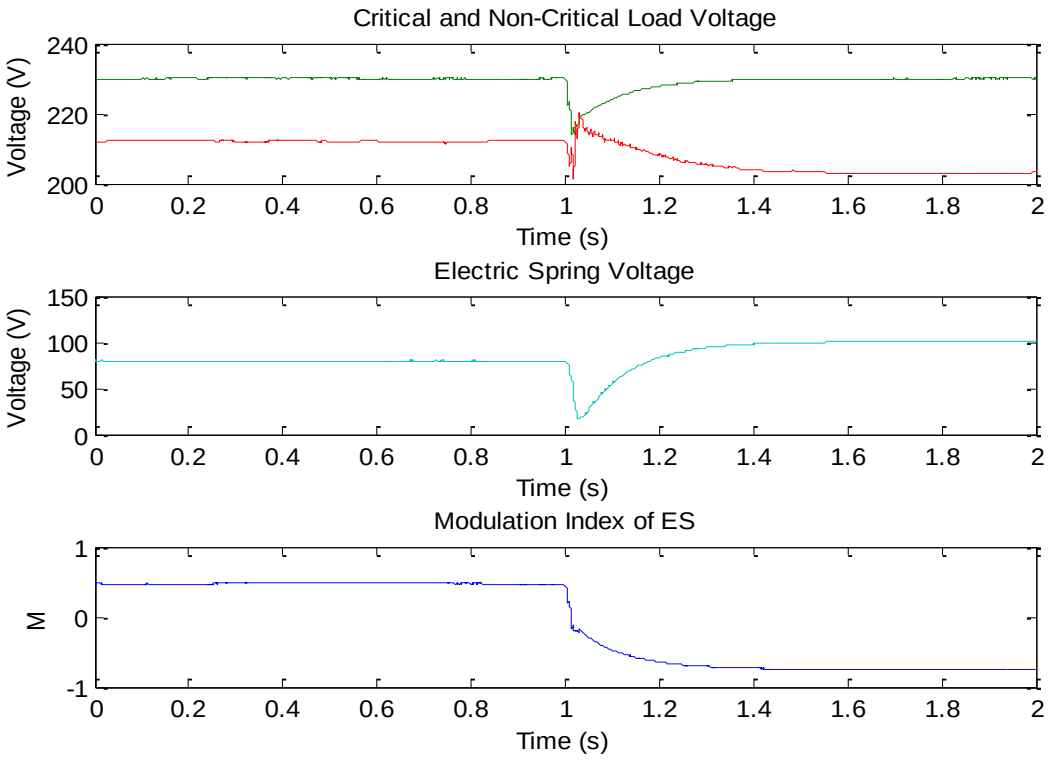

Figure 4-14 Critical, non-critical loads and ES voltages and modulation index response

The inserted inductive load consumes more reactive power which flows in the network and causes a voltage drop to the system. This situation of voltage drop enforces ES to reverse its mode by injecting reactive power to the system instead of consuming it. To keep the main voltage constant after inserting the inductive load, ES will inject higher voltage value at its terminal.

- Resistive load variations

In this case, simulation is carried out for 3s and it is divided into 3 equal time periods. During the first time period, the critical and non-critical loads are 50 Ω each. During the second period, loads are changed by inserting 75 Ω in parallel with non-critical load and 20 Ω in series with critical load. In the last period, the non-critical load resistance increases by inserting 20 Ω in series and the critical load resistance varies by

inserting 75 Ω in parallel. Critical and non-critical load voltages, ES voltage and modulation index response are shown in Figure 4-15

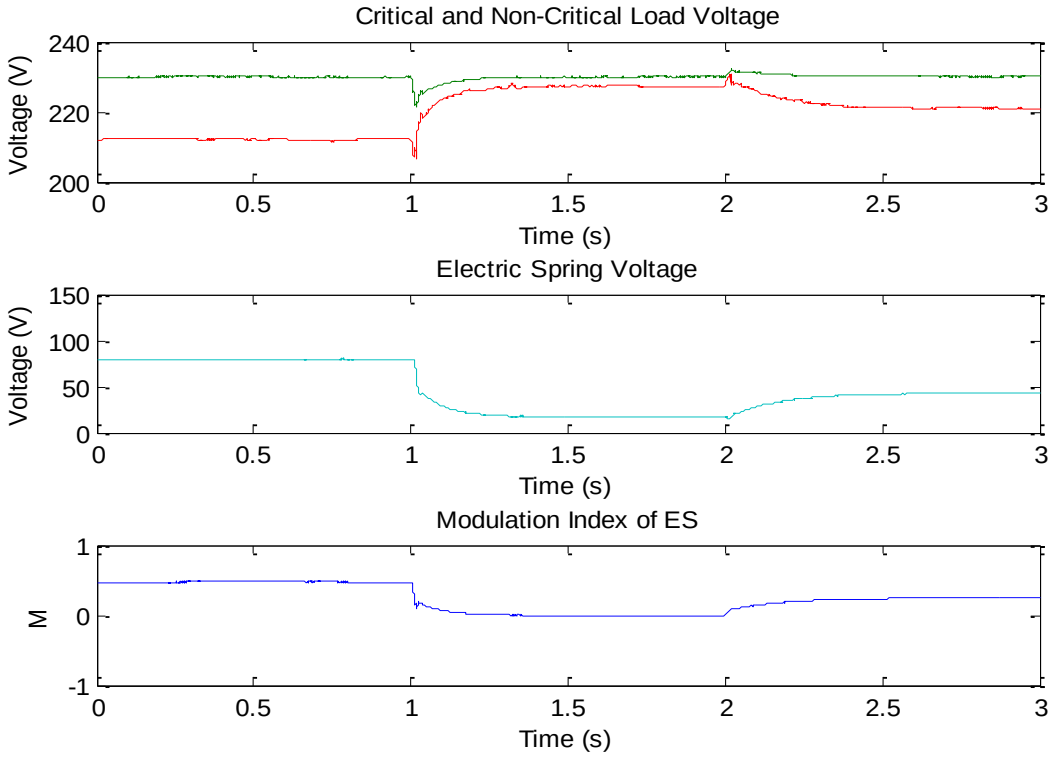

Figure 4-15 Critical, non-critical loads and ES voltages and modulation index response for three time periods

The first time period represents the normal case when the system isn't disturbed. It is noted in the second period that the ES voltage is decreased lower than the previous period. However, ES capacity is improved. It occurs when the non-critical load current (same as ES current) is increased because of the non-critical load resistance is decreased. In the last period, non-critical load current is reduced. Means that ES capacity is decreased and ES needs to inject higher voltage to generate sufficient amount of reactive power to do the same work of regulating the main voltage.

CHAPTER 5

ELECTRIC SPRING CONTROL DESIGN USING AVERAGING MODEL

5.1 Basic Principles of Averaged Model

In chapter 4, a switching model is adopted for its accuracy as it describes the dynamics of the converter. However, there are several disadvantages of this model as follows:

1- Difficulty to understand the relationship between the control signal indicated by $m(t)$ and the instantaneous resulting values of the voltage and current.
2- Switching model gives more details on variables which are not needed in dynamic analysis and control design purposes.

Therefore, average model is more suitable in analysis as compared to the switching model. Moreover, the dynamics of the converter are considered as a function of modulating signal.

ES converter with low pass filter is considered as shown in Figure 5-1. Applying KVL loop on ac side of the single phase inverter, the following equation can be written:

$$L_f \frac{d}{dt} I_{inj}(t) + R_f I_{inj}(t) = V_t(t) - V_{es} \tag{5.1}$$

Where V_t, V_{es}, I_{inj} are the output voltage with switching period T_s, electric spring voltage and injected current respectively.

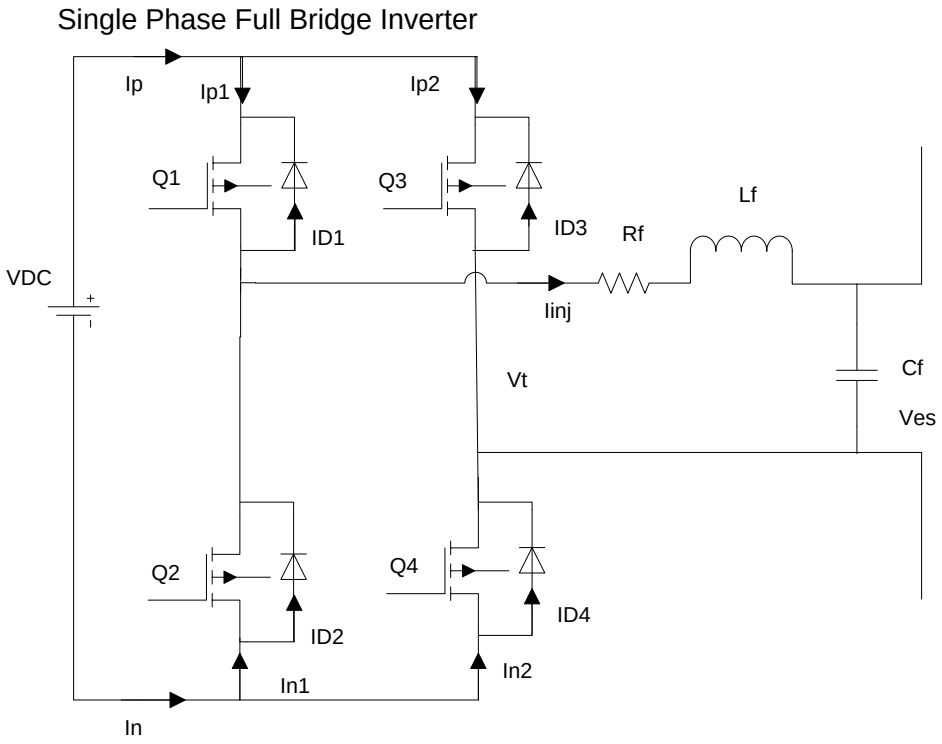

Figure 5-1 Single phase inverter connected with low pass filter

V_t can be represented using Fourier series analysis as:

$$V_t(t) = \frac{1}{T_s}\int_0^{T_s} V_t(\tau)\, d\tau + \sum_{h=1}^{h=+\infty} [a_h \cos(h\omega_s t) + b_h \sin(h\omega_s t)] \qquad (5.2)$$

Where h is the harmonic order from 0 to $+\infty$ and $\omega_s = \frac{2\pi}{T_\omega}$.

a_h and b_h factors are described by the following formulas:

$$a_{h=}\frac{2}{T_s}\int_0^{T_s} V_t(\tau)\cos(h\omega_s t)\, d\tau \qquad (5.3)$$

$$b_{h=}\frac{2}{T_s}\int_0^{T_s} V_t(\tau)\sin(h\omega_s t)\,d\tau \tag{5.4}$$

After substituting (5.2) into (5.1), it becomes as follows:

$$L\frac{d\boldsymbol{I_{inj}(t)}}{dt} + R\boldsymbol{I_{inj}(t)} = \left(\frac{1}{T_s}\int_0^{T_s} V_t(\tau)\,d\tau - V_s\right) = \sum_{h=1}^{h=+\infty}[a_h\cos(h\omega_s t) + b_h\sin(h\omega_s t)] \tag{5.5}$$

Eq. (5.5) can be separated to dc and periodic signal equations as shown in Eq. (5.6)-Eq.(5.8)

$$L\frac{d\bar{I}_{inj}}{dt} + R\bar{I}_{inj} = \left(\frac{1}{T_s}\int_0^{T_s} V_t(\tau)\,d\tau - V_{es}\right) \tag{5.6}$$

$$L\frac{d\tilde{I}_{inj}}{dt} + R\tilde{I}_{inj} = \sum_{h=1}^{h=+\infty}[a_h\cos(h\omega_s t) + b_h\sin(h\omega_s t)] \tag{5.7}$$

Where

$$I_{inj}(t) = \bar{I}_{inj}\,(t) + \tilde{I}_{inj}\,(t) \tag{5.8}$$

The average operator where the average value is changed from one switching cycle to another one can be expressed as:

$$\bar{x}(t) = \frac{1}{T_s}\int_{t-T_s}^{t} x(\tau)\,d\tau \tag{5.9}$$

As the modulating signal varies with time, the switched waveforms s_1, s_2, s_3, s_4will not maintain their constant periodic forms. Therefore, the switched waveforms can be added in the averaging process as follows:

$$\bar{s}_1(t) = \bar{s}_4(t) = d\text{ , when } V_t \neq 0 \tag{5.10}$$

$$\bar{s}_3(t) = \bar{s}_2(t) = 1 - d\text{, when } V_t \neq 0 \tag{5.11}$$

Where d is the duty ratio between 0 and 1.

Substituting Eq. (5.10) and Eq. (5.11) into Eq. (4.6), averaged terminal voltage is obtained

$$\overline{V_t} = V_{DC}(2d - 1) \tag{5.12}$$

The relationship between the modulating signal and the duty ratio can be realized using Figure 5-2 where

$$m = 2d - 1 \text{ or } d = (m + 1)/2 \tag{5.13}$$

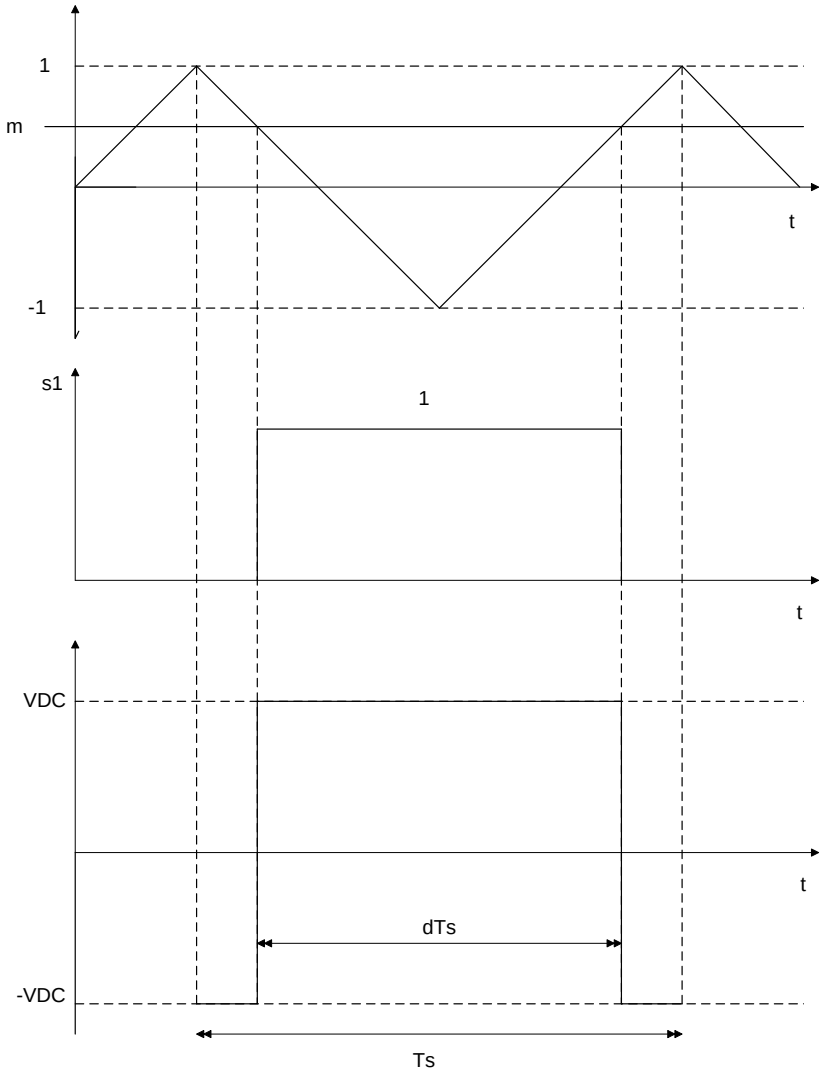

Figure 5-2 Relationship between modulation signal, switching waveform and terminal voltage and the duty cycle

It is concluded that when the modulating signal changes from -1 to 1, the duty ratio changes from 0 to 1. Hence, the terminal voltage V_t varies between -V_{DC} to V_{DC}.

5.2 Electric Spring Averaged Model

Averaged model of the test system shown in Figure 4-2 has been mathematically derived and validated. It consists of a grid voltage source, intermittent renewable energy current source, distribution feeders and connected critical and non-critical loads.

5.2.1 Power System Model

Test system equations have been derived in two different cases whether loads are classified as a resistive or inductive loads as shown in Figure 5-3. Power system has five states variables represented by V_{dc}, I_{inj}, V_{es}, I_{es} and I_d where:

V_{dc}: ES voltage at the dc terminal

I_{inj}: Injected current flows out the converter towards the power system

V_{es}: ES voltage at the terminal of the low pass filter capacitor

I_{es}: ES current which is same as non-critical load current

I_d: Distribution current provided by the network to the loads

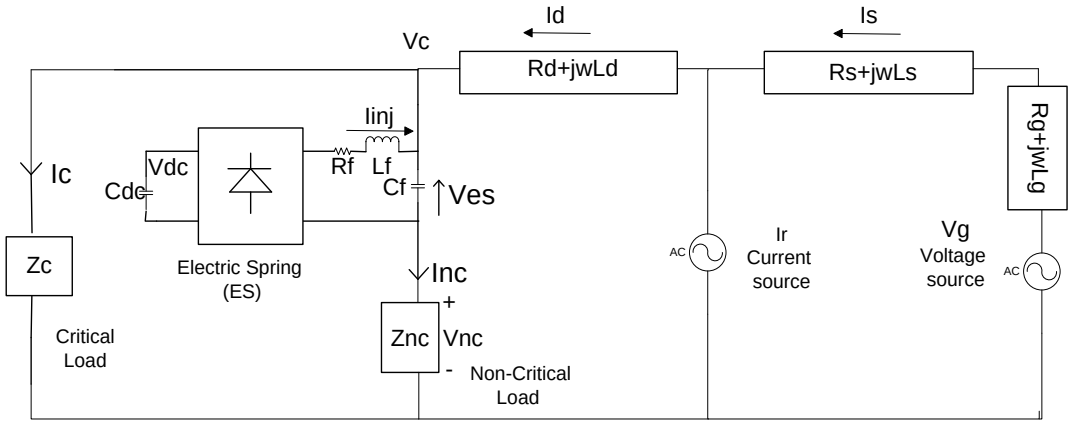

Figure 5-3 Test system including ES, loads, feeders and energy sources

Case 1: Critical and Non-Critical Resistive Loads

In this case, resistive loads are considered for both critical and non-critical loads. In other words, I_{es} state variable will be ignored. Applying KCL on the ac side of the power inverter yields

$$I_{inj} + I_{ES} = C_f \frac{dV_{es}}{dt} \tag{5.14}$$

Also, the smart load bus voltage is described as

$$V_c = I_{ES} * R_{nc} + V_{es} \tag{5.15}$$

Substituting Eq. (5.15) into Eq. (5.14) gives

$$\dot{V}_{es} = \left(\frac{1}{C_f}\right) I_{inj} + \left(\frac{1}{R_{nc} * C_f}\right) V_c - \left(\frac{1}{R_{nc} * C_f}\right) V_{es} \tag{5.16}$$

The relationship between V_c and I_d and V_{es} can be written as:

$$V_c = \frac{\left(I_d + \frac{V_{es}}{R_{nc}}\right)}{\left(\frac{1}{R_c} + \frac{1}{R_{nc}}\right)} \tag{5.17}$$

Substituting Eq. (5.17) into Eq. (5.16) gives

$$\dot{V}_{es} = \left(\frac{1}{C_f}\right) I_{inj} + \left(\frac{R_c}{C_f * (R_c + R_{nc})}\right) I_d - \left(\frac{1}{(R_c + R_{nc}) * C_f}\right) V_{es} \tag{5.18}$$

Applying KVL on the ac side of power converter yields

$$\dot{I}_{inj} = -\left(\frac{R_f}{L_f}\right) I_{inj} + \left(\frac{m}{L_f}\right) V_{dc} - \left(\frac{1}{L_f}\right) V_{es} \tag{5.19}$$

V_{dc} can be expressed as follows:

$$\dot{V}_{dc} = \left(\frac{R_f}{C_{dc}}\right) * \left(\frac{I^2{}_{inj}}{V_{dc}}\right) \tag{5.20}$$

Distribution current I_d is derived by applying KVL on the power system as:

$$\dot{I}_d = \left(\frac{1}{L_s + L_d + L_g}\right) \left(-\left(R_g + R_s + R_d\right) I_d + \left(R_g + R_s\right) I_r + \left(L_g + L_s\right) \dot{I}_r + V_g - V_c\right) \tag{5.21}$$

Substituting Eq. (5.17) into Eq. (5.21) gives

$$\dot{I}_d = \left(\frac{1}{L_s + L_d + L_g}\right) \left(-\left(\frac{R_c}{R_c + R_{nc}}\right) V_{es} - \left(\left(\frac{R_c R_{nc}}{R_c + R_{nc}}\right) + \left(R_g + R_s + R_d\right)\right) I_d + \left(R_g + R_s\right) I_r + \left(L_g + L_s\right) \dot{I}_r + V_g\right) \tag{5.22}$$

Grid voltage source V_g, intermittent renewable current source I_r and its derivation $\dot{I}_r$ are expressed in Eq. (5.23), Eq. (5.24) and Eq. (5.25) respectively.

$$V_g = N * sin(\omega t + \theta) \tag{5.23}$$

$$I_r = P * sin(\omega t + \varphi) \tag{5.24}$$

$$\dot{I}_r = P * \omega * sin(\omega t + \varphi) \tag{5.25}$$

Where N and P are the amplitude of the grid and current source while θ and φ represent the angle displacement of the aforementioned signals.

Case 2: Critical and Non-Critical Inductive Loads

As derived previously for resistive loads, the mathematical equations for inductive loads are represented with five state variables. Unlike case 1, there are 5 state variables in this case. This will increase the complexity of the model.

ES voltage can be derived as:

$$\dot{V}_{es} = \left(\frac{1}{C_f}\right) I_{inj} + \left(\frac{1}{C_f}\right) I_{es} \tag{5.26}$$

Applying KCL on the ac side yields

$$\dot{I}_{inj} = -\left(\frac{R_f}{L_f}\right) I_{inj} + \left(\frac{m}{L_f}\right) V_{dc} - \left(\frac{1}{L_f}\right) V_{es} \tag{5.27}$$

The voltage dynamics of the capacitor at dc side is represented as:

$$\dot{V}_{dc} = \left(\frac{R_f}{C_{dc}}\right) * \left(\frac{I^2{}_{inj}}{V_{dc}}\right) \tag{5.28}$$

Main bus voltage V_c is expressed as follows:

$$V_c = V_{es} + I_{es} R_{nc} + L_{nc} \dot{I}_{es} \tag{5.29}$$

Rearrange Eq. (5.29), $\dot{I}_{es}$ can be obtained as:

$$\dot{I}_{es} = -\left(\frac{R_{nc}}{L_{nc}}\right) I_{es} - \left(\frac{1}{L_{nc}}\right) V_{es} + \left(\frac{1}{L_{nc}}\right) V_c \tag{5.30}$$

I_d current is obtained by applying KVL for the power system as:

$$\dot{I}_d = \left(\frac{1}{L_s + L_d + L_g}\right) * \left(-\left(R_s + R_d + R_g\right) I_d + \left(R_g + R_s\right) I_R + \left(L_g + L_s\right) \dot{I}_R + V_g - V_c\right) \quad (5.31)$$

Main voltage can be written as:

$$V_c = (I_d - I_{es}) R_c + L_c \left(\dot{I}_d - \dot{I}_{es}\right) \quad (5.32)$$

Substituting Eq. (5.30) into Eq. (5.32) yields

$$V_c = \left(\frac{R_{nc} L_c - R_c L_{nc}}{L_c + L_{nc}}\right) I_{es} + \left(\frac{R_c L_{nc}}{L_c + L_{nc}}\right) I_d + \left(\frac{L_c L_{nc}}{L_c + L_{nc}}\right) \dot{I}_d + \left(\frac{L_c}{L_c + L_{nc}}\right) V_{es} \quad (5.33)$$

Substituting Eq. (5.33) into Eq. (5.31) gives

$$\begin{aligned} \dot{I}_d = \left(\frac{1}{L_c L_{nc} + (L_s + L_d + L_g)(L_c + L_{nc})}\right) \Big(& \left[-\left(R_s + R_d + R_g\right)(L_c + L_{nc}) + (L_{nc} R_c)\right] I_d \\ & + \left[\left(R_g + R_s\right)(L_c + L_{nc})\right] I_R + \left[\left(L_g + L_s\right)(L_c + L_{nc})\right] \dot{I}_R + [(L_c + L_{nc})] V_g \\ & - [(L_c R_{nc} - L_{nc} R_c)] I_{es} \\ & - L_c V_{es}\Big) \end{aligned} \quad (5.34)$$

Substituting Eq. (5.31) into Eq. (5.32) gives

$$\begin{aligned} V_c = \left(\frac{1}{L_s + L_d + L_g + L_c}\right) \Big(& \left[R_c\left(L_s + L_d + L_g\right) - L_c(R_s + R_d + R_g)\right] I_d \\ & - \left[R_c\left(L_s + L_d + L_g\right)\right] I_{es} - \left[L_c\left(L_s + L_d + L_g\right)\right] \dot{I}_{es} + \left[L_c\left(R_s + R_g\right)\right] I_R \\ & + \left[L_c\left(L_s + L_g\right)\right] \dot{I}_R + L_c V_g\Big) \end{aligned} \quad (5.35)$$

Substituting Eq. (5.35) into Eq. (5.30), electric spring current can be expressed as:

$$\dot{I}_{es} = \left(\frac{1}{L_{nc}(L_s + L_d + L_g + L_c) + L_c(L_s + L_d + L_g)}\right)\Big(\big[R_c(L_s + L_d + L_g) - L_c(R_s + R_d + R_g)\big]I_d + \big[-R_c(L_s + L_d + L_g) - R_{nc}(L_s + L_d + L_g + L_c)\big]I_{es} + \big[L_c(R_s + R_g)\big]I_R + \big[L_c(L_s + L_g)\big]\dot{I}_R + L_c V_g + \big[-(L_s + L_d + L_g + L_c)\big]V_{es}\Big) \quad (5.36)$$

5.2.2 Power System Controller

To facilitate the derivations, the proposed controllers are derived in two parts: single phase locked loop PLL and PIs controller as follows:

- Single Phase Phase Locked Loop (PLL)

Single phase phase looked loop (PLL) is represented as shown in Figure 5-4. It consists of filter blocks on the left side and alpha-beta to d-q conversion in addition to PI controller in the right side.

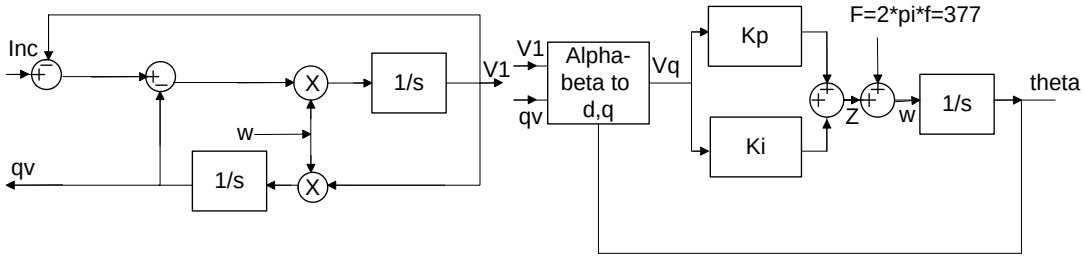

Figure 5-4 Phase locked loop schematic diagram

Mathematical derivations for filter blocks are written sequentially in Eq. (5.37) and Eq. (5.38)

$$\dot{q}_v = w * V1 \quad (5.37)$$

$$\dot{V}_1 = w * (I_{nc} - V_1 - q_v) \quad (6.38)$$

Alpha-beta to d-q conversion equations are given in Eq. (5.39)- Eq. (5.41)

$$V_q = q_v * \sin(\theta) + V_1 * \cos(\theta) \tag{5.39}$$

$$\dot{V}_q = q_v * \cos(\theta) * \dot{\theta} + \dot{q}_v * \sin(\theta) + V_1 * -\sin(\theta) * \dot{\theta} + \cos(\theta) * \dot{V}_1 \tag{5.40}$$

$$\dot{V}_q = q_v * \cos(\theta) * w + w * V1 * \sin(\theta) + V_1 * -\sin(\theta) * w + \cos(\theta) * w * (I_{nc} - V_1 - q_v) \tag{5.41}$$

$$\dot{V}_q = w * \cos(\theta) * (I_{nc} - V_1) \tag{5.42}$$

The PI controller side derivations are expressed in (5.43)-(5.46)

$$Z = K_p * V_q + K_I \int V_q dt \tag{5.43}$$

$$\dot{Z} = \dot{w} = K_p * \dot{V}_q + K_I * V_q \tag{5.44}$$

$$\dot{w} = K_p * \dot{V}_q + K_I * V_q \tag{4.45}$$

$$\dot{\theta} = w \tag{5.46}$$

- PI controllers

The following Figure 5-5 is an ES with dc and ac controllers. Each one of these controllers has been derived as below:

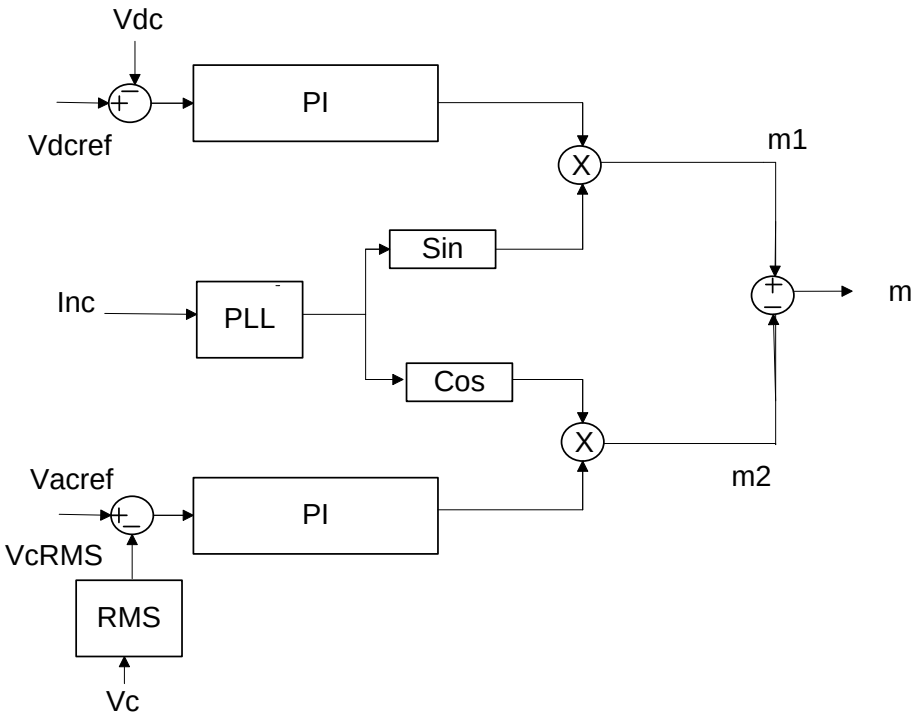

Figure 5-5 Full schematic diagram of ES controller

- DC PI Controller:

According to Figure 5-5, $m_1$signal is multiplication of an output of dc controller and the sine values of the tracked angle of non-critical load current.

$$m_1 = \left(V_{dcref} - V_{dc}\right) * \left(K_{pdc} + \frac{K_{idc}}{s}\right) * si\,n(\theta) \tag{5.47}$$

Then,

$$\dot{m_1} = \left(\left(V_{dcref} - V_{dc}\right)^{\cdot} * K_{pdc} + \left(V_{dcref} - V_{dc}\right) * K_{idc}\right) * sin(\theta) \tag{5.48}$$

$$\dot{m_1} = \left(-\dot{V}_{dc} * K_{pdc} + V_{dcref} * K_{idc} - V_{dc} * K_{idc}\right) * sin(\theta) \tag{5.49}$$

Substituting (5.20) into (5.48) yields

$$\dot{m_1} = -\left(\frac{R_f}{C_{dc}}\right) * \left(\frac{{I^2}_{inj}}{V_{dc}}\right) * K_{pdc} * sin(\theta) + V_{dcref} * K_{idc} * \sin(\theta) - V_{dc} * K_{idc} * \sin(\theta) \tag{5.50}$$

- Ac PI Controller:

m_2 is considered as an output control signal of ac controller block multiplied with the output cosine signal of non-critical load current

$$m_2 = \left(V_{cref} - V_{cRMS}\right) * \left(K_{pac} + \frac{K_{iac}}{s}\right) * co\,s(\theta) \tag{5.51}$$

Then,

$$\dot{m_2} = \left(\left(V_{cref} - V_{cRMS}\right)^{\cdot} * K_{pac} + \left(V_{cref} - V_{cRMS}\right) * K_{iac}\right) * cos(\theta) \tag{5.52}$$

$$\dot{m_2} = \left(-\dot{V}_{cRMS} * K_{pac} + V_{cref} * K_{iac} - V_{cRMS} * K_{iac}\right) * \cos(\theta) \tag{5.53}$$

V_c and V_{cRMS} are the magnitude and RMS values of the main bus voltage. These values can be expressed mathematically as follows:

$$V_{cRMS} = \sqrt{\left(\frac{1}{T}\right)\int {V_c}^2 dt} \tag{5.54}$$

$$\dot{V}_{cRMS} = \left(\frac{1}{T}\right) * \left(\frac{{V_c}^3}{V_{cRMS}}\right) * \dot{V}_c \tag{5.55}$$

$$V_c = \frac{\left(I_d + \frac{V_{es}}{R_{nc}}\right)}{\left(\frac{1}{R_c} + \frac{1}{R_{nc}}\right)} \tag{5.56}$$

$$\dot{V}_c = \frac{\left(\dot{I}_d + \frac{\dot{V}_{es}}{R_{nc}}\right)}{\left(\frac{1}{R_c} + \frac{1}{R_{nc}}\right)} \tag{5.57}$$

The final control signal m is expressed as:

$$\dot{m} = \dot{m}_1 - \dot{m}_2 \tag{5.58}$$

The non-linearity of the power system comes from Eq. (5.20). To simplify the method, V_{dc} dynamics will be neglected. The dc side of electrical spring is considered constant such that no significant change in the dc voltage.

5.2.3 Power System Linearization

To optimize the controller parameters, the linearized model of the system consisting of a power plant in addition to the plant controller is developed. This approach aims at constructing a closed loop matrix and optimizing the proposed controller parameters by investigating the Eigen values for each candidate solution. The linearized model is given in appendix.

5.3 Particle Swarm Optimization Technique (PSO)

Particle swarm optimization technique has been developed and enhanced by Eberhart and Kennedy in 1995. First of all, PSO was used to represent social behavior of the swarms like bird flock or fish school. It is a computational method used by many researchers to optimize their problems by finding the best solutions or candidates. PSO is considered as a stochastic based optimization problem. It is a robust technique and can find the best solution regardless initial populations. The initial generation is represented by n-particles. Each one of these particles has a certain number of optimized parameters which represent a dimension of that problem [72]. PSO optimization steps are roughly described in the following points:

1- In the first step, initial positions (particles) and velocities are generated randomly within constraints. The constraints of the controller parameters are selected based on the experience with the system. Lower and upper boundaries of these velocities are selected accordingly.

2- Candidate solutions are evaluated based on objective function (non-linear cost function). Then, individual and global best solutions are updated and stored.

3- To control the swarm velocity, two different approaches can be applied during optimization process either inertia weight method or constriction factor method as shown in the following expressions:

- Inertia weight method is:

$$w(t) = \alpha * w(t-1), \tag{5.59}$$

where

$\alpha = 0.9, w(0) = 1.0$

Also, the velocity expression is:

$$v_{j,k}(t) = w(t)v_{j,k}(t-1) + c_1 r_1 \left(x^{*}_{j,k}(t-1) - x_{j,k}(t-1)\right) + c_2 r_2 \left(x^{**}_{j,k}(t-1) - x_{j,k}(t-1)\right) \tag{5.60}$$

Where

$v_{j,k}(t-1)$ and $v_{j,k}(t)$: Previous and updated iteration velocity where j and k represent the number of row and column numbers respectively.

c_1 & c_2 : Acceleration constants

$x^{*}_{j,k}(t-1)$ and $x^{**}_{j,k}(t-1)$: individual best position and global best position respectively.

- Constriction factor method is:

$$v_{j,k}(t) = c_{factor}\left[v_{j,k}(t-1) + c_1 r_1 \left(x^{*}_{j,k}(t-1) - x_{j,k}(t-1)\right) + c_2 r_2 \left(x^{**}_{j,k}(t-1) - x_{j,k}(t-1)\right)\right] \tag{5.61}$$

Where

c_f : constriction factor

4- Updating the positions for the next iteration as :

$$x_{j,k}(t) = v_{j,k}(t-1) + x_{j,k}(t-1) \quad (5.62)$$

Where

$x_{j,k}(t), x_{j,k}(t-1)$: Previous and updated positions

$v_{j,k}(t-1)$: Previous iteration velocity

5- Each updated velocities and positions values have to be investigated whether these values are feasible or not. If not, each value outside the range should be forced to its nearest limit.

6- Updating the values of individual positions and global position for each calculated iteration.

7- The stopping criteria limit is examined. If the search reaches the maximum number of iterations, the optimization process is stopped and the best solution is reported.

These steps are also provided and clarified as a flowchart in Figure 5-6

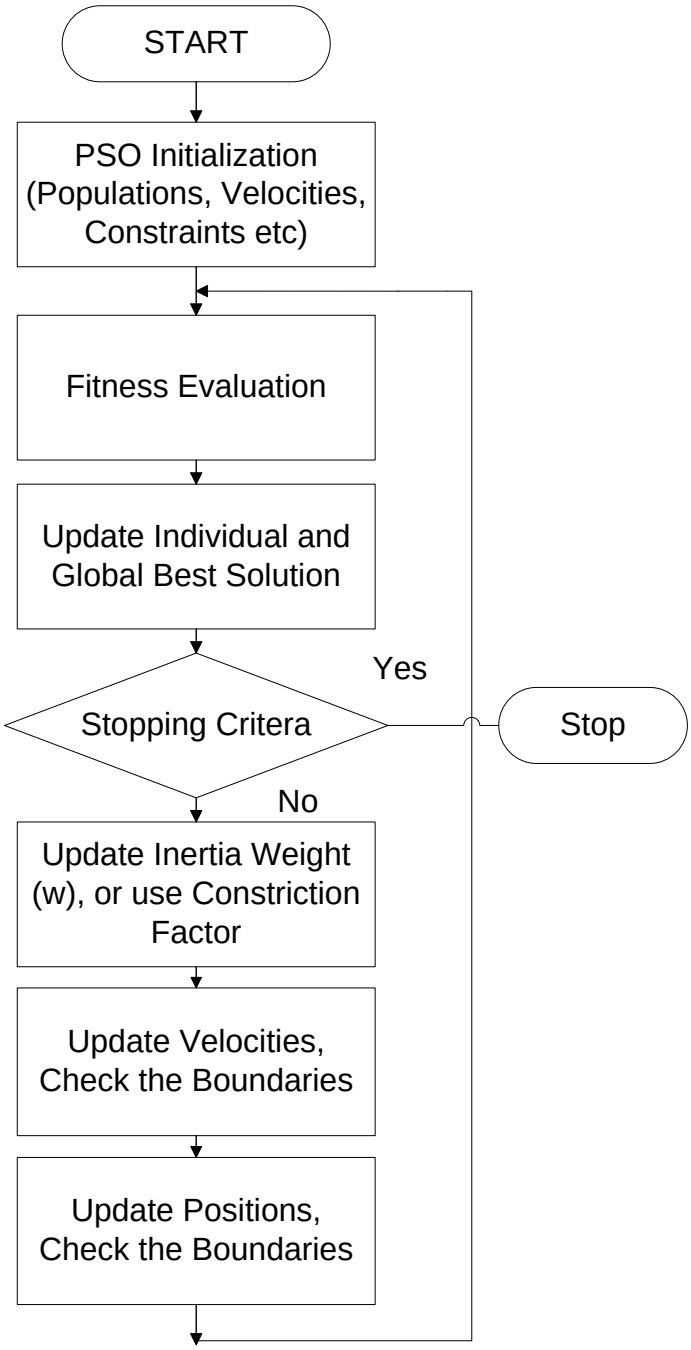

Figure 5-6 Flowchart of PSO technique

5.4 Simulation Results

Power system non-linear model described in the previous chapter is considered to examine the performance of ES. The system includes ac side controller in addition to PLL. Two cases have been considered in this study. In the first one, the critical and non-critical loads are resistive loads while in the second case, the loads are inductive. All details and results are shown and discussed in the following sections where the power system performance is tested for different kinds of disturbances.

5.4.1 Case 1: Critical and Non-Critical Resistive Loads

In this case study, one ac PI controller parameters has been optimized using two different PSO velocities, inertia factor and constriction factor method. It is concluded that the constriction factor is better than inertia factor regarding convergence time and quality of the solutions. The bridge and PI controller are shown in Figure 5-7.

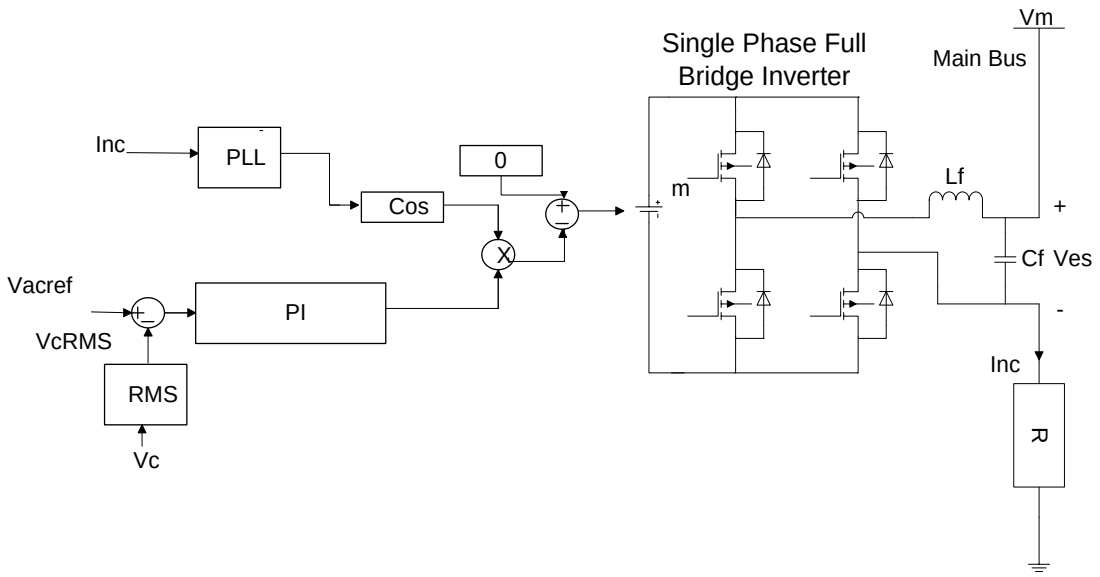

Figure 5-7 Control blocks for the electric spring (single phase full bridge inverter)

Objective function utilized in this optimization is non-linear cost function to minimize the error resulting from the difference between the actual main voltage (V_m) and the reference value. The objective function can be expressed as:

$$\mathbf{J} = \left(\int \boldsymbol{t} \, |\Delta \boldsymbol{V_{ac}}| \, \boldsymbol{dt} \right) \tag{5.63}$$

Subject to

$$\begin{cases} \boldsymbol{K_p}^{\boldsymbol{min}} \leq \boldsymbol{K_p} \leq \boldsymbol{K_p}^{\boldsymbol{max}} \\ \boldsymbol{K_i}^{\boldsymbol{min}} \leq \boldsymbol{K_i} \leq \boldsymbol{K_i}^{\boldsymbol{max}} \end{cases} \tag{5.64}$$

Where $\boldsymbol{t}$ is the simulation time, $\boldsymbol{\alpha}$ is a weighting factor, $\Delta \boldsymbol{V_{ac}}$ is the ac main voltage deviation and $\mathbf{K_p}$ and $\mathbf{K_i}$ are the parameters of ac PI voltage controllers.

As seen in Figure 5-8, PSO algorithm has been performed for 100 iterations and the objective functions are calculated and compared.

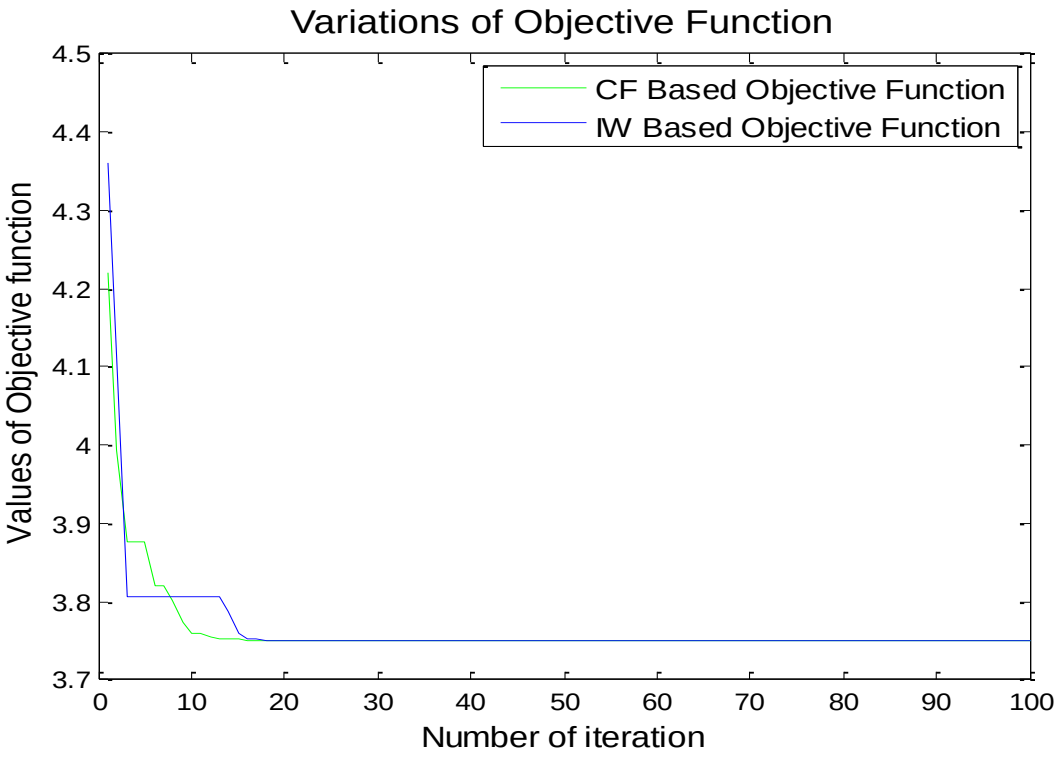

Figure 5-8 Objective function variation using non-linear cost objective function

Different kinds of simulations were carried out such as multi-disturbances, resistive load variation, inserting inductive load to critical resistive load.

- Multi-disturbances

Simulation of multiple disturbances is carried out for 3s to investigate the performance of the electric spring. The simulation is divided into three time periods. Each time period is one second. Renewable energy current source injects $\mathbf{0}\ \boldsymbol{A}, \mathbf{10}\ \boldsymbol{A}$ and $\mathbf{2}\ \boldsymbol{A}$ for each time period respectively. To keep the main voltage ($\boldsymbol{V_m}$) constant, ES is activated and starts injecting a compensation voltage at its terminal as depicted in Figure 5-9

The output power of renewable energy source ($\boldsymbol{P_r}$), real power consumption by critical and non-critical loads ($\boldsymbol{P_c}, \boldsymbol{P_{nc}}$) respectively and the generated power by the grid connected ($\boldsymbol{P_g}$) are depicted in Figure 5-10.

ES modulation index ($\boldsymbol{m}$), the angle difference between electric spring voltage and the non-critical load current ($\boldsymbol{\theta}$), and the reactive power generated by the electric spring ($\boldsymbol{Q_{es}}$) are shown in Figure 5-11. It is noted that the angle difference ($\boldsymbol{\theta}$) is very close to $\pm\ \mathbf{90^o}$ because there is no need for real power to regulate the dc side of ES. Figure 5-12 shows that the dc side of ES is constant and the real power consumption by ES is close to zero.

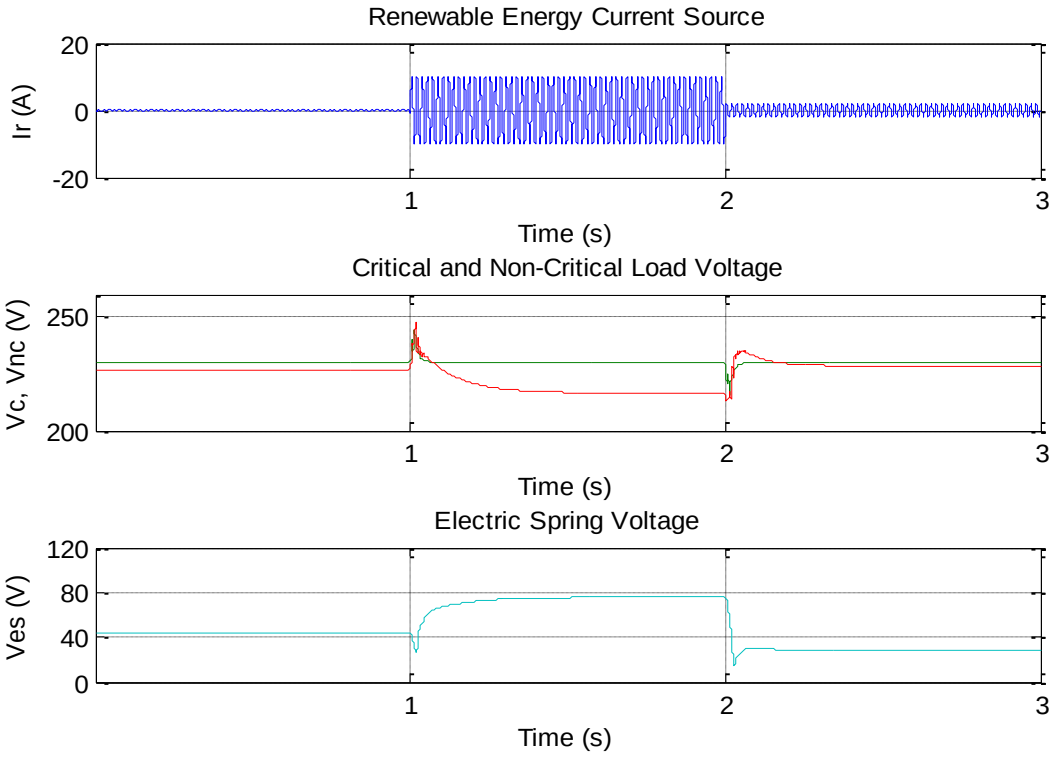

Figure 5-9 Voltage analysis of ES averaged model in different modes

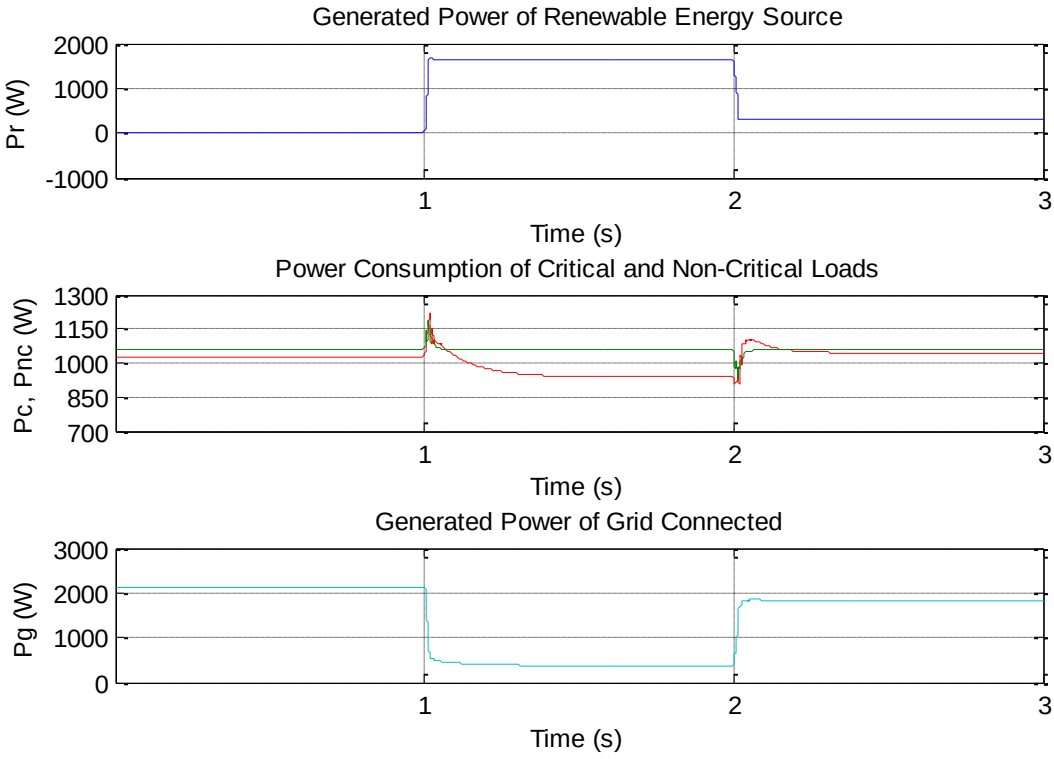

Figure 5-10 Power analysis of ES averaged model in different modes

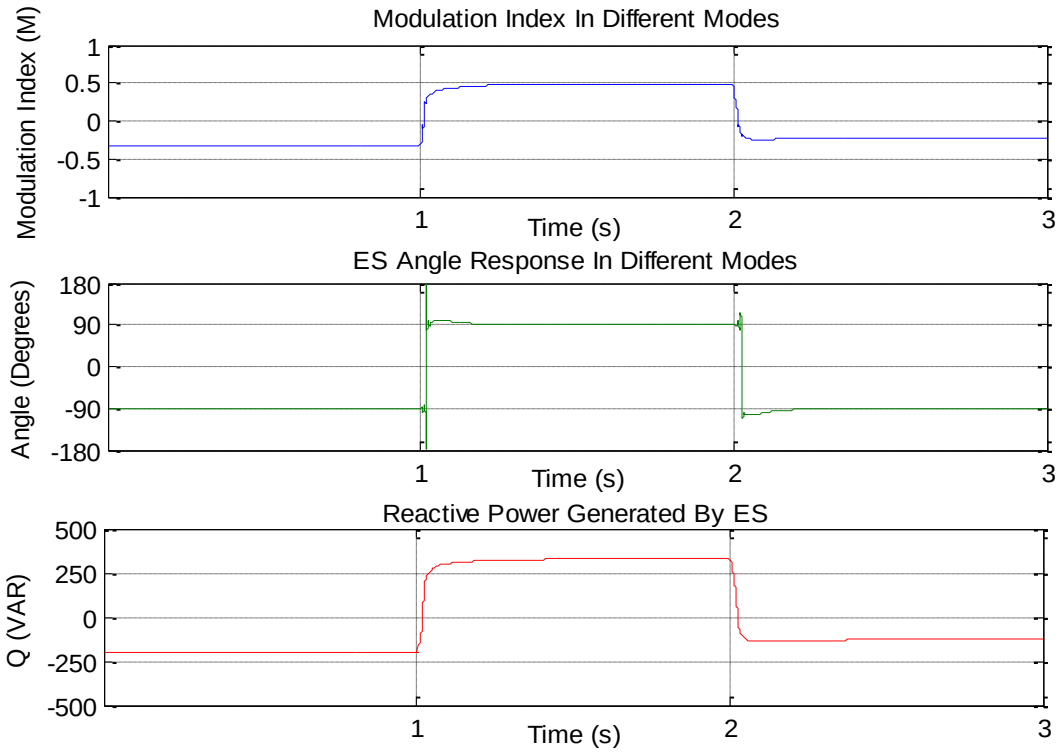

Figure 5-11 Modulation index, Angle and reactive power of ES averaged model in different modes

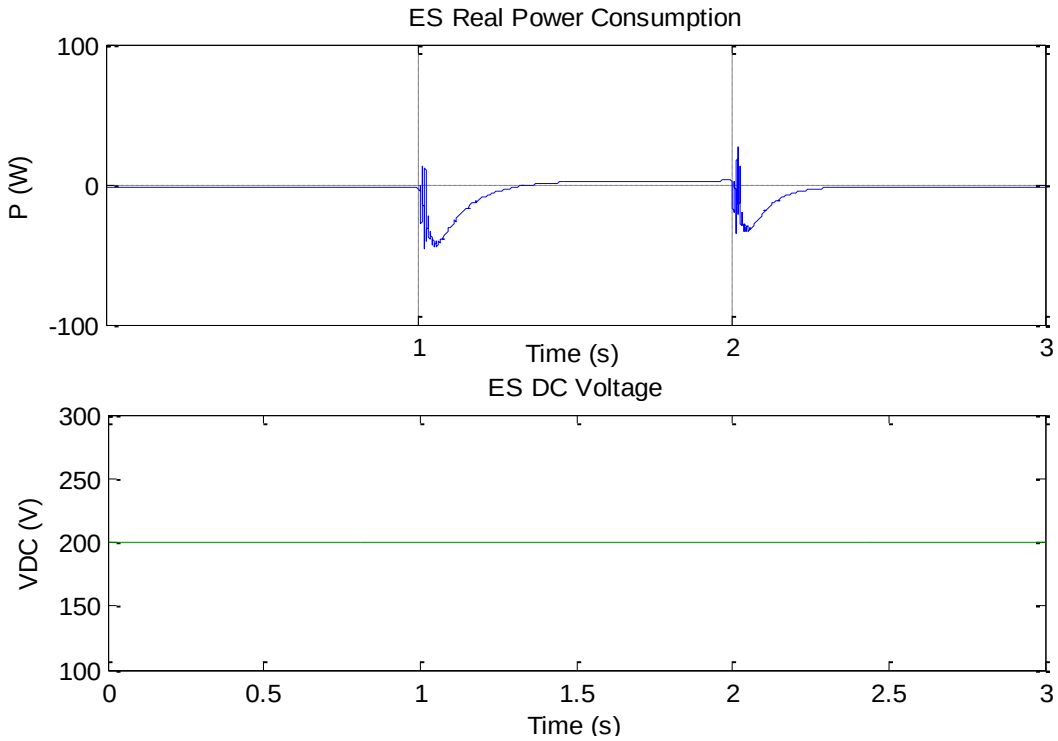

Figure 5-12 ES real power consumption and dc voltage responses in different modes

- Resistive loads variations

The simulation is carried out when the renewable energy source injects 10 A to the distribution system. Simulation is divided in three time periods. Each time period is one second. In the first time period, critical and non-critical loads are 50 Ω each. In the second period, the non-critical load resistance becomes lower than the previous period by inserting 30 Ω in parallel with its terminal. At the same time, 70 Ω is connected in series with the critical loads. In the third period, 70 Ω is connected in series with the non-critical load and 30 Ω is connected in parallel with the critical load. Critical, non-critical load, and ES voltages response are shown in Figure 5-13.

It is noted that the ES is capable to handle all of these three resistive variations by generating sufficient amount of reactive power to regulate the main voltage. Also, ES voltage is affected significantly when the value of non-critical load varies. However, when the resistance of non-critical loads is becomes lower, non-critical load current becomes higher. So, ES injects lower value of voltage at its terminal to generate the required amount of reactive power as shown in the second period. In the third period, ES injects higher voltage at its terminal as compared to the previous period because the non-critical load current is decreased.

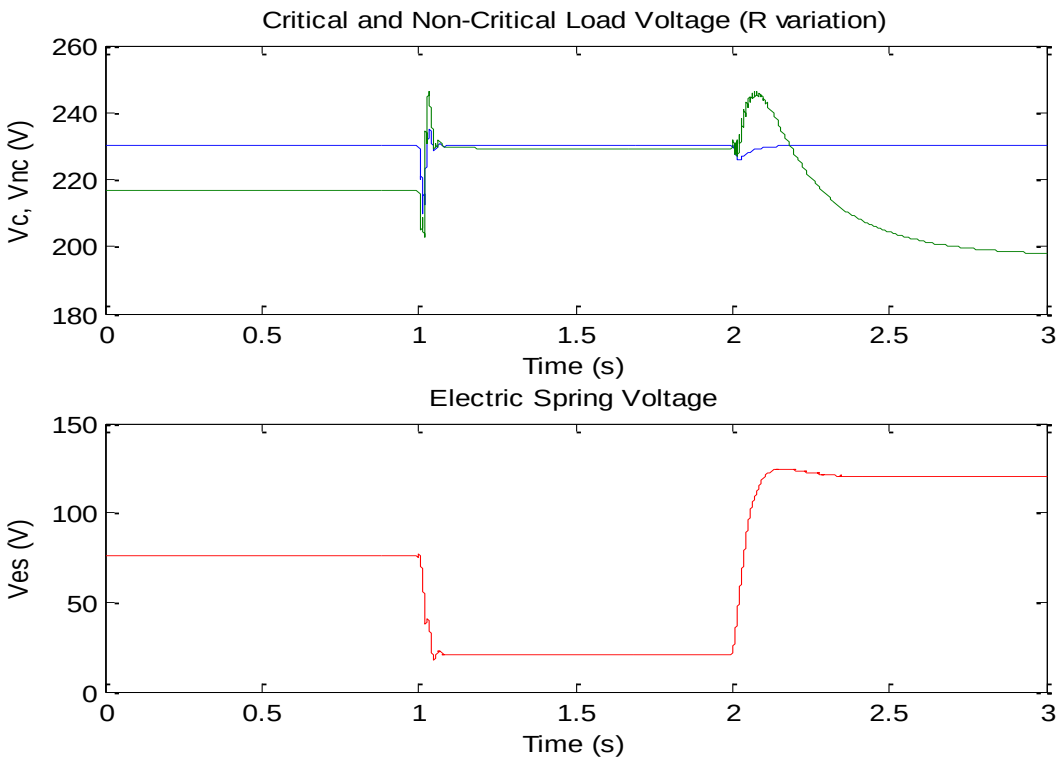

Figure 5-13 Critical, non-critical load and ES voltages

It is clear that the ES mode is changed in these three time periods. Reactive power is also changed accordingly. Modulation index (m) and reactive power compensation response (Q_{es}) are shown in Figure 5-14.

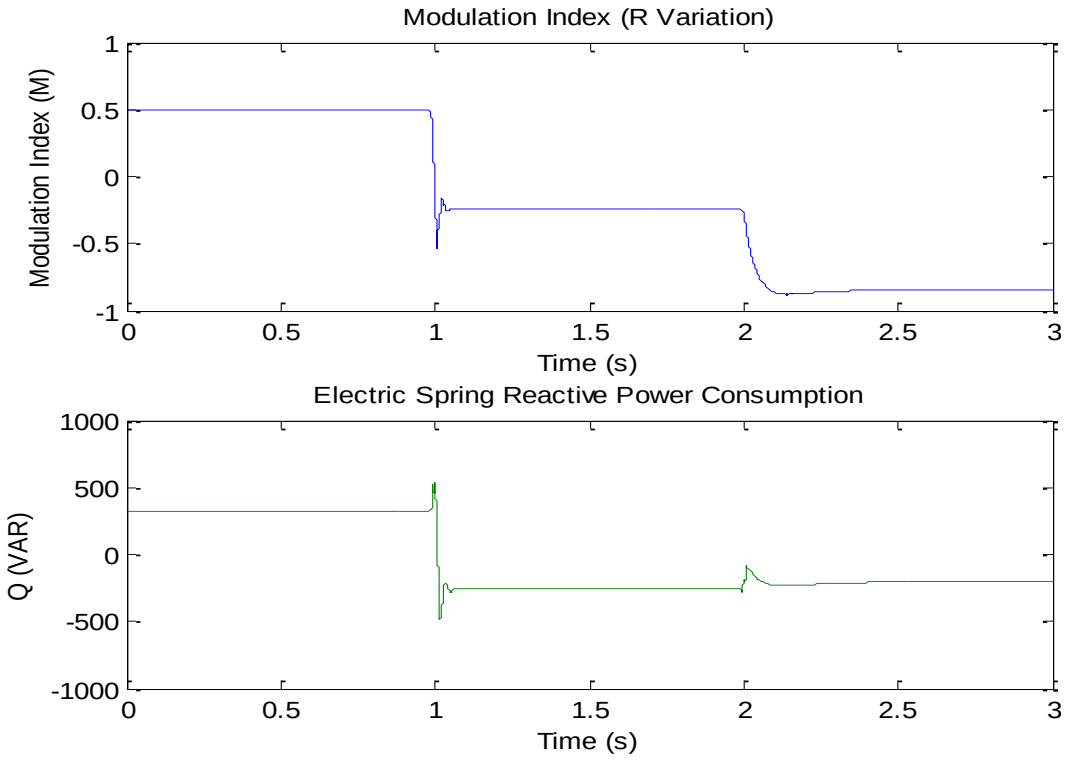

Figure 5-14 ES modulation index and reactive power compensation

- Switching of Inductive Load:

Inductive loads with 0.95 power factor causes a disturbance for power system when it is suddenly switched on and off. These disturbances are done with two different cases when the intermittent renewable current source is 7 A and 10A as follows:

- Renewable current source is 7 A

In this case, current source is kept to be 7 A during the simulation while critical load is disturbed by switching on and off an inductive load. Different power signals are investigated such as critical, non-critical load and ES voltages as seen in Figure 5-15. In addition, the modulation index signal and reactive power compensation are shown in Figure 5-16. Figure 5-17and Figure 5-18 show the power system response when the

inductive load is switched off. It is noted that ES is capable to regulate the bus in this case.

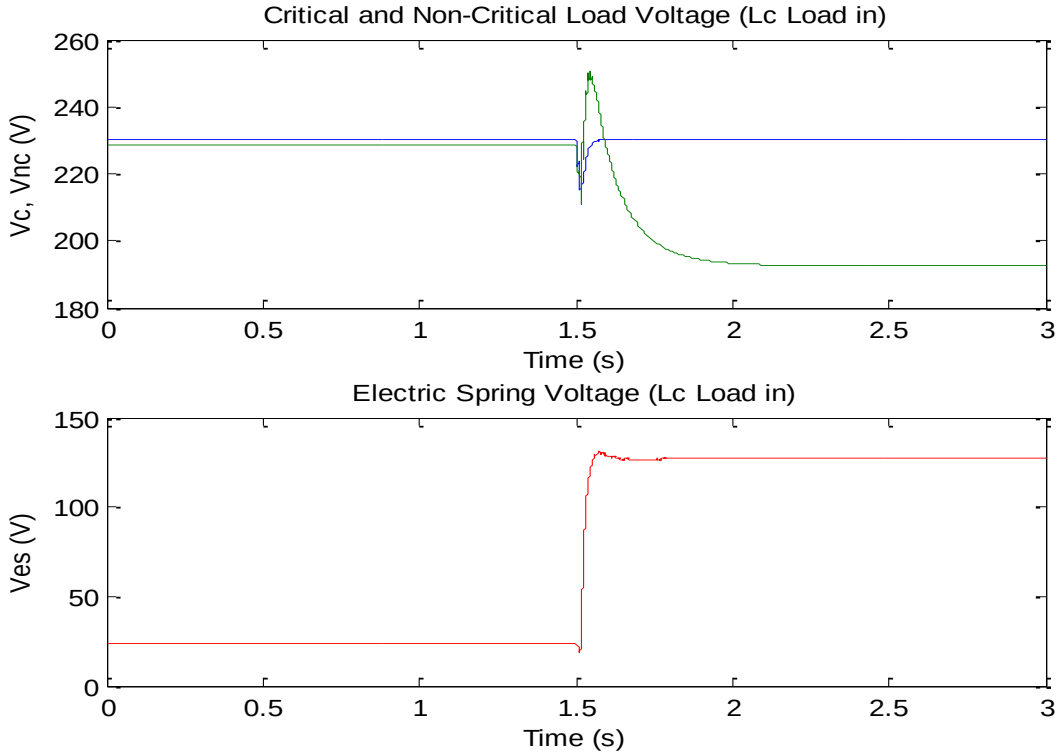

Figure 5-15 Critical, non-critical load and ES voltages response when inductive load is switched on and renewable source current is 7A

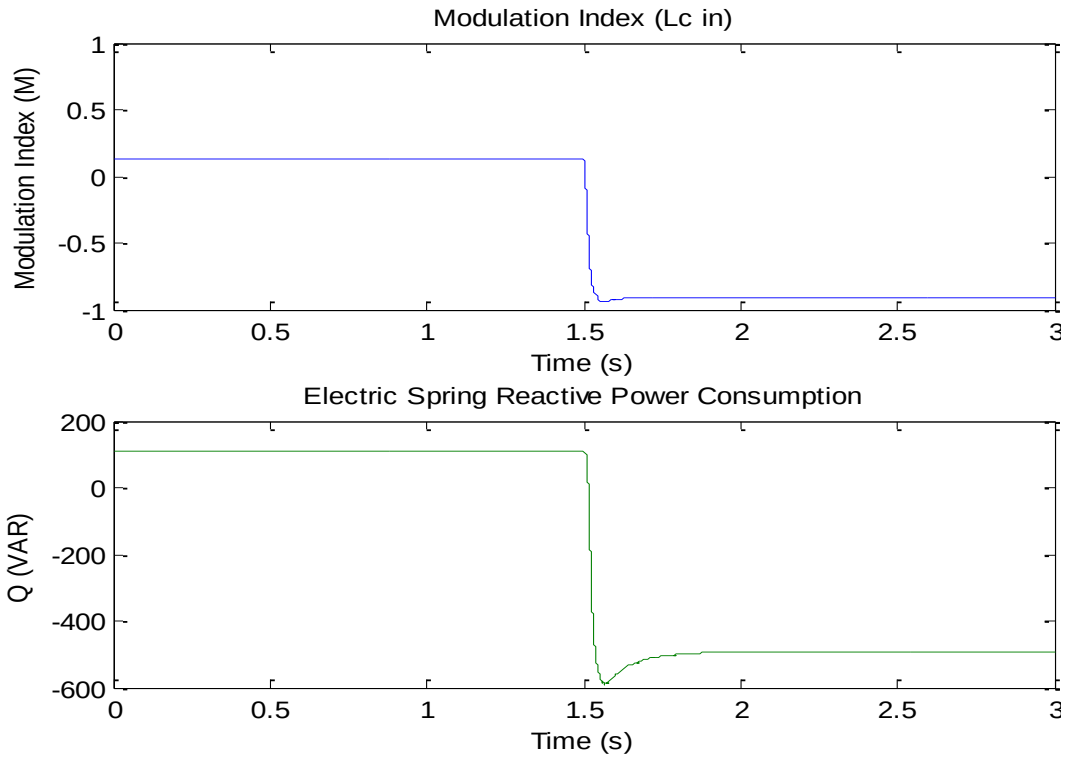

Figure 5-16 ES modulation index and reactive power compensation response when inductive load is switched on and renewable source current is 7A

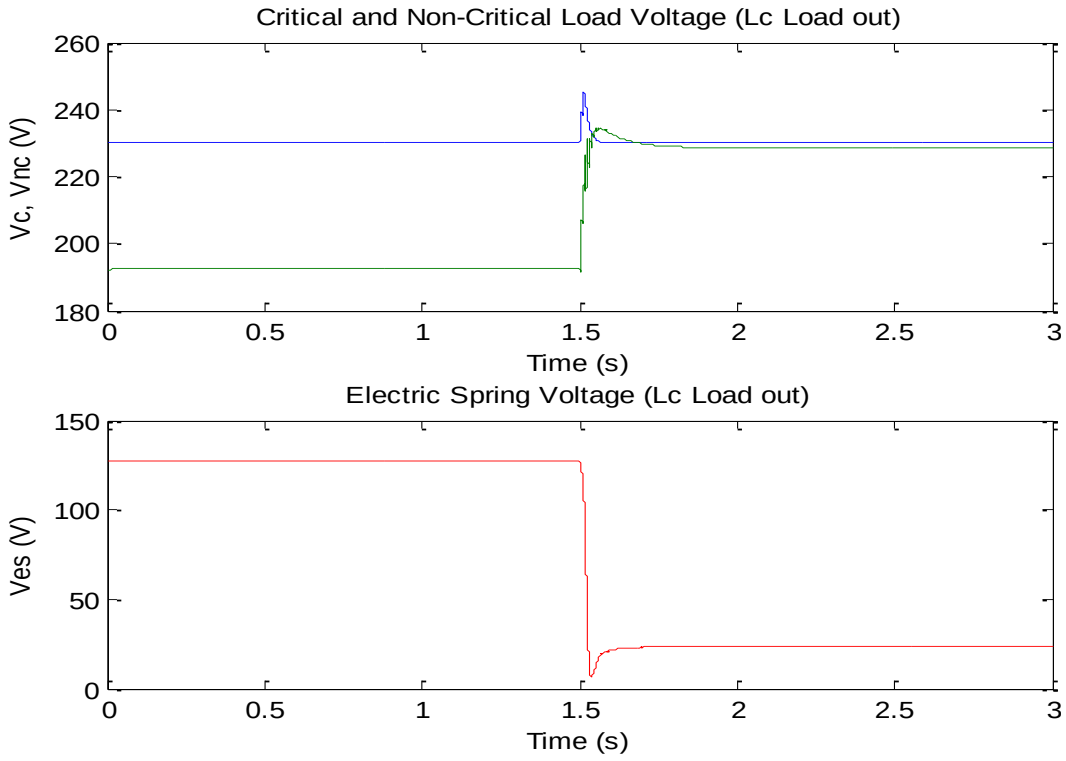

Figure 5-17 Critical, non-critical load and ES voltages response when inductive load is switched off and renewable source current is 7A

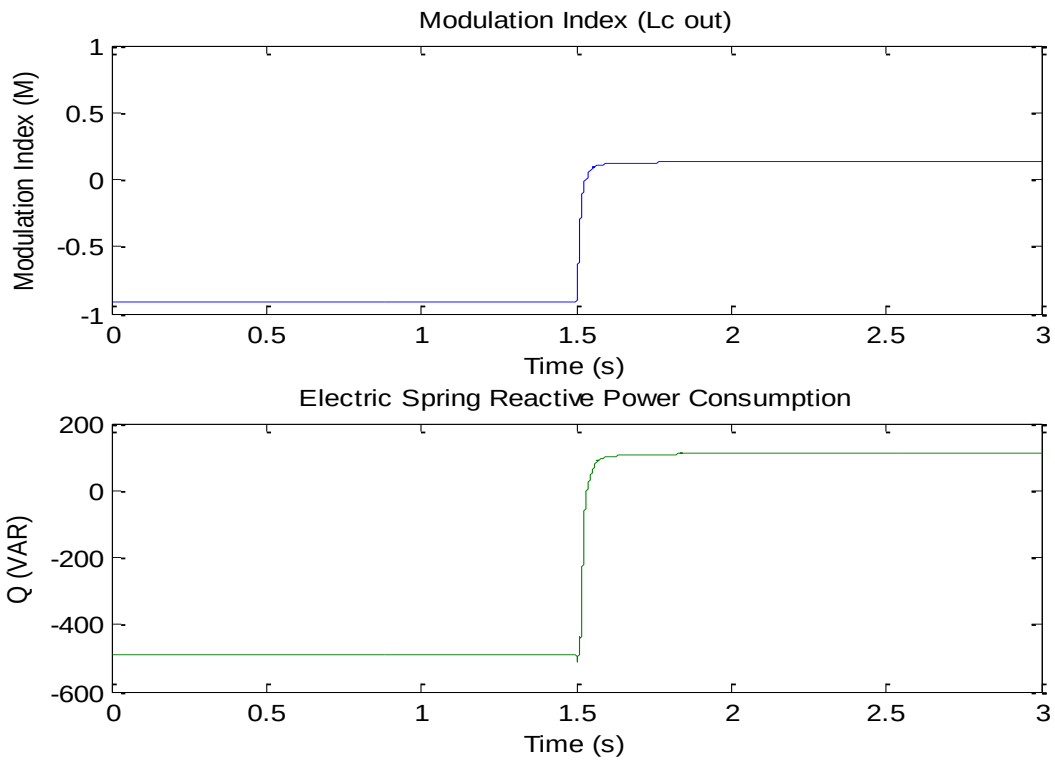

Figure 5-18 ES modulation index and reactive power compensation response when inductive load is switched off and renewable source current is 7A

- Renewable current source is 10 A

In this case, current source is 10 A during the simulation while critical load is disturbed by switching on and off an inductive load. Critical, non-critical load and ES voltages are shown in Figure 5-19. The modulation index signal and reactive power compensation are shown in Figure 5-20. Figure 5-21 and Figure 5-22show the power system response when the inductive load is switched off.

As a conclusion, ES generates lower voltage as compared to 7 A case. That is because 10 A generated current supports the main voltage of the distribution bus better than 7 A. Also, the main bus is well regulated in this kind of disturbance.

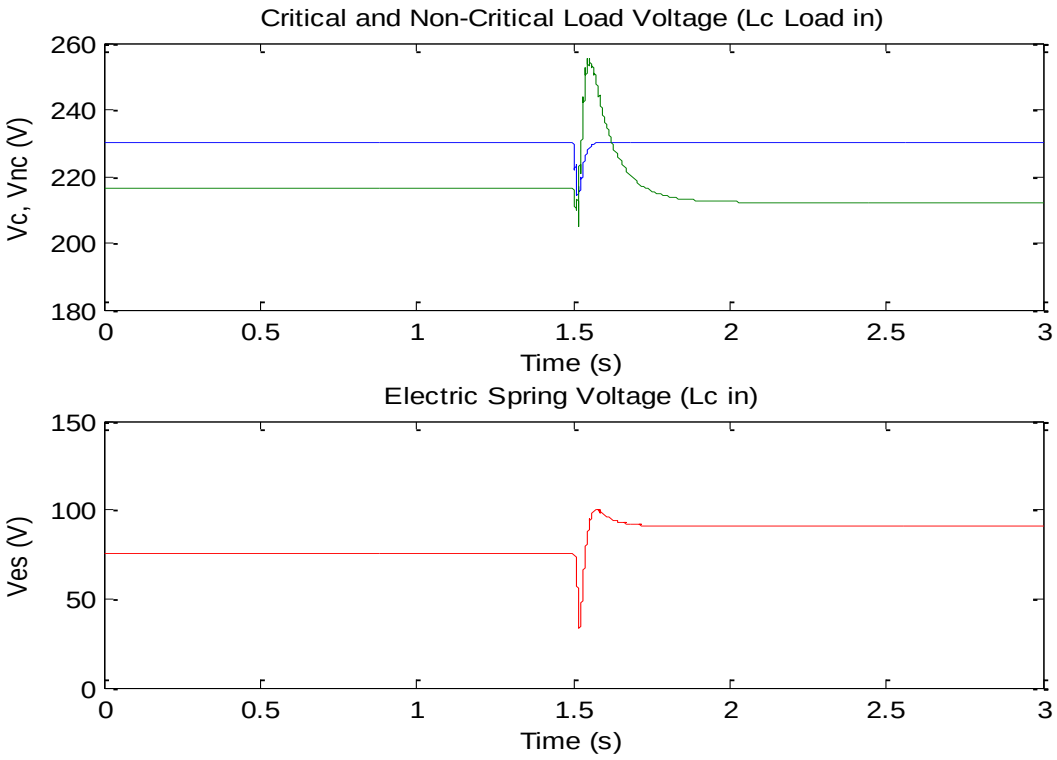

Figure 5-19 Critical, non-critical load and ES voltages response when inductive load is switched on and renewable source current is 10A

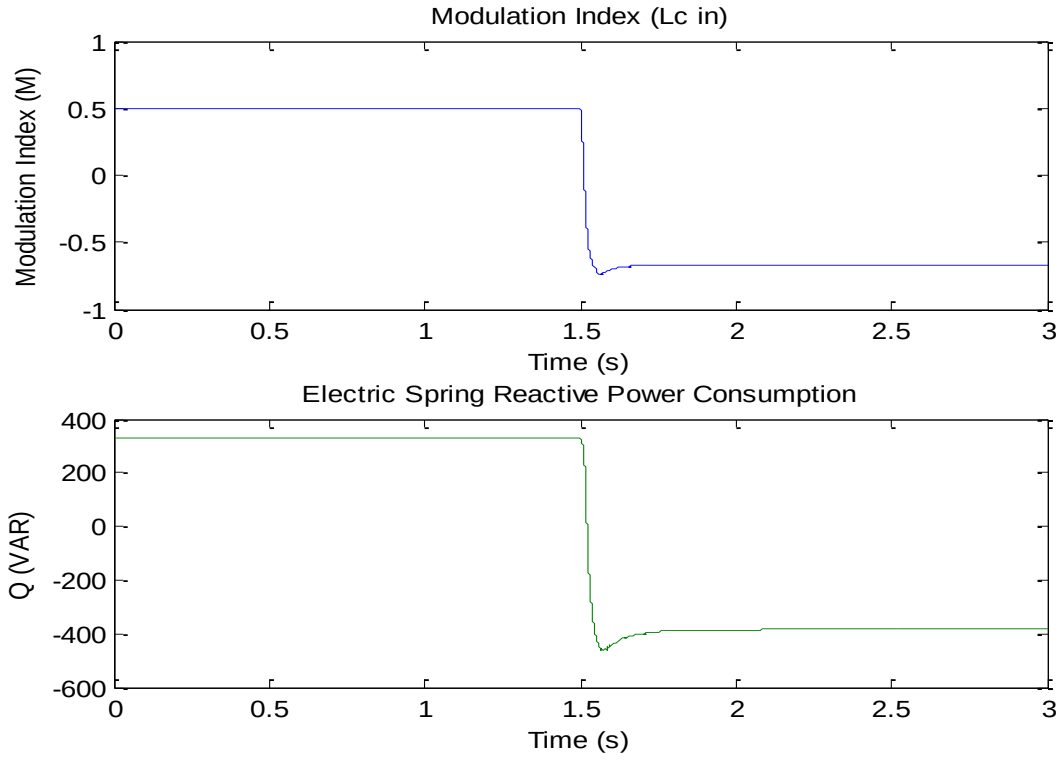

Figure 5-20 ES modulation index and reactive power compensation response when inductive load is switched on and renewable source current is 10A

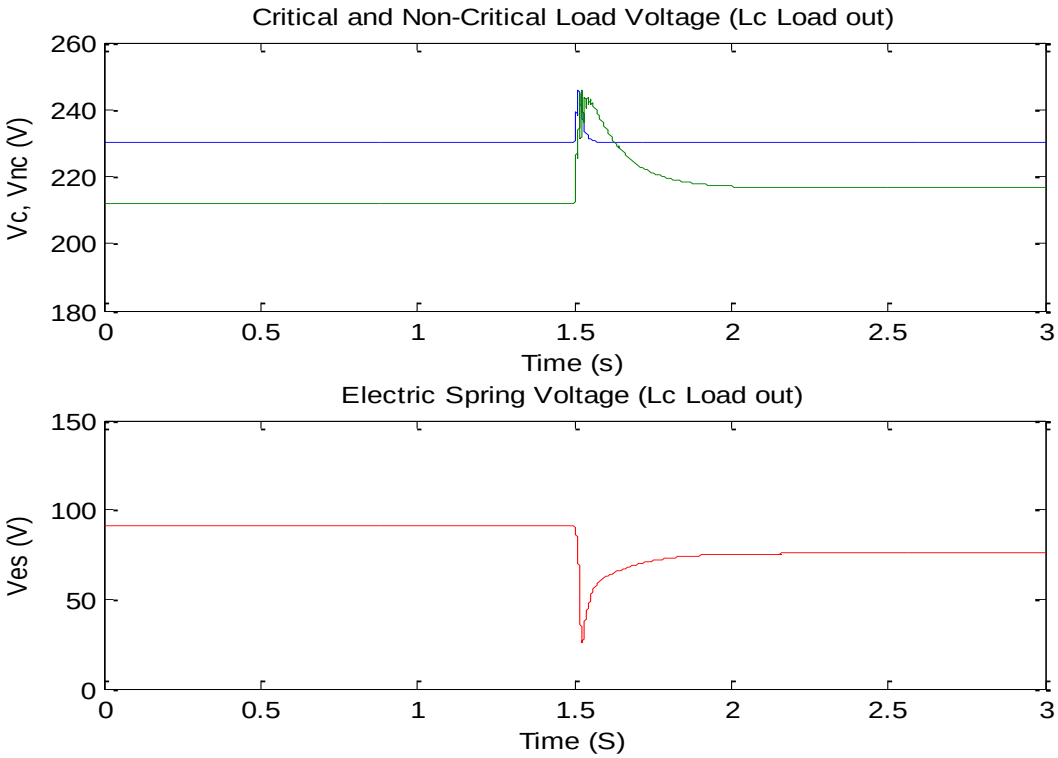

Figure 5-21 Critical, non-critical load and ES voltages when response when inductive load is switched off and renewable source current is 10A

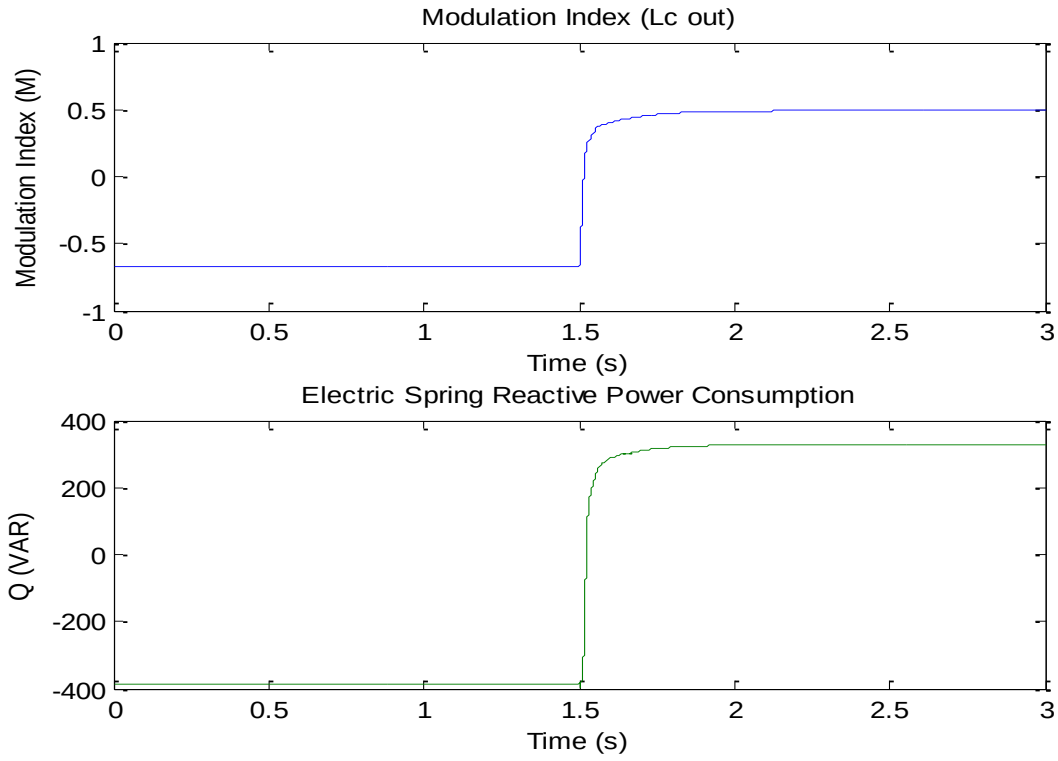

Figure 5-22 ES modulation index and reactive power compensation response when inductive load is switched off and renewable source current is 10A

5.4.2 Case 2: Critical and non-critical Inductive loads

In this case study, ac PI controller parameters has been optimized using two different PSO velocities, inertia factor and constriction factor method and the results are compared together as shown in Figure 5-23. The objective function is non-linear cost function to minimize the error resulting from the difference between the actual main voltage (V_m) and the reference value. The objective function, constraints, and the controller are considered the same as in case 1. Different kinds of simulations were carried out such as multi-disturbances and different kinds of loads are switching on with the non-critical load.

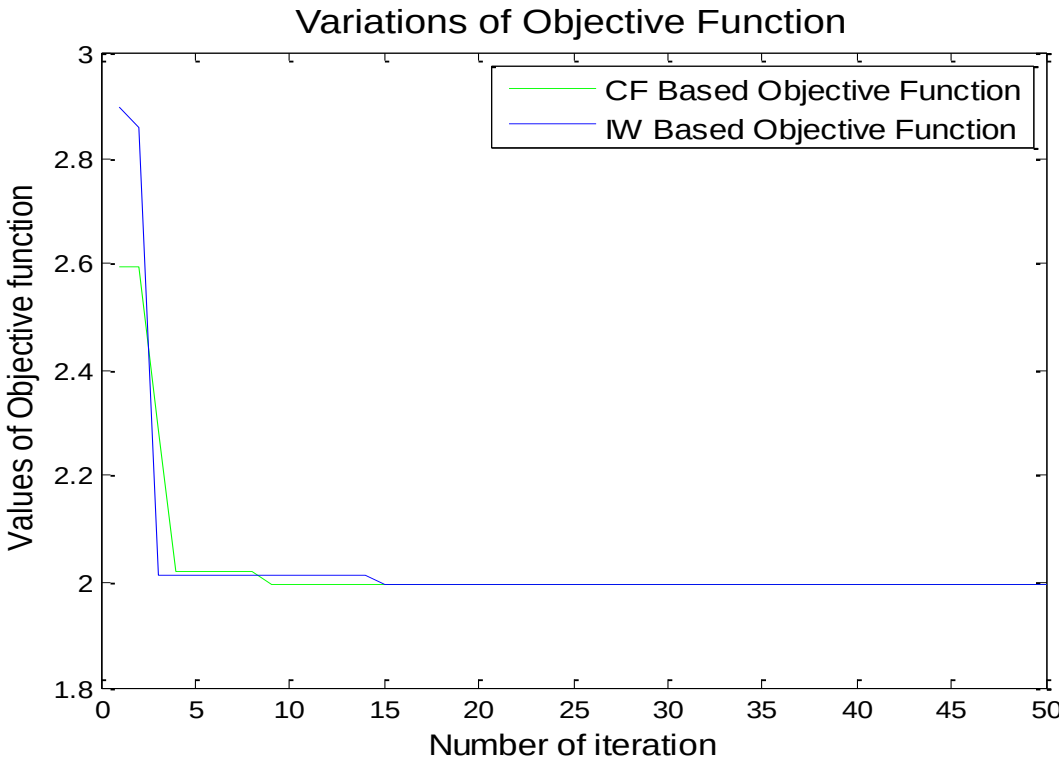

Figure 5-23 Objective function variation using non-linear cost objective function

- Multi-disturbances

Two cases are applied in this section. In the first case, three multiple disturbances are carried out in ascending way starting from 0 A renewable energy source current passing through 2.5 A up to 5 A in the third time period. The time step is 1s for each current level. In the second case, the renewable energy source current is 3 A for the first period and 11 A for the second period. The time step is 1s for each current level. In this case, the critical load is 50 Ω while the non-critical load is inductive with 0.95 PF.

As indicated in Figure 5-24, the main voltage (V_m) is maintained constant while the non-critical load voltage is automatically increased higher than the nominal value (230 V). When the renewable energy source current is increased, ES injects less voltage at its terminal to regulate the main bus. Also, the non-critical load voltage becomes higher. ES operates in capacitive mode for all of these three time periods and generates less reactive power for each upcoming time period as shown in Figure 5-25

Figure 5-26 and Figure 5-27 shows ES response when renewable energy current generates 3 A and 11 A respectively. ES operates in capacitive and inductive modes. Also, ES generates the reactive power for the first period and consumes reactive power for the second period.

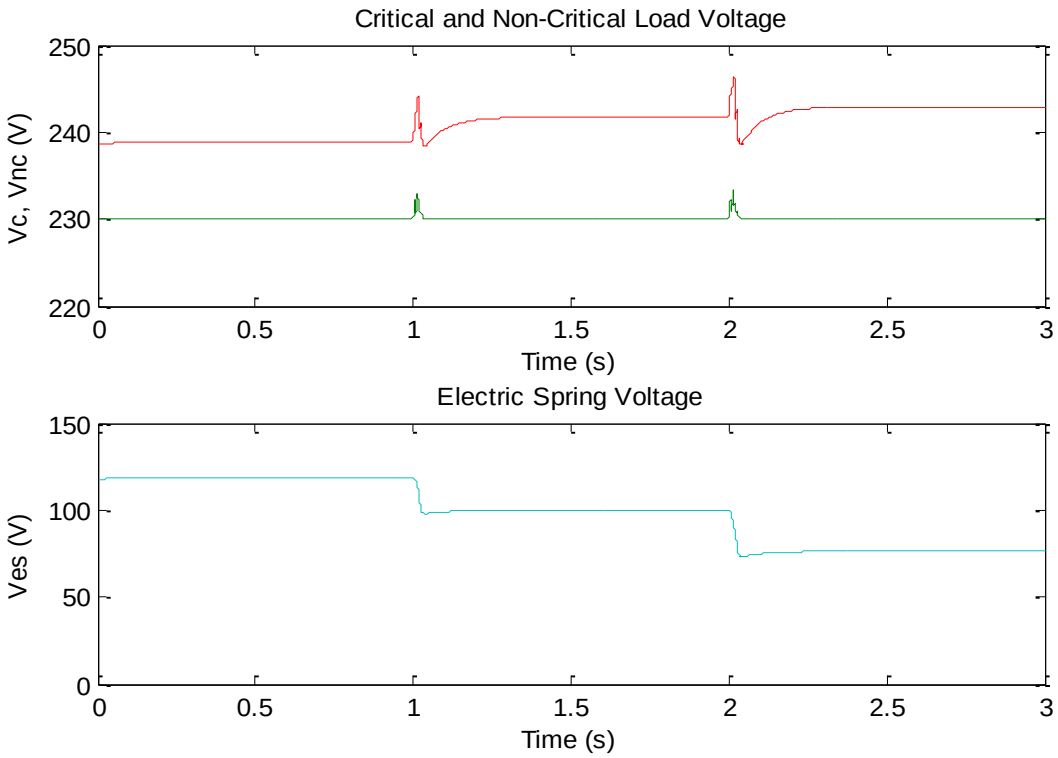

Figure 5-24 Critical, non-critical load and ES voltages in capacitive mode when ES is connected in series with non-critical inductive load

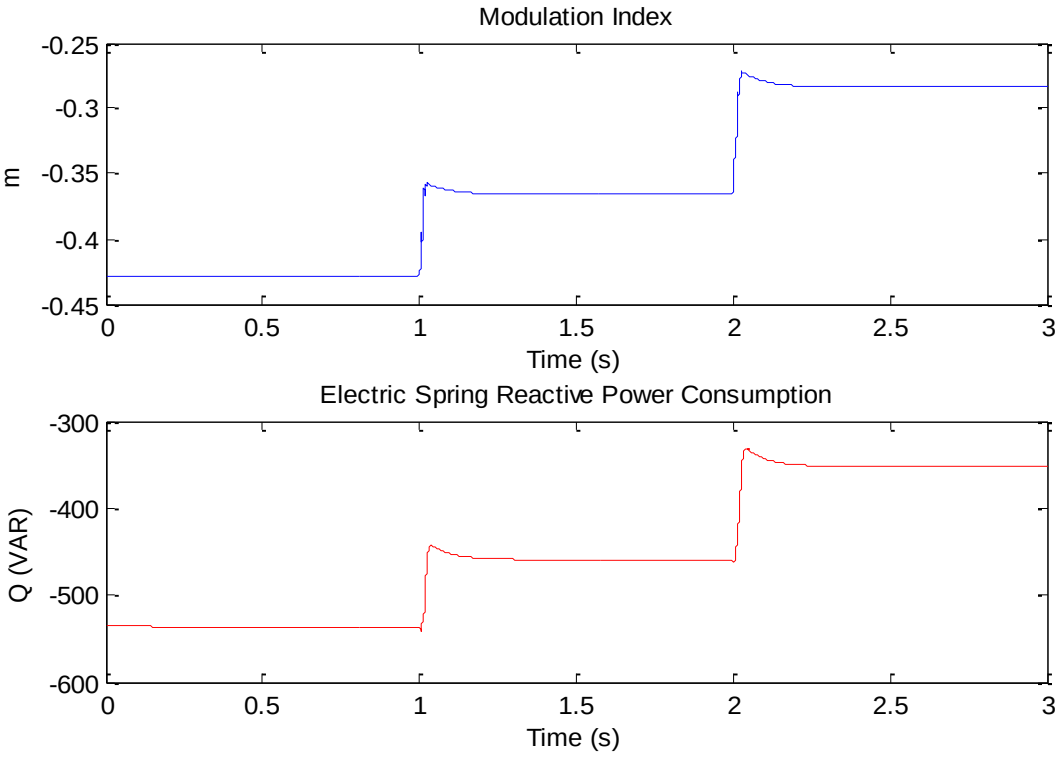

Figure 5-25 Modulation index and reactive power compensation when ES operates in capacitive mode and when ES connected in series with non-critical inductive load

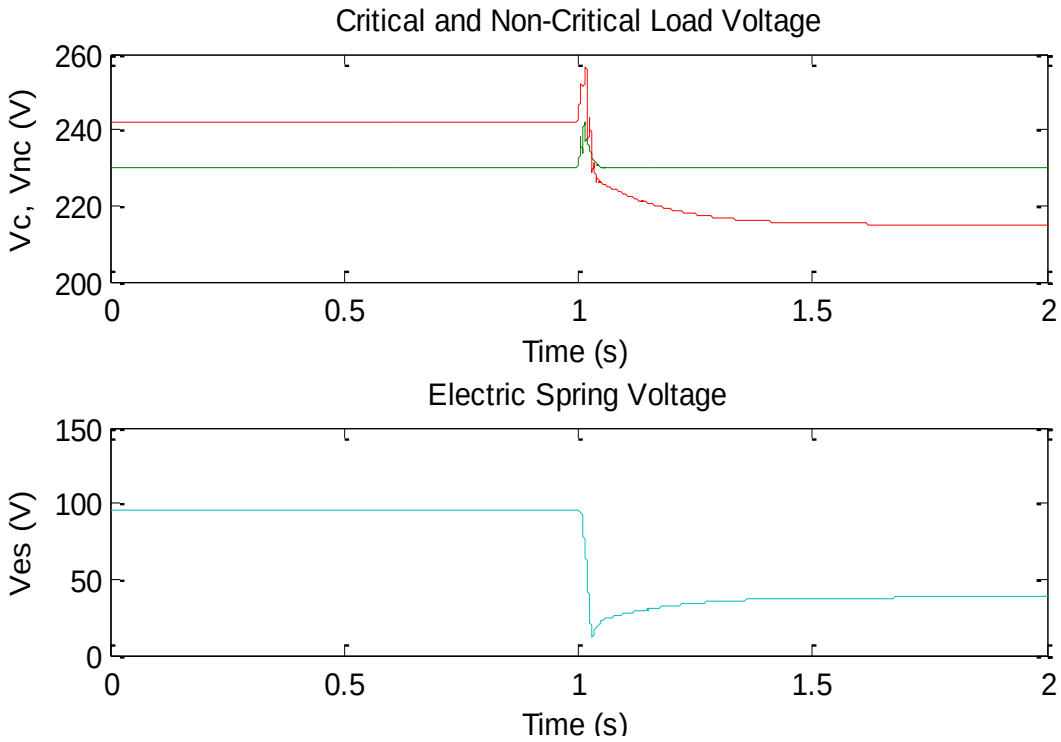

Figure 5-26 Critical, non-critical load and ES voltages in capacitive and inductive modes when ES is connected in series with non-critical inductive load

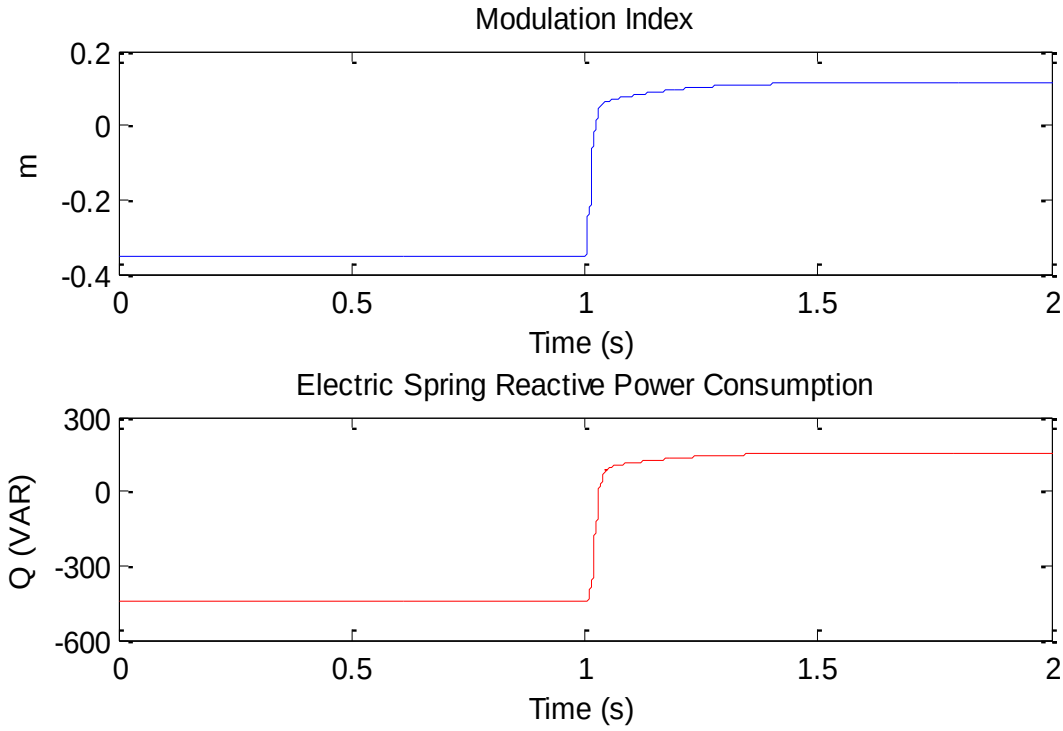

Figure 5-27 Modulation index and reactive power compensation when ES operates in capacitive and inductive modes and when ES connected in series with non-critical inductive load

- Different loads characterization are connected with non-critical load

In this case, the non-critical load is disturbed by switching on three different kinds of loads at a time. These loads are resistive, inductive and capacitive loads. The renewable energy source current is 5 A.

- Switching on a resistive load in parallel with non-critical inductive load

Power system is simulated for two time periods. Each one is 1s. In the first time period, the main voltage is regulated at it nominal value of 230 V. The voltage of non-critical load is higher than the nominal value. ES operates in capacitive mode. However, in the second time period, the non-critical load is disturbed by switching on a 50 Ω resistive load. So, non-critical load becomes more resistive and consumes more real power. It increases the voltage drop in the feeders. However, ES will generate more reactive power compensation to regulate the main bus. Figure 5-28 shows the critical, non-critical load voltages and ES voltage responses while Figure 5-29 shows the ES modulation index and reactive power generation.

- Switching on an inductive load in parallel with non-critical inductive load

In this case, inductive load with PF of 0.95 lagging is switched on in parallel with the non-critical inductive load. Non-critical load becomes more inductive and consumes more reactive power. ES will generate more reactive power compensation to cover the increasing of reactive power demand. Figure 5-30 shows the critical, non-critical load voltages and ES voltage responses while Figure 5-31 shows the ES modulation index and reactive power generation.

- Switching on a capacitive load in parallel with non-critical inductive load

Capacitive load is switched on in parallel with inductive non-critical load with PF of 0.95 leading. The connected capacitor cancels out the reactive power consumption by the inductive load partially or completely. So, the voltage drop through the distribution feeder is reduced. ES generates lower value of ac voltage at its terminal and lower reactive power compensation as compared to the previous time step. Figure 5-32shows the critical, non-critical load voltages and ES voltage responses while Figure 5-33 shows the ES modulation index and reactive power generation.

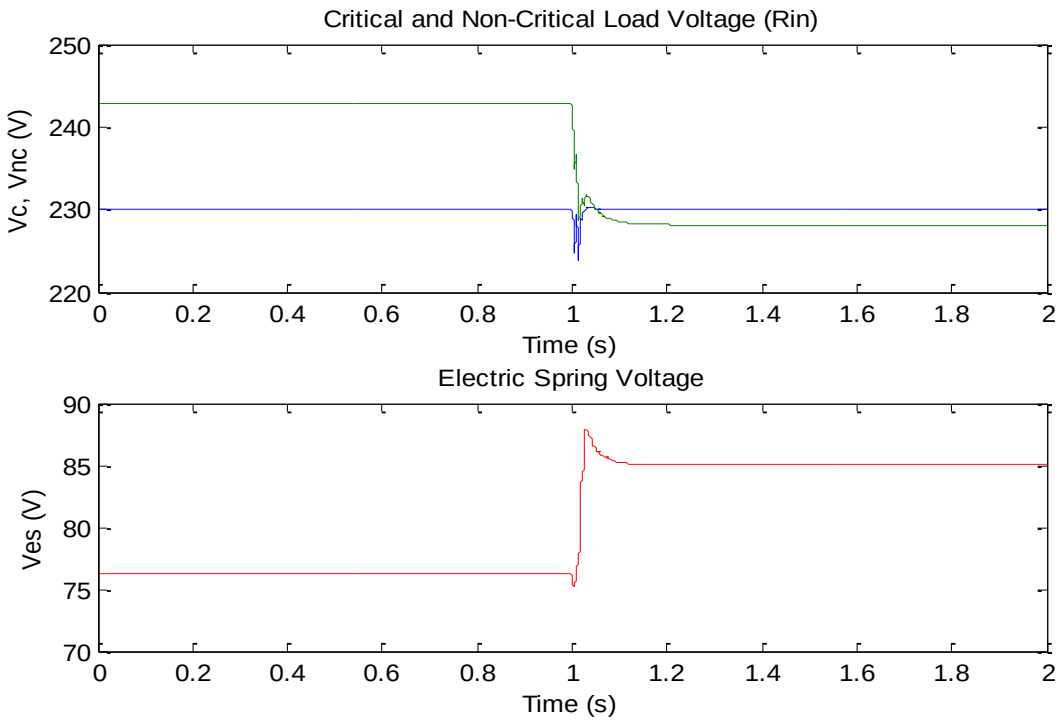

Figure 5-28 Critical, non-critical loads and ES voltages when resistive load is switched on in parallel with non-critical load

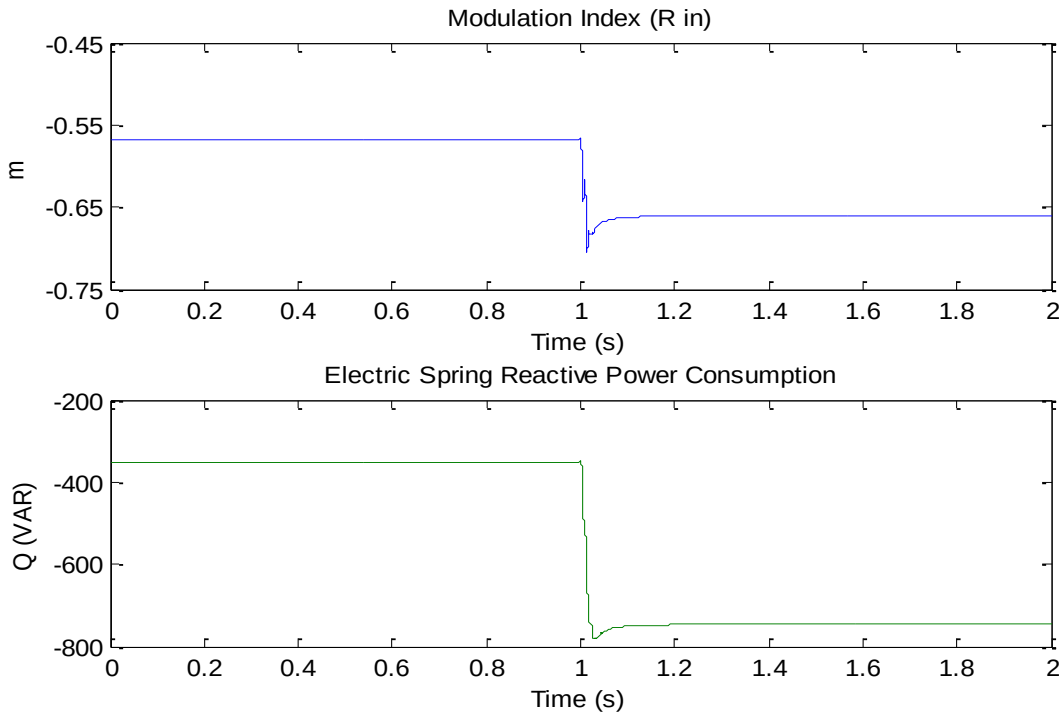

Figure 5-29 Modulation index and reactive power compensation when resistive load is switched on in parallel with non-critical load

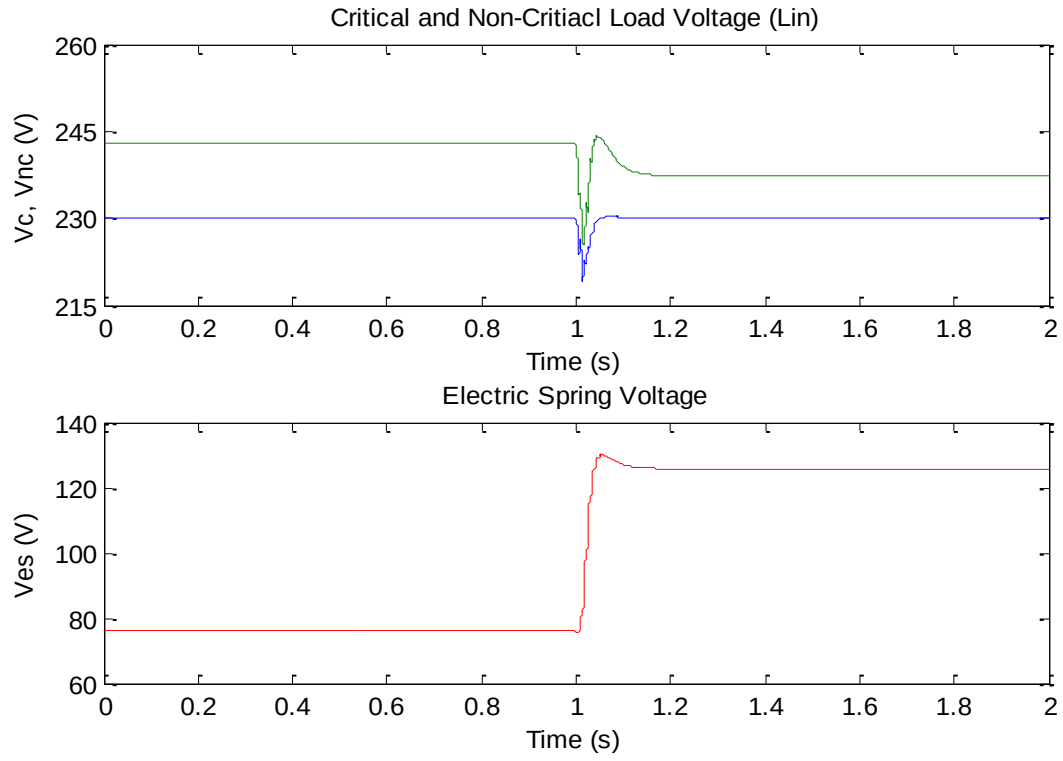

Figure 5-30 Critical, non-critical loads and ES voltages response when inductive load is switched on in parallel with non-critical load

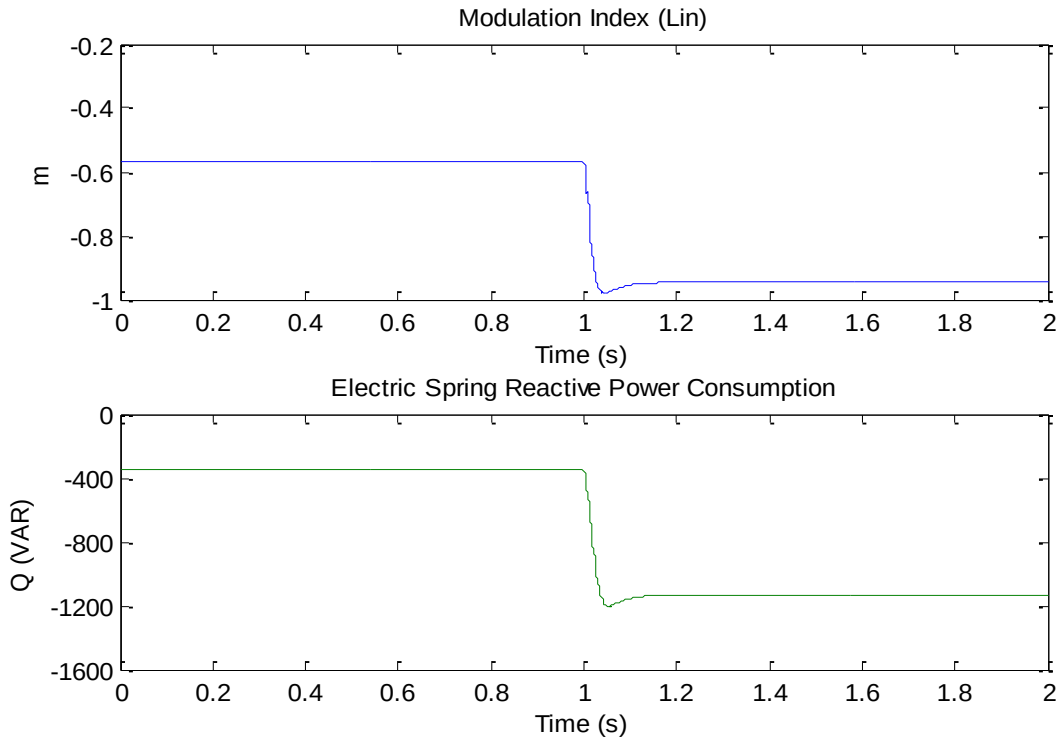

Figure 5-31 Modulation index and reactive power compensation when inductive load is switched on in parallel with non-critical load

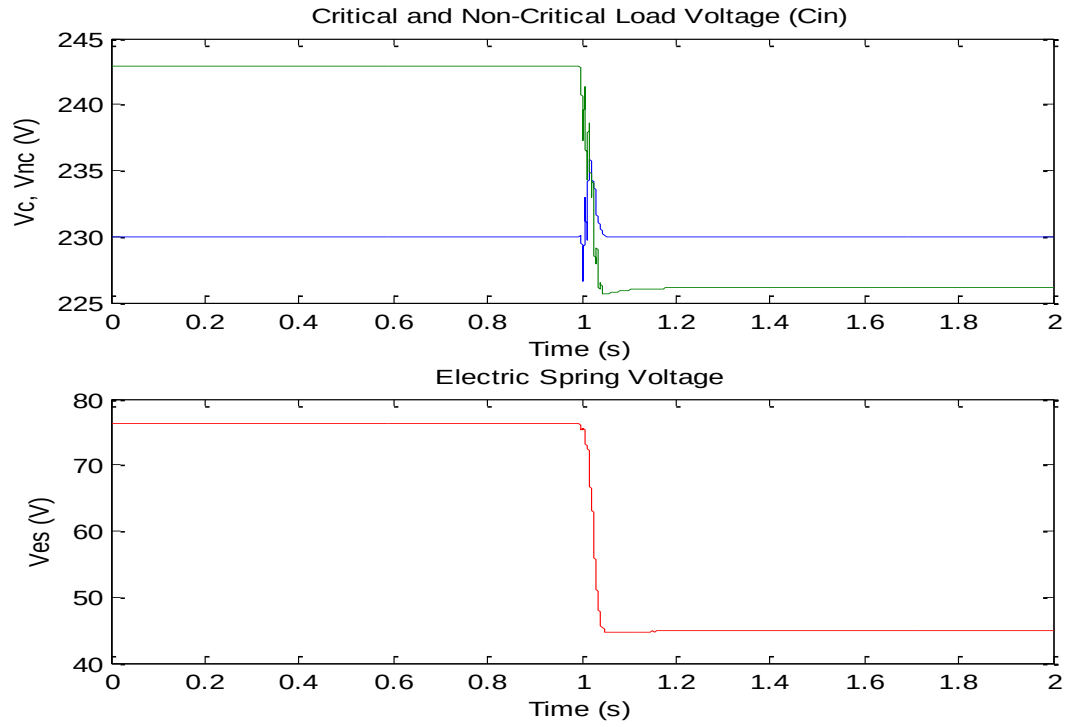

Figure 5-32 Critical, non-critical loads and ES voltages response when capacitive load is switched on in parallel with non-critical load

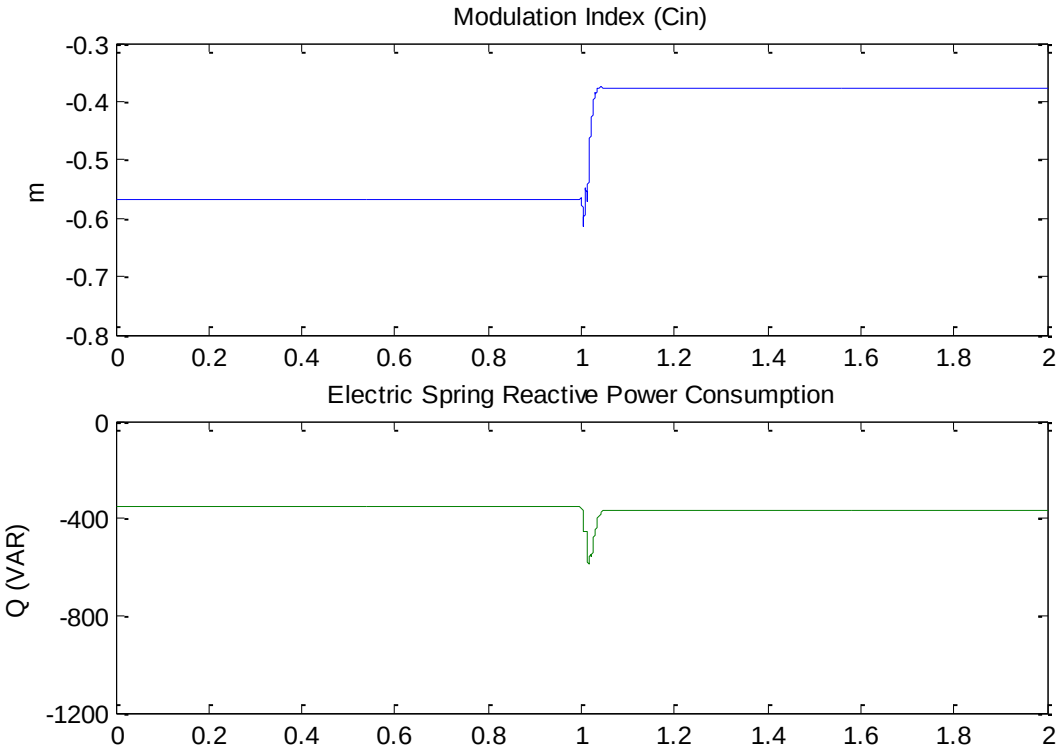

Figure 5-33 Modulation index and reactive power compensation when capacitive load is switched on in parallel with non-critical load

CHAPTER 6

ANALYSIS OF ELECTRIC SPRING PERFORMANCE

The modes of operation of the electric spring are analogous to the operational modes of mechanical spring. The ES like the mechanical spring has operational constraints such as extension of displacement of the mechanical spring is limited to a certain range.

One of these constraints is the dc link voltage which controls the maximum value of the ES output voltage. In addition, there still exists a minimum voltage for the non-critical load to work properly within the specifications. However, lighting loads operate in the range of 170 V-265 V in the system of 230 V. The minimum voltage for the heating system can be theoretically between 0 V and its allowed maximum voltage [62]. The value of non-critical load plays a crucial rule in ES limitations. It can affect the ES capacity by controlling the non-critical load current.

6.1 Renewable Energy Current Source Variation

In this section, there are two cases regarding the characteristics of critical and non-critical loads. In the first case, critical and non-critical loads are resistive and equal 50 Ω each. The relationship between $V_c, V_{nc}, V_{es,} Q_{es}$ and m versus renewable energy current source variation is shown in Figure 6-1. It is noted that ES operates in capacitive mode when renewable energy current source generates less than 5 A. ES generates reactive power compensation and the modulation index has a negative value. When the current source generates 5 A, the main bus is automatically regulated to its nominal value

of 230V. No need for ES at this stage. However, ES operates in inductive mode when the current source generates higher than 5 A. ES consumes reactive power and the modulation index sign becomes positive. In inductive and capacitive modes, the voltage of the critical load is regulated to its nominal value while the voltage of non-critical load is reduced lower than the nominal voltage.

In the second case, the non-critical load is considered inductive with 0.95 PF. It is observed in Figure 6-2, the neutral mode occurs when the current source generates 10 A. That is because the non-critical load consumes reactive power which means the main voltage is dropped higher than the previous case through the distribution feeders. Non-critical load voltage is higher than the nominal value in capacitive mode while it becomes lower in the inductive mode. The relationship between $V_c, V_{nc}, V_{es,} Q_{es}$ and m versus current source are shown in Figure 6-2 where 11 simulations have been conducted. Each simulation has been performed for a certain value of current source.

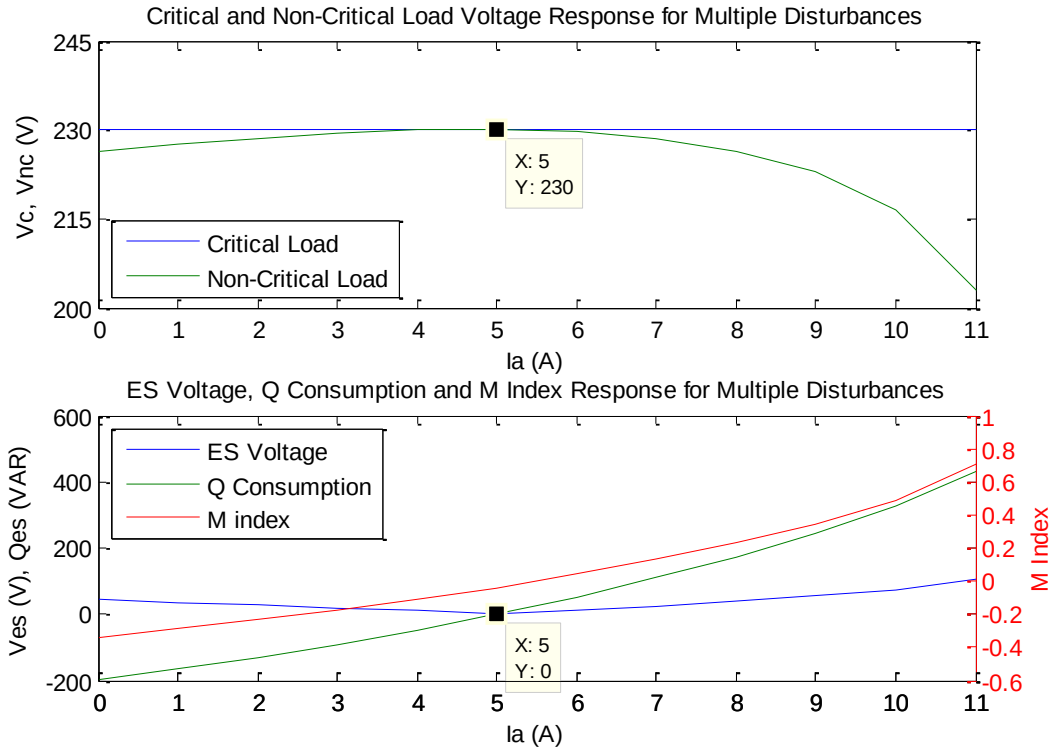

Figure 6-1 Relationship between critical, non-critical loads, and ES voltages, reactive power compensation and modulation index versus current source variation in case of resistive loads

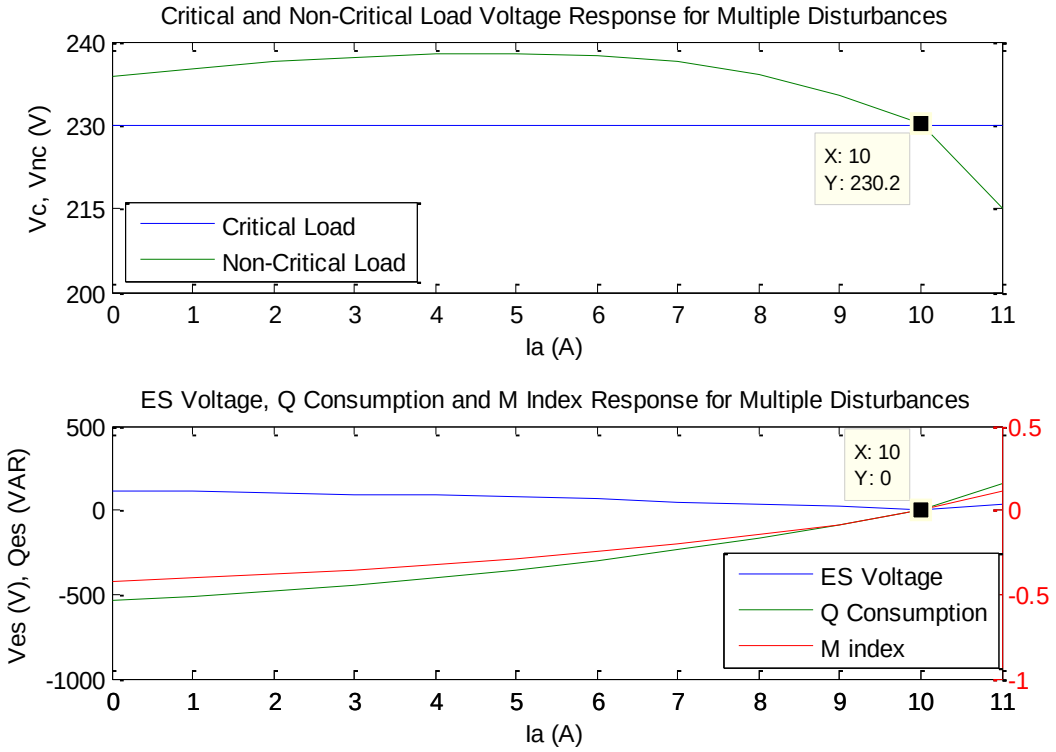

Figure 6-2 Relationship between critical, non-critical loads, and ES voltages, reactive power compensation and modulation index versus current source variation in case of inductive loads

6.2 Modulation Index Variation

To investigate the limitations of ES, two tests have been performed by varying the modulating signal value m. The tests are as follows:

6.2.1 Test 1: Critical and Non-Critical Loads Are Resistive

- Voltage Boosting

Critical and non-critical resistive loads are 50 Ω each. Different voltage levels; +5%, +7.5% and +10%, higher than the nominal value of 230 V are considered across the critical load. ES operates in inductive mode to suppress the voltage level when the modulation index is in the range of $(0-1)$. Otherwise, the voltage level keeps rising higher than the nominal value. It is noted that when the voltage of the main bus is increased, the capability of ES for regulation is decreased as seen in Figure 6-3. ES voltage response and reactive power compensation are depicted in Figure 6-4

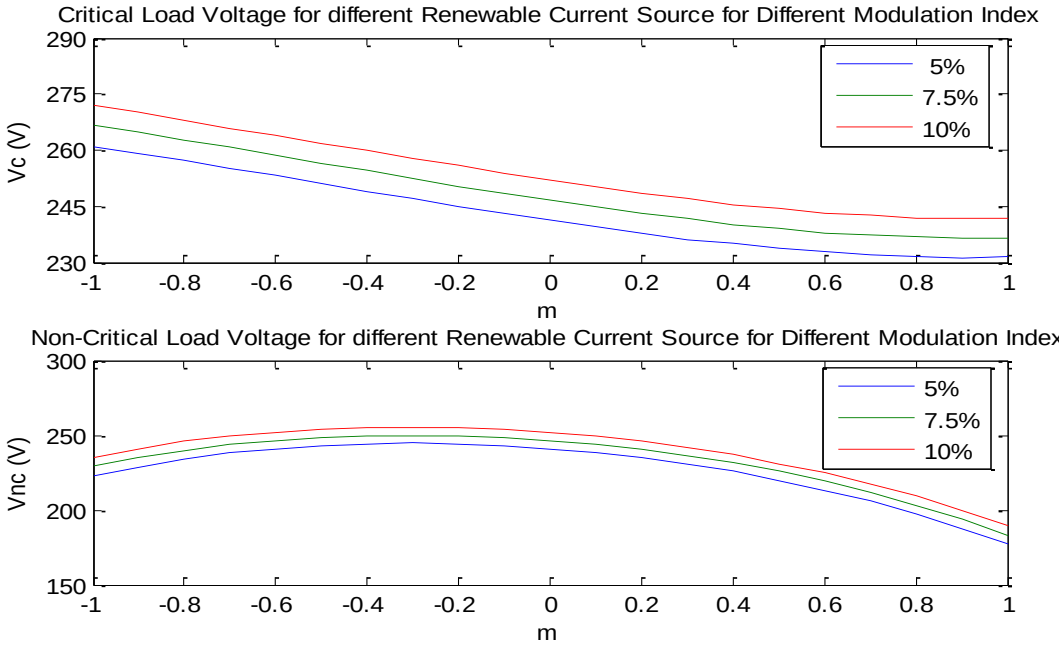

Figure 6-3 Relationship between critical and non-critical loads voltages versus the modulation index variation in case of resistive loads

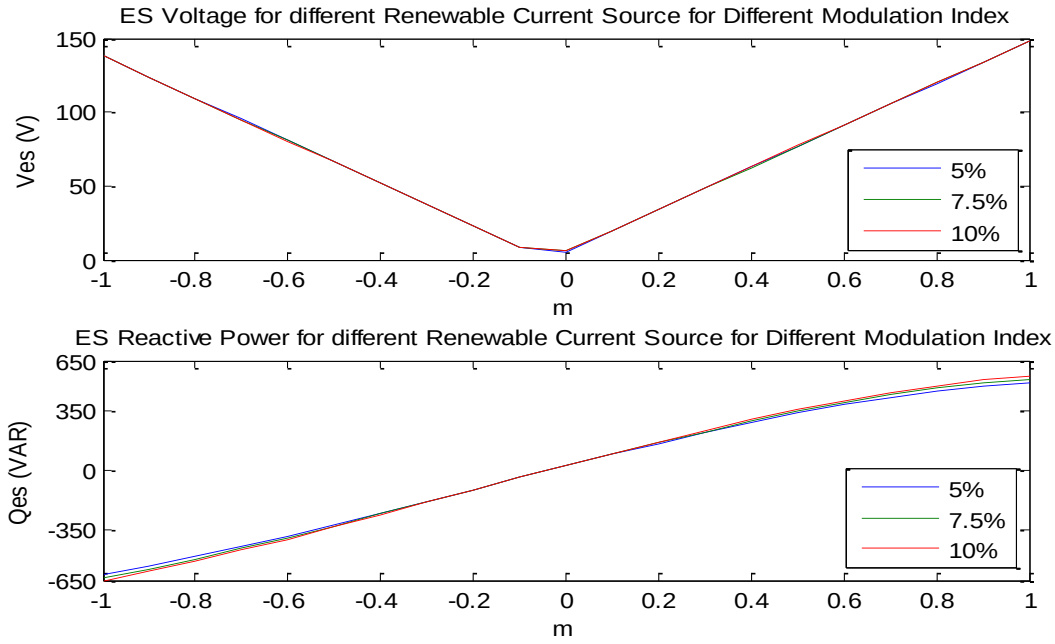

Figure 6-4 ES voltage response and reactive power compensation versus modulation index variation

- Voltage Reduction

In this case, critical and non-critical resistive loads are 50 Ω each. Different voltage levels; -5%, -7.5% and -10%, lower than the nominal value of 230 V are considered across the critical load. ES operates in capacitive mode to support the voltage level when the modulation index is in the range of $(-1 - 0)$. Otherwise, the voltage level keeps declining lower than the nominal value. It is noted that when the voltage of the main bus is decreased, the capability of ES for regulation is decreased as shown in Figure 6-5. ES voltage response and reactive power compensation are depicted in Figure 6-6

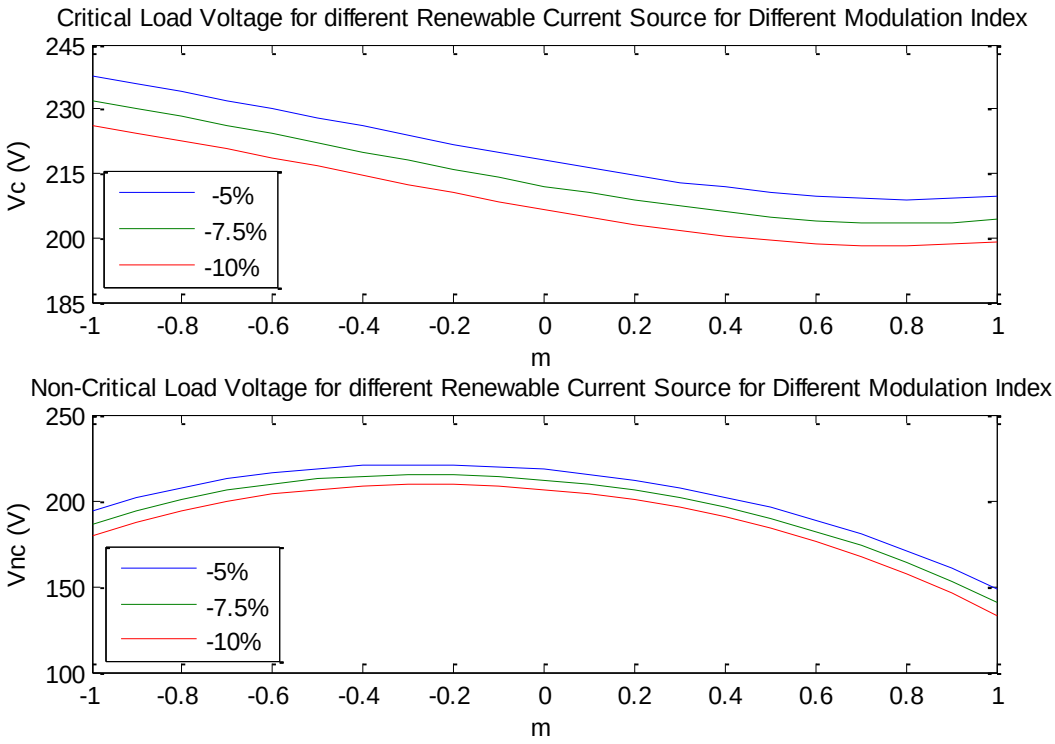

Figure 6-5 Relationship between critical and non-critical loads voltages versus the modulation index variation in case of resistive loads

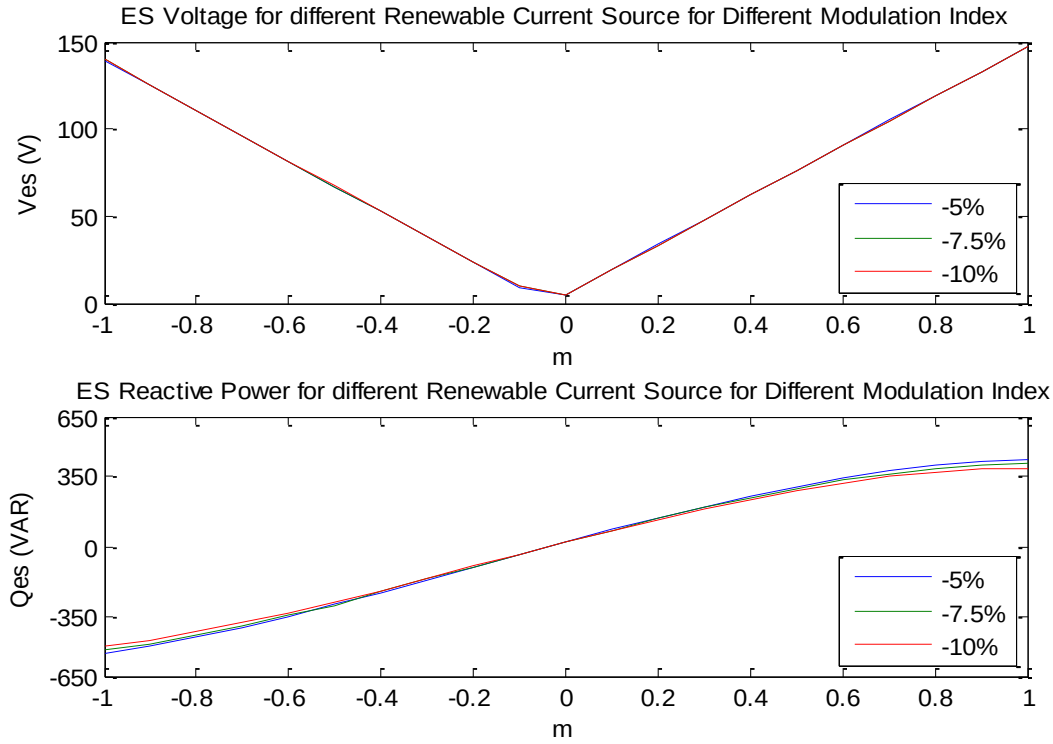

Figure 6-6 ES voltage response and reactive power compensation versus modulation index variation

➢ Comparison

To get a clear picture, the previous voltage boosting and voltage reduction cases are combined in one graph as shown in Figure 6-7, Figure 6-8, Figure 6-9 and Figure 6-10 respectively. The critical load voltage response is shown in Figure 6-9. The non-critical load voltage response is non-linear with respect to the modulation index variation as seen in Figure 6-8. Furthermore, the ES voltage are close in different voltage levels as shown in Figure 6-9. Lastly, the reactive power compensation response is depicted in Figure 6-10

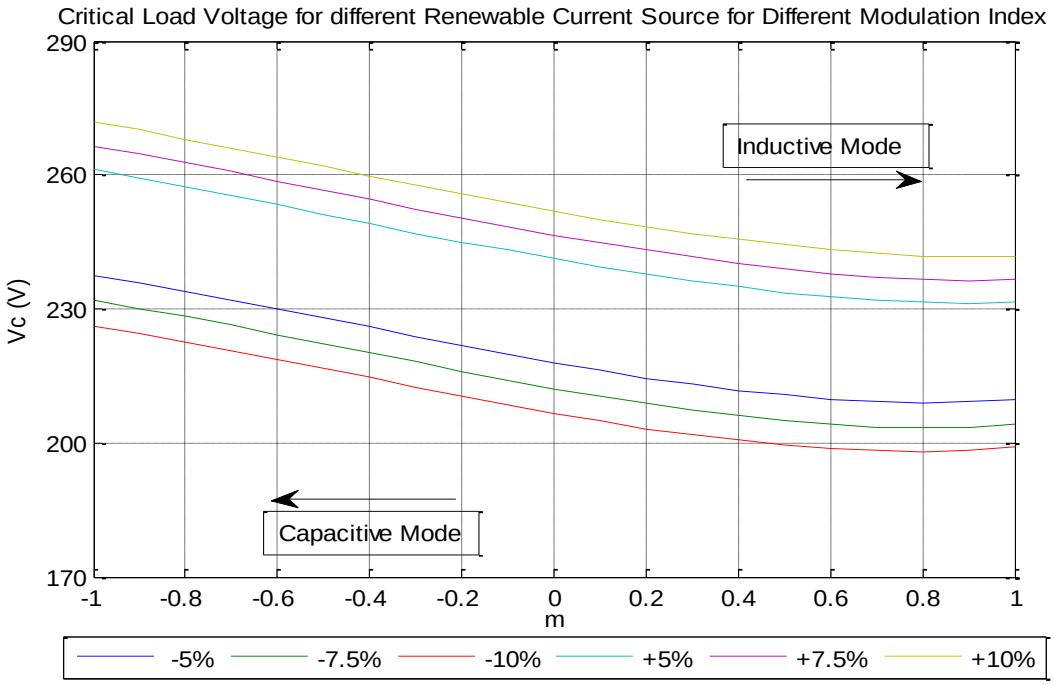

Figure 6-7 Critical load voltage comparison in case of resistive loads

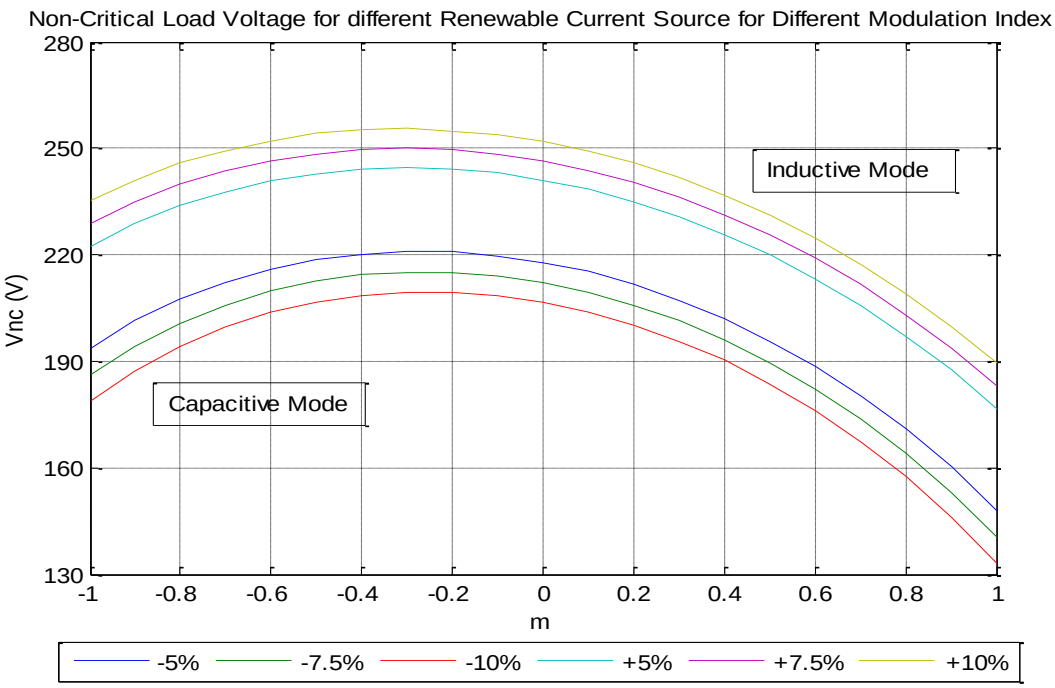

Figure 6-8 Non-critical load voltage comparison in case of resistive loads

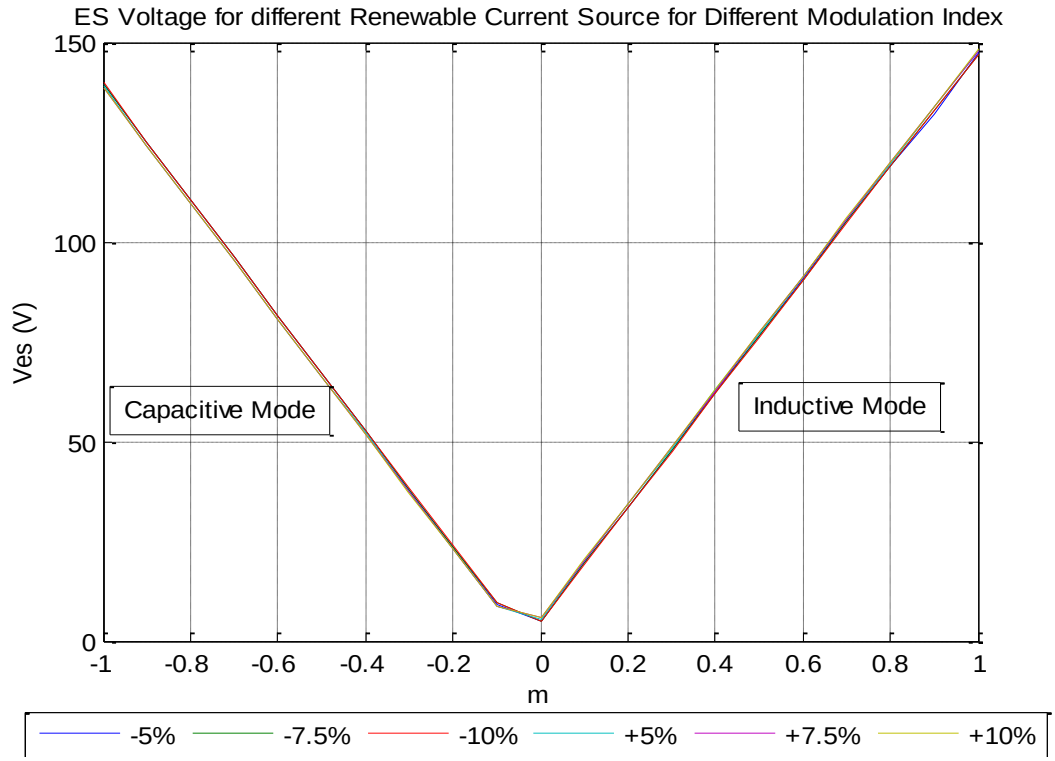

Figure 6-9 ES voltage comparison in case of resistive loads

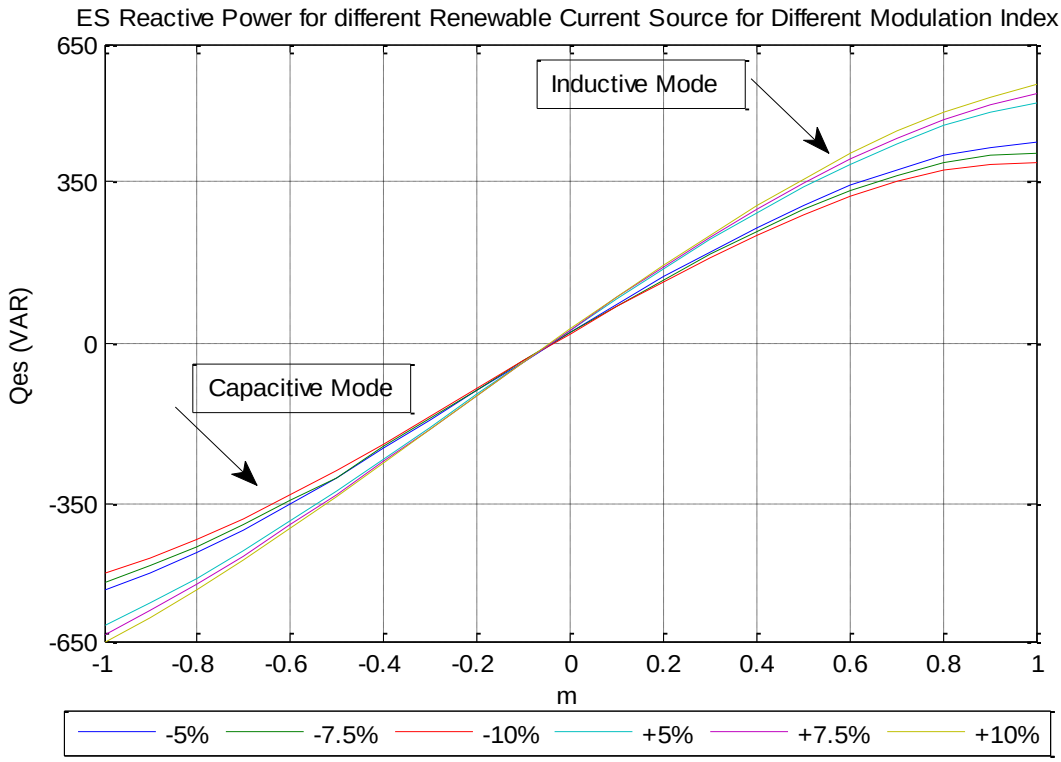

Figure 6-10 Reactive power comparison in case of resistive loads

6.2.2 Test 2: Non-Critical load is Inductive

- Voltage Boosting

Non-critical inductive load with 0.95 PF is considered. Different voltage levels; +5%, +7.5% and +10%, higher than the nominal value across the critical load are taken into consideration. In Figure 6-11, ES operates in inductive mode to reduce the voltage level. However, after a certain value of the modulation index, ES adversely affects the bus voltage. The voltage across the non-critical load is reduced which means decreasing the consumption of the reactive power. Therefore, the main voltage increases again. It is noted that the voltage across the non-critical load is decreased when ES operates in inductive mode. The ES voltage response and reactive power compensation are depicted in Figure 6-12

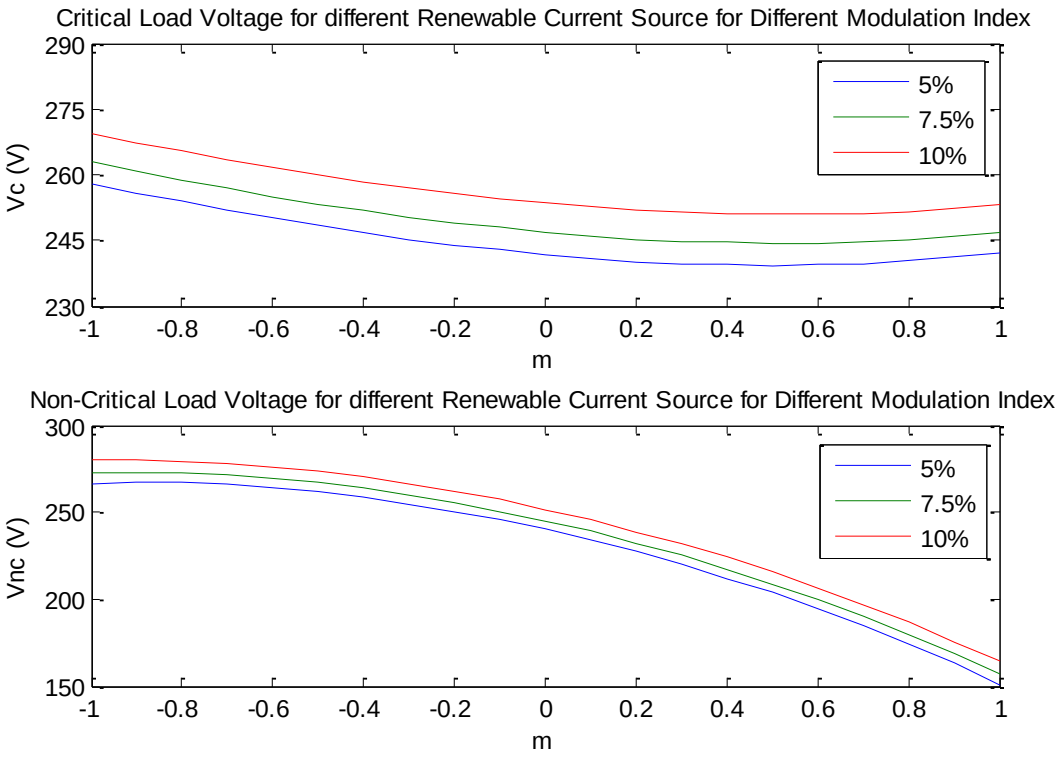

Figure 6-11 Relationship between critical and non-critical loads voltages versus the modulation index variation in case of inductive loads

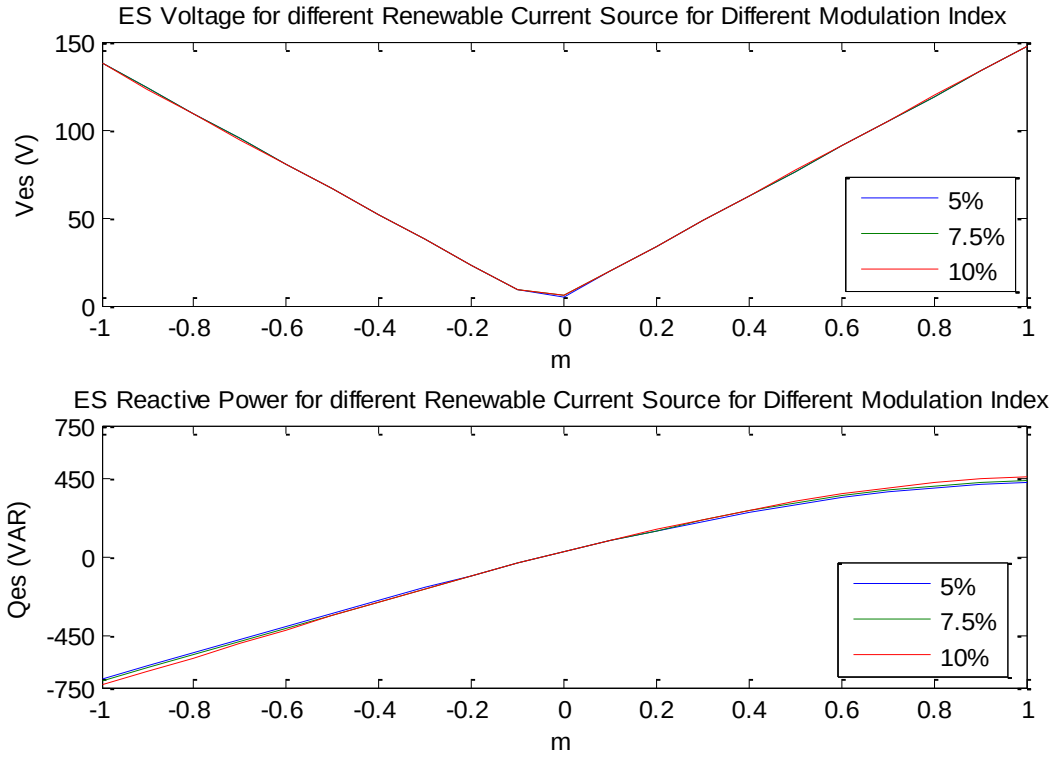

Figure 6-12 ES voltage response and reactive power compensation versus modulation index variation

➢ Voltage Reduction

In this case, different voltage levels; -5%, -7.5% and -10%, lower than the nominal value across the critical load are considered. ES operates in capacitive mode to increase the voltage level. However, the voltage across the non-critical load is increased which means increasing the consumption of the reactive power as seen in Figure 6-11. The ES voltage response and reactive power compensation are depicted in Figure 6-12

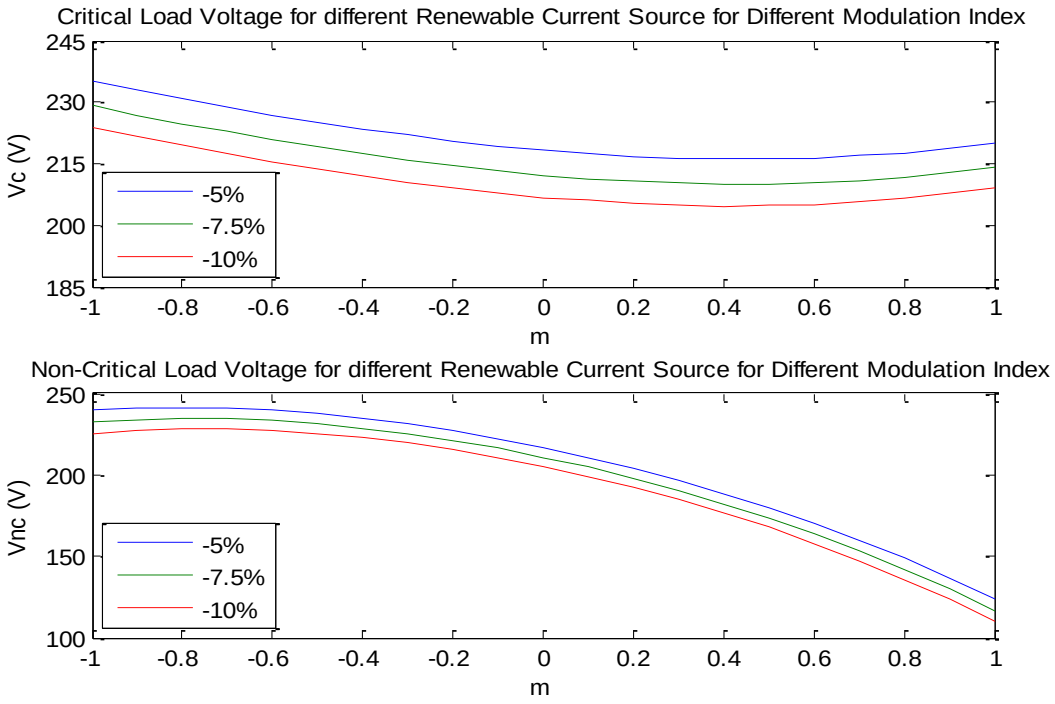

Figure 6-13 Relationship between critical and non-critical loads voltages versus the modulation index variation in case of inductive loads

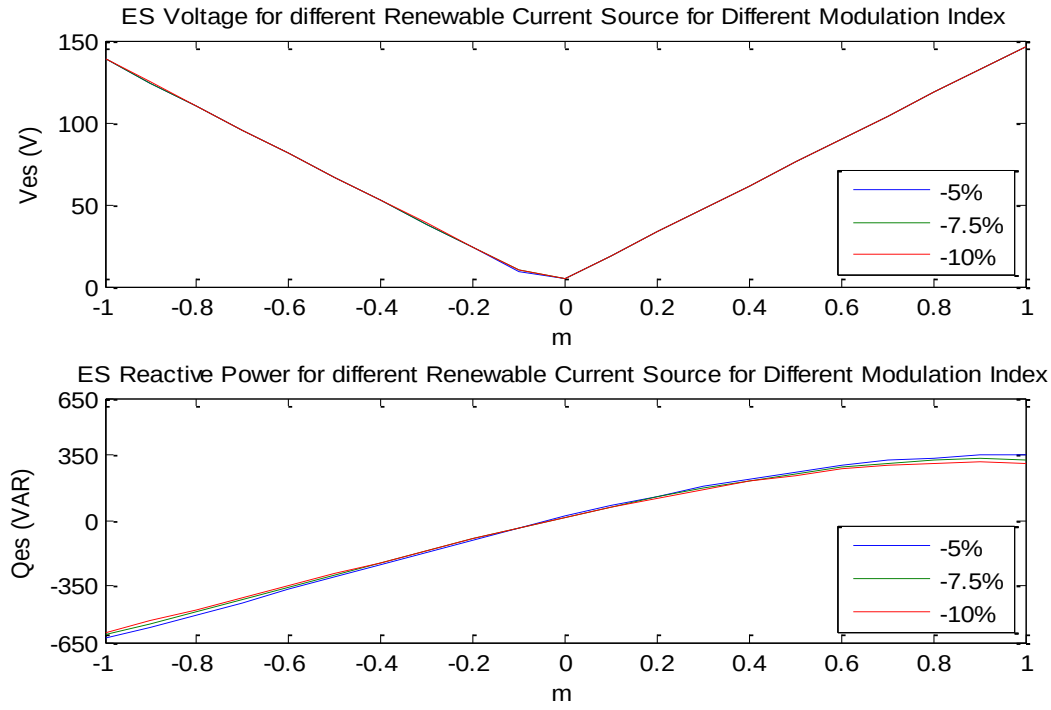

Figure 6-14 ES voltage response and reactive power compensation versus modulation index variation

- Comparison

Voltage boosting and voltage reduction cases are combined in one graph as shown in Figure 6-15, Figure 6-16, Figure 6-17 and Figure 6-18 respectively. The critical load voltage response is shown in Figure 6-15. The non-critical load voltage response with respect to the modulation index variation is seen in Figure 6-16. Furthermore, the ES voltage are close in different voltage levels as shown in Figure 6-17. Lastly, the reactive power compensation response is depicted in Figure 6-18

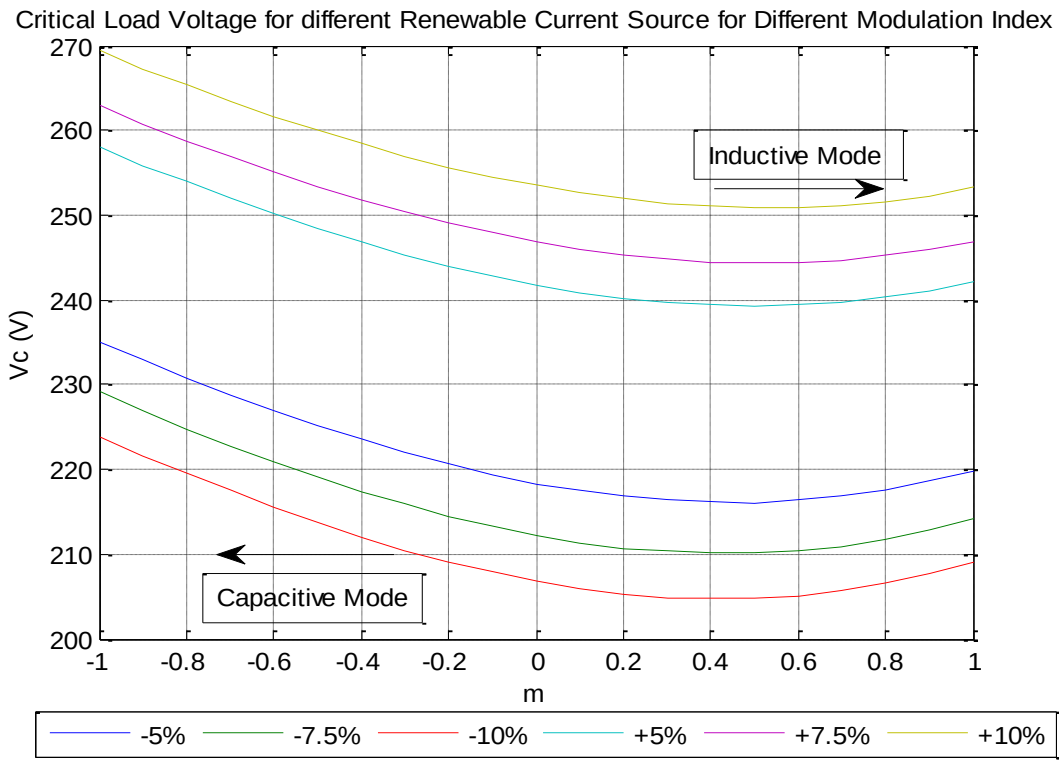

Figure 6-15 Critical load voltage comparison in case of inductive loads

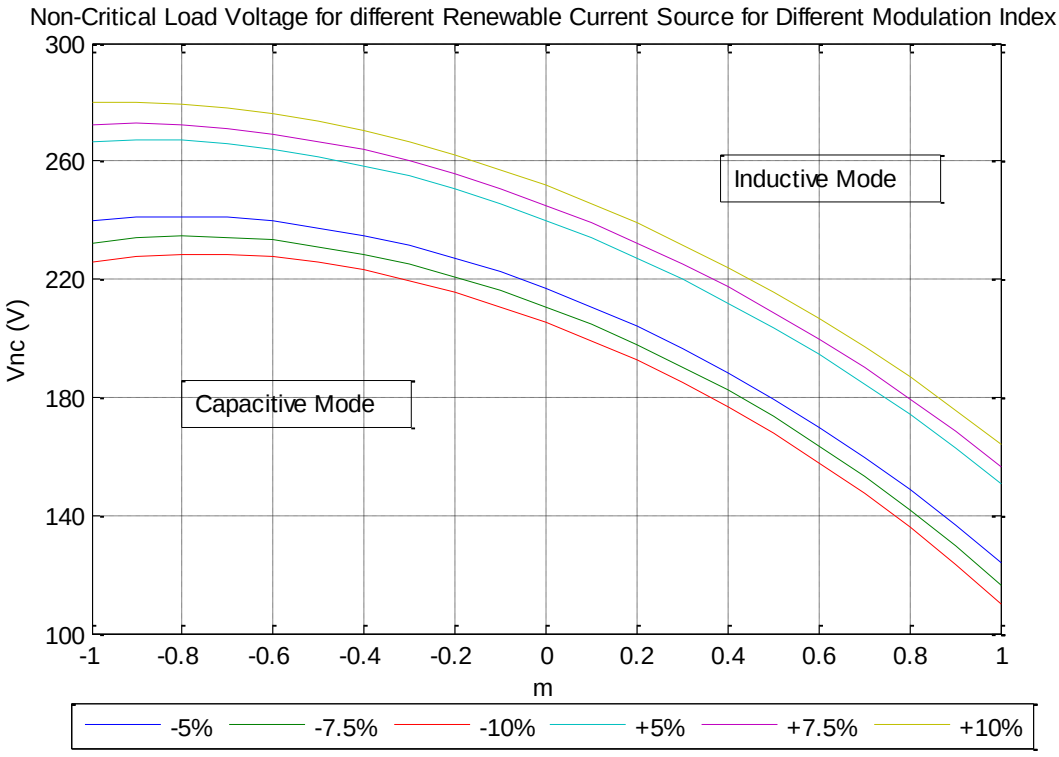

Figure 6-16 Non-critical load voltage comparison in case of inductive loads

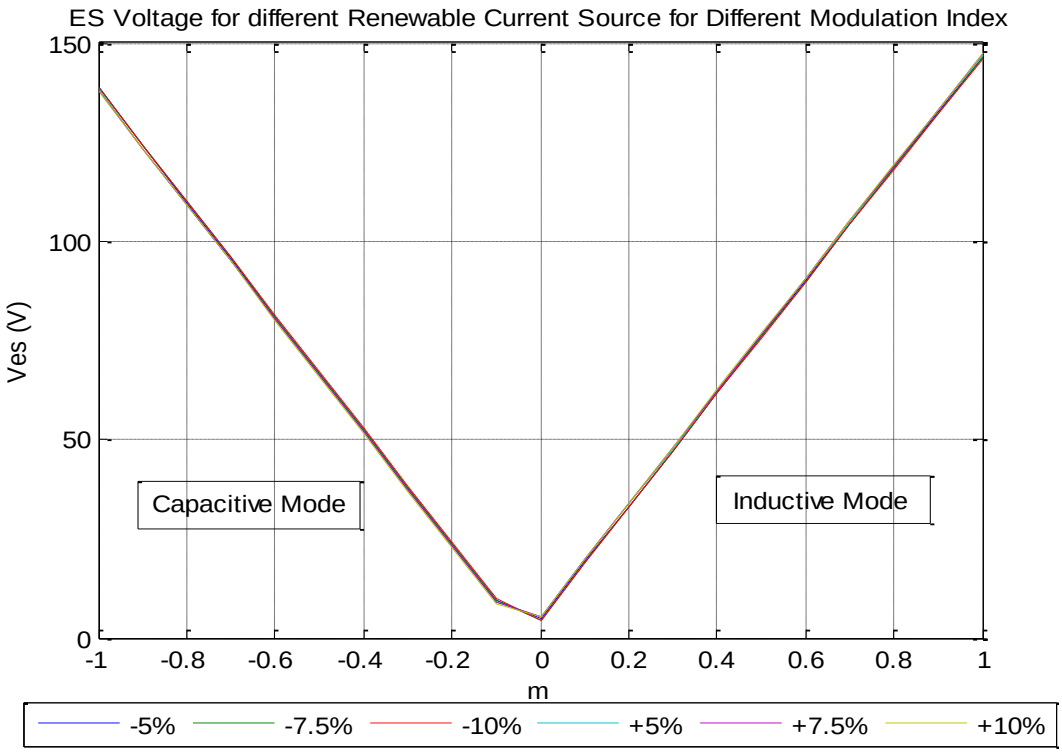

Figure 6-17 ES voltage comparison in case of inductive loads

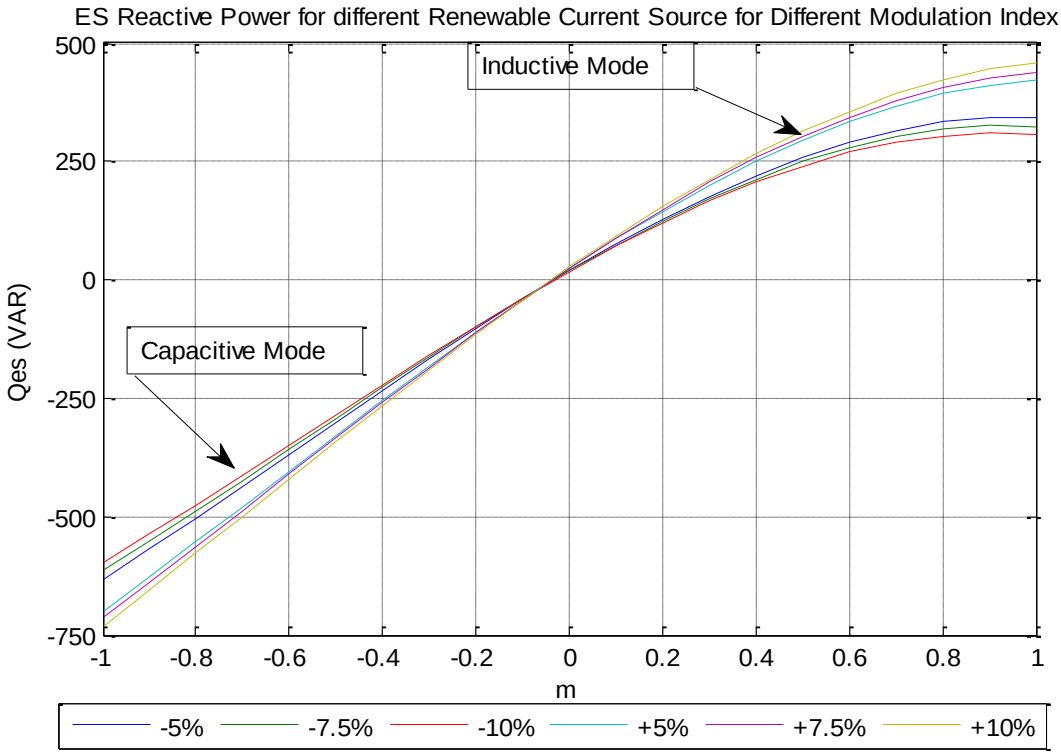

Figure 6-18 Reactive power comparison in case of inductive loads

6.3 Electric Spring Limitation with Respect to Rnc Load

6.3.1 Reducing Non-Critical Resistive Load Impedance

In this section, the non-critical load impedance is reduced to 15 Ω. Different voltage levels; +5%, +10% and +15%, higher than the nominal value of 230 V are considered across the critical load. Results show that the ES behavior is improved by reducing the non-critical load impedance. ES can handle with higher voltage levels as compared to the previous cases. The voltage across the non-critical load is reduced which means increasing the non-critical load current. Thus, ES capacity is improved. Critical and non-critical voltage response is depicted in Figure 6-19. ES voltage and reactive power compensation responses versus modulating signal variation m are indicated in Figure 6-20

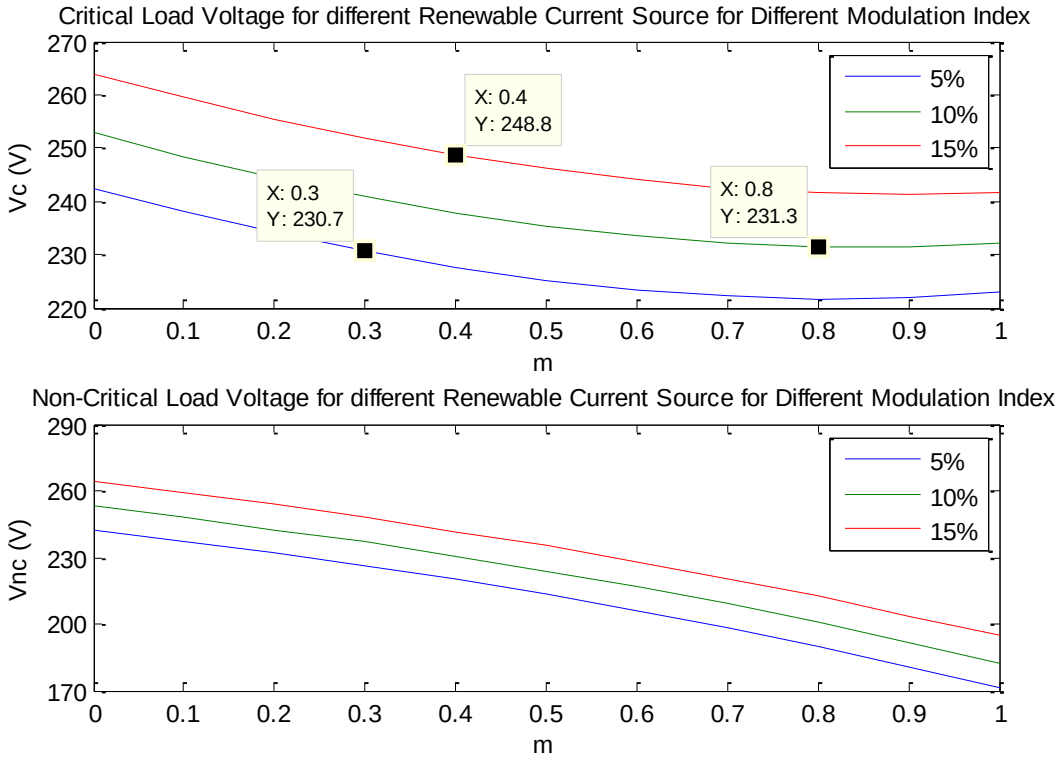

Figure 6-19 critical and non-critical loads responses versus modulating signal variation

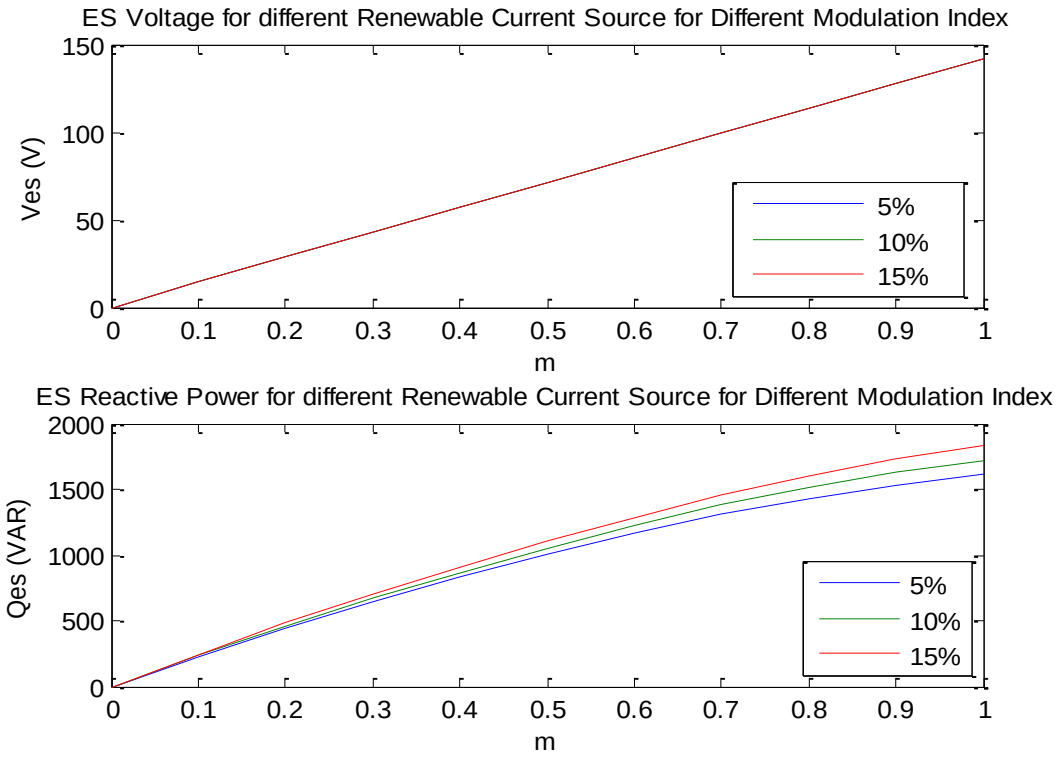

Figure 6-20 ES voltage and reactive power compensation responses versus modulating signal variation

6.3.2 Non-Critical Inductive Load Variation by Changing the Values of Power Factor

The power factor of non-critical load is changed in the range of $0.9 - 1$ while the resistive part is kept constant 15 Ω. For each power factor, renewable energy current source is changed in a special manner to have $\pm 5\%$ voltage level higher than the nominal value across the loads. Modulation index is tuned to get the best response of ES with respect to voltage regulation as shown in Figure 6-21 and Figure 6-22.

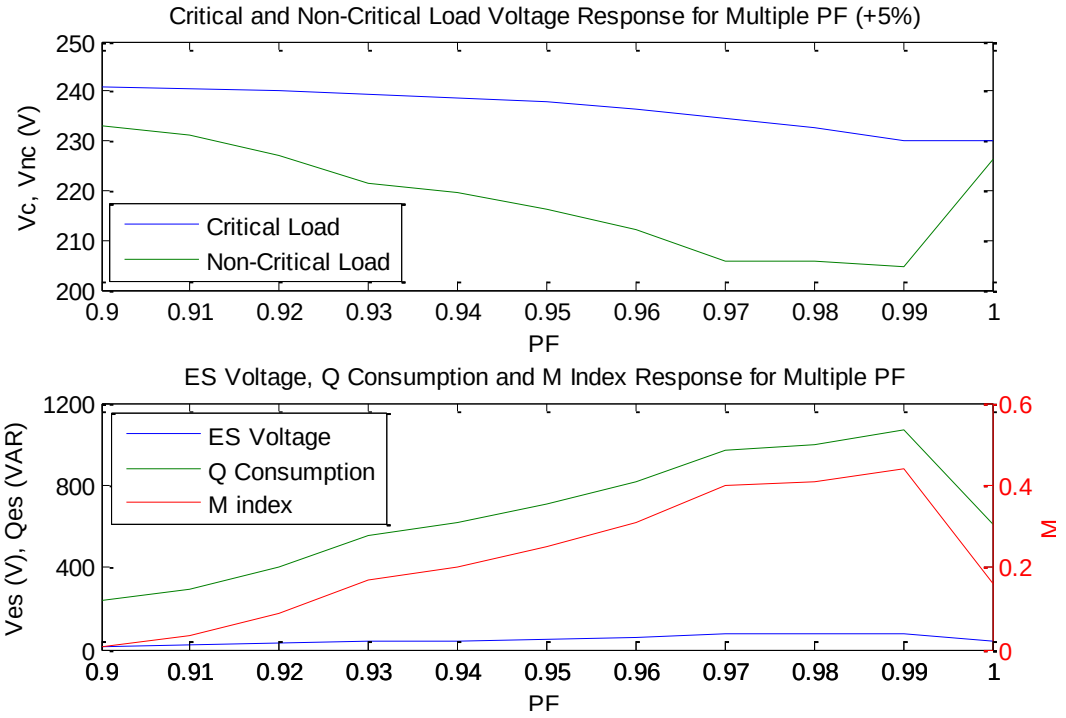

Figure 6-21 Power system response with respect to power factor variation for positive voltage level

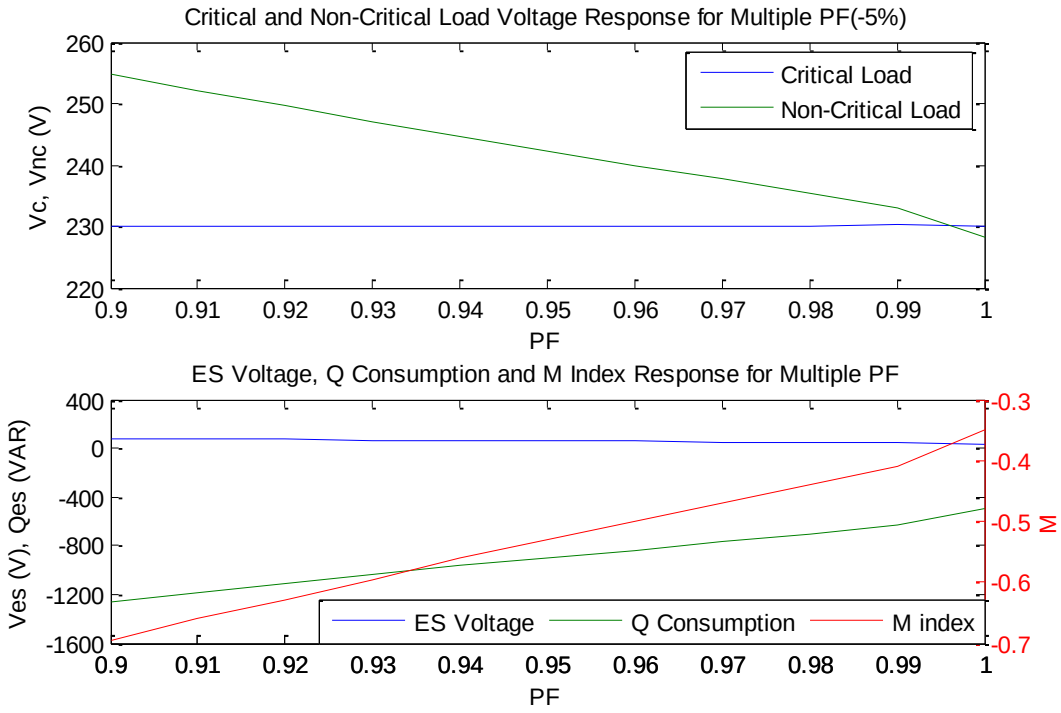

Figure 6-22 Power system response with respect to power factor variation for positive voltage level

Figure 6-21 shows the main voltage is going to be well regulated when the power factor is close to unity factor. On the other hand, non-critical load voltage is decreased when the modulation index, ES voltage and reactive power compensation is increased. It is noted that the main voltage is well regulated for all values of PF variation as depicted in Figure 6-22.

CHAPTER 7

HRADWARE IN THE LOOP (HIL) SETUP AND EXPERIMENTAL WORK VALIDATION

Electric spring (ES) as a new approach to demand side management has been implemented and verified experimentally by using real time digital simulator (RTDS) and dSPACE controller. To do so, the power part of the test system is constructed on RTDS while the control part is implemented externally on dSPACE controller. Both equipments are integrated as a hardware in the loop implementation (HIL). Experimental work is carried out to validate the switching model of the ES in different kinds of disturbances. ES model is validated in sudden change inductive mode, sudden change capacitive mode, multi-disturbances, and load variations. Then, Simulation and experimental work results are compared together.

7.1 Electric Spring Sudden Change Case

- Electric Spring Inductive Mode

In this case, ES operates in inductive mode when the voltage level of the main voltage is higher than the nominal value. However, Renewable energy current source generates 10 A. Figure 7-1 to Figure 7-6 describe the sudden change response of the power system in inductive mode where ES consumes sufficient amount of pure reactive power to regulate the main bus.

Figure 7-1 and Figure 7-2 show the charging of dc capacitor and the angle difference response between electric spring terminal voltage and non-critical load current. Figure 7-3 and Figure 7-4 show the ES real and reactive power response while Figure 7-5 and Figure 7-6 show the response voltage of ES, critical and non-critical loads respectively. M and R in figures refer to MATLAB and RTDS results respectively.

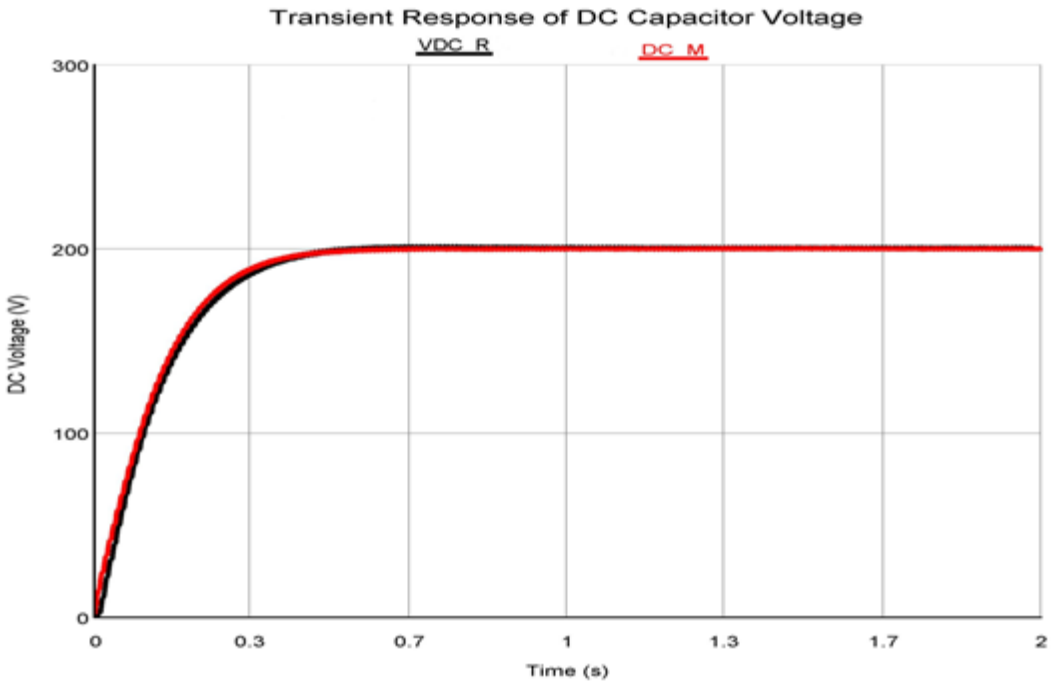

Figure 7-1 Comparison of dc voltage response in sudden change inductive mode

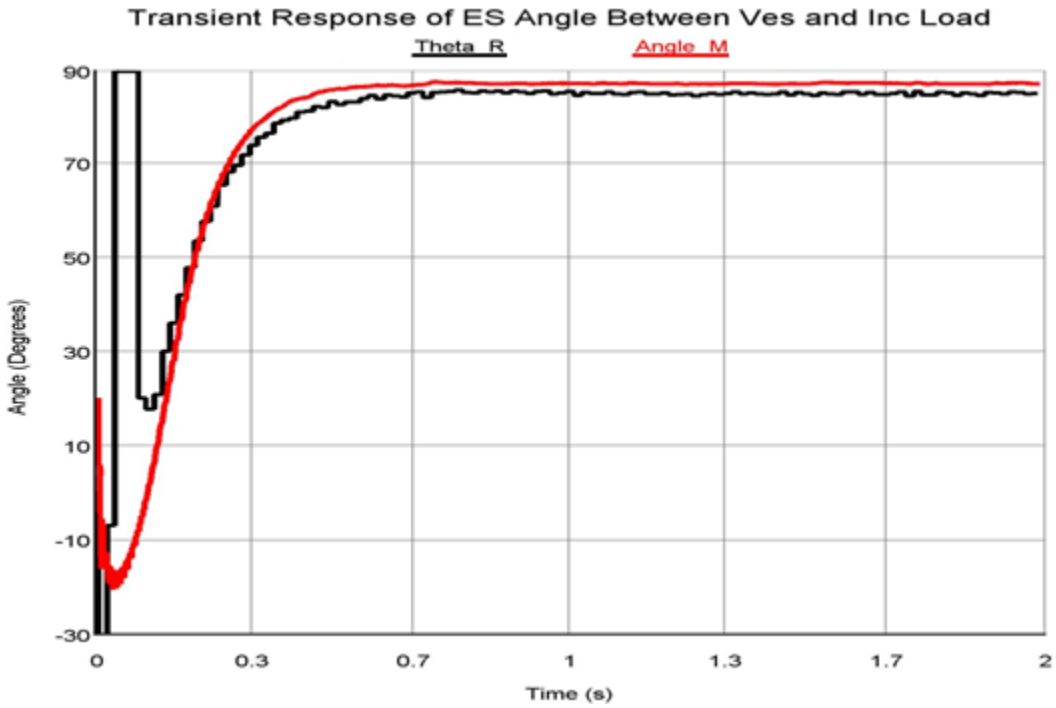

Figure 7-2 Comparison of ES angle difference between Ves and Inc response in sudden change inductive mode

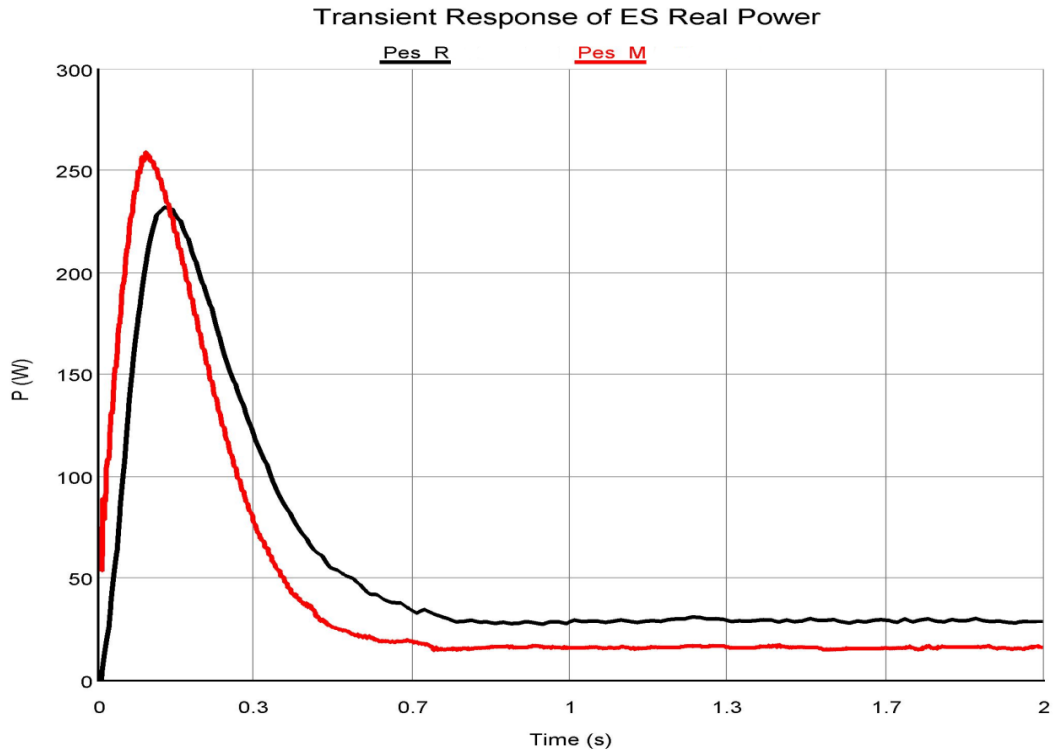

Figure 7-3 Comparison of ES active power response in sudden change inductive mode

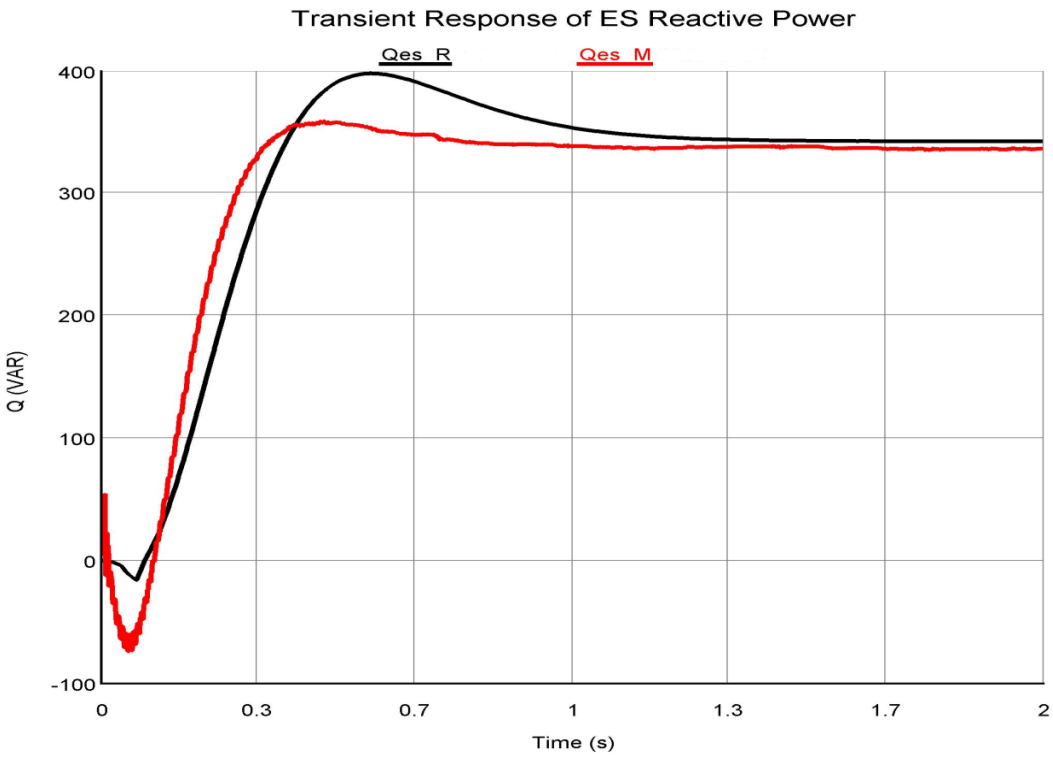

Figure 7-4 Comparison of ES reactive power response in sudden change inductive mode

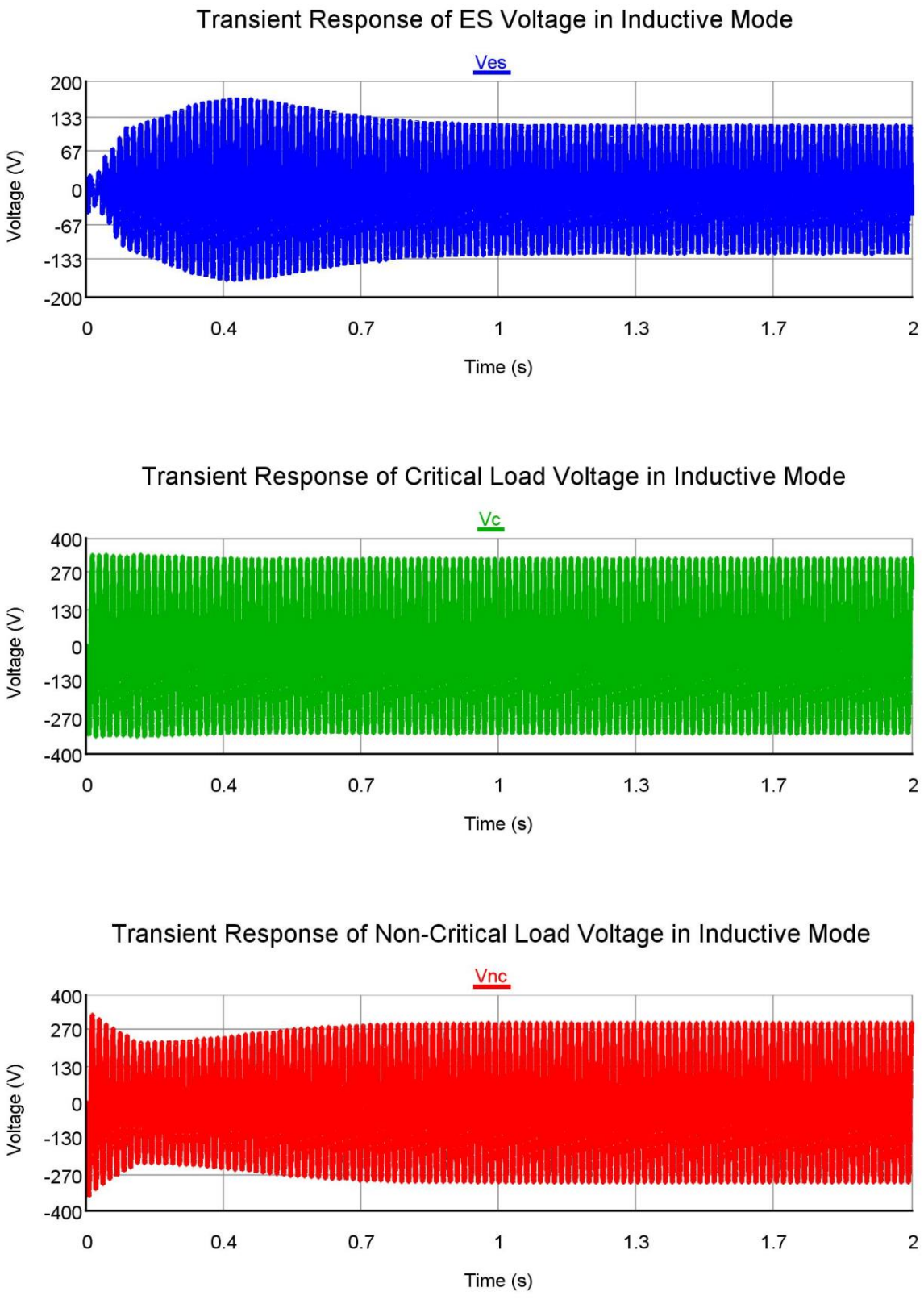

Figure 7-5 ES, critical and non-critical time varying voltage responses in sudden change inductive mode

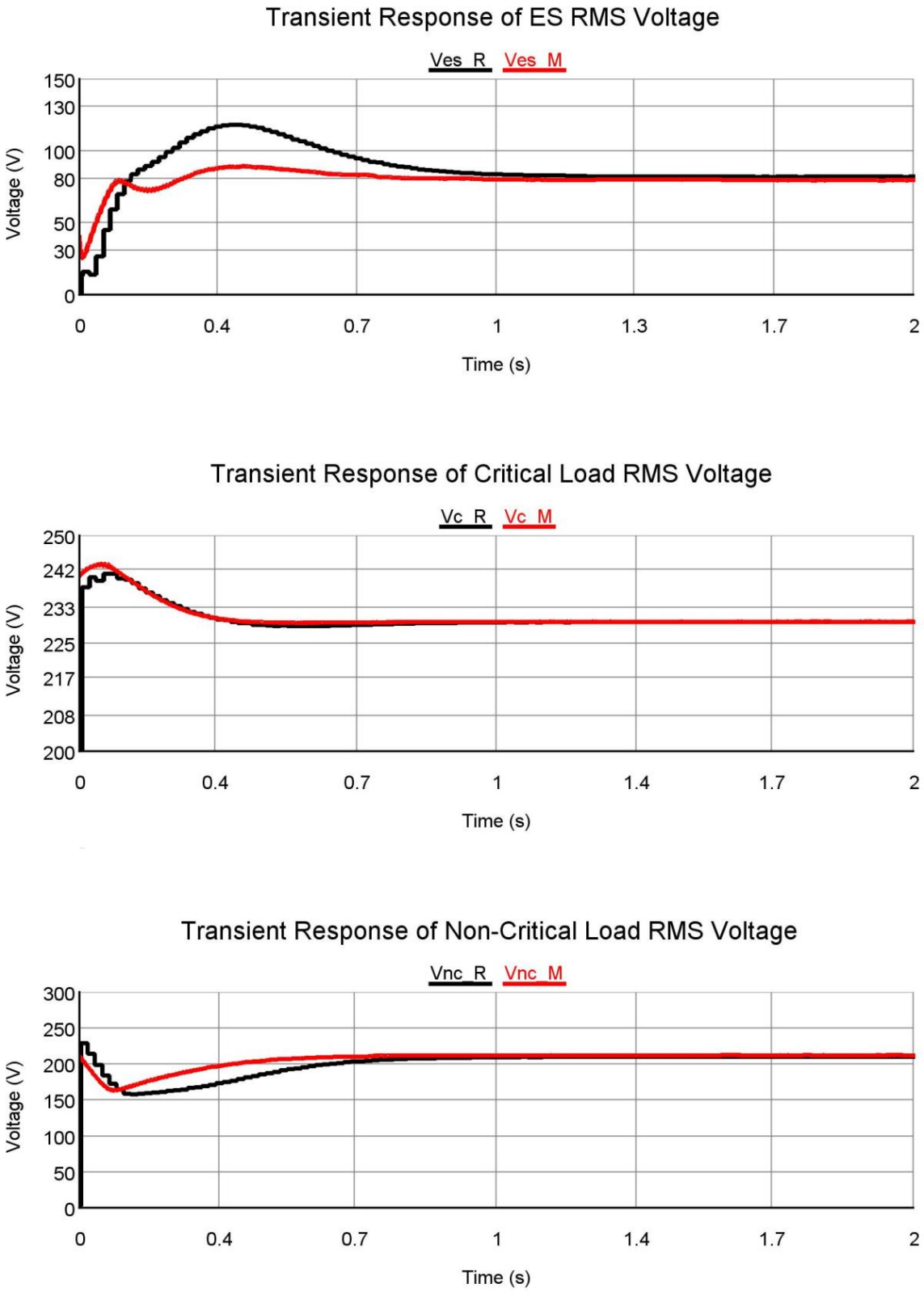

Figure 7-6 ES, critical and non-critical rms voltage responses in sudden change inductive mode

- Electric Spring Capacitive Mode

In this case, ES operates in capacitive mode when the voltage level of the main voltage is less than the nominal value. However, Renewable energy current source generates 0 A. Figure 7-7 to Figure 7-12 describe the sudden change response of the power system in capacitive mode where ES generates sufficient amount of pure reactive power to regulate the main bus.

Figure 7-7and Figure 7-8 show the charging of dc capacitor and the angle difference response between electric spring terminal voltage and non-critical load current. Figure 7-9 and Figure 7-10 show the ES real and reactive power response while Figure 7-11 and Figure 7-12 show the response voltage of ES, critical and non-critical loads respectively. M and R in figures refer to MATLAB and RTDS results respectively.

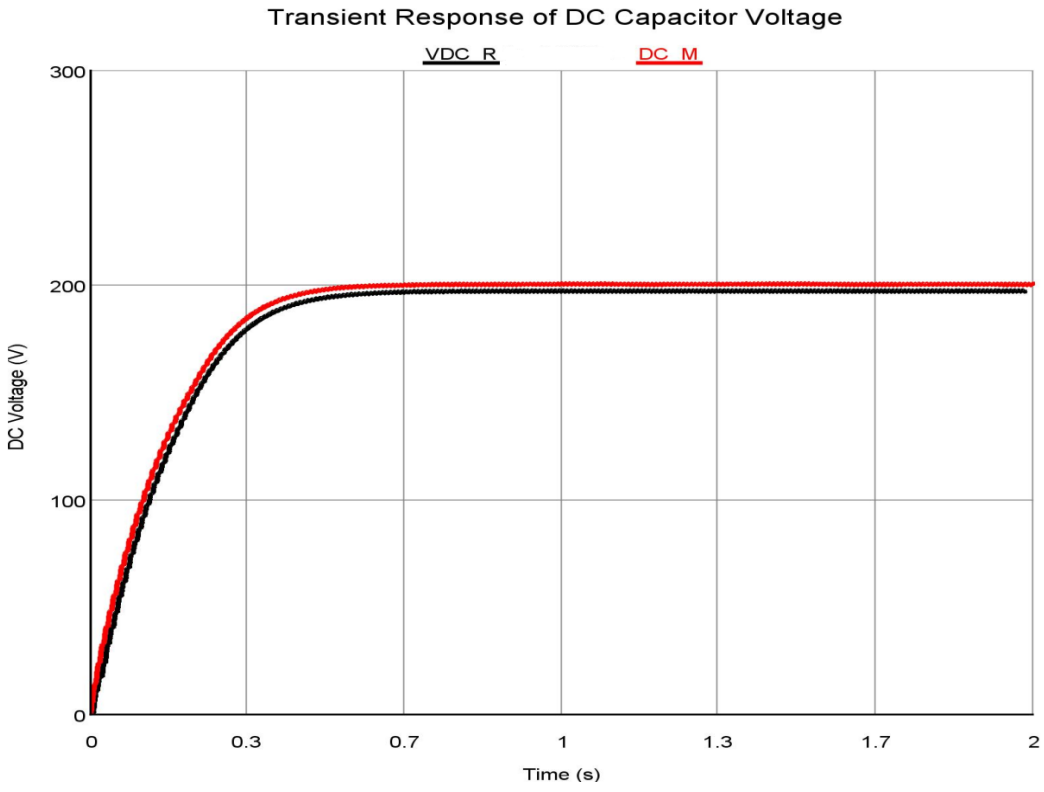

Figure 7-7 Comparison of dc voltage response in sudden change capacitive mode

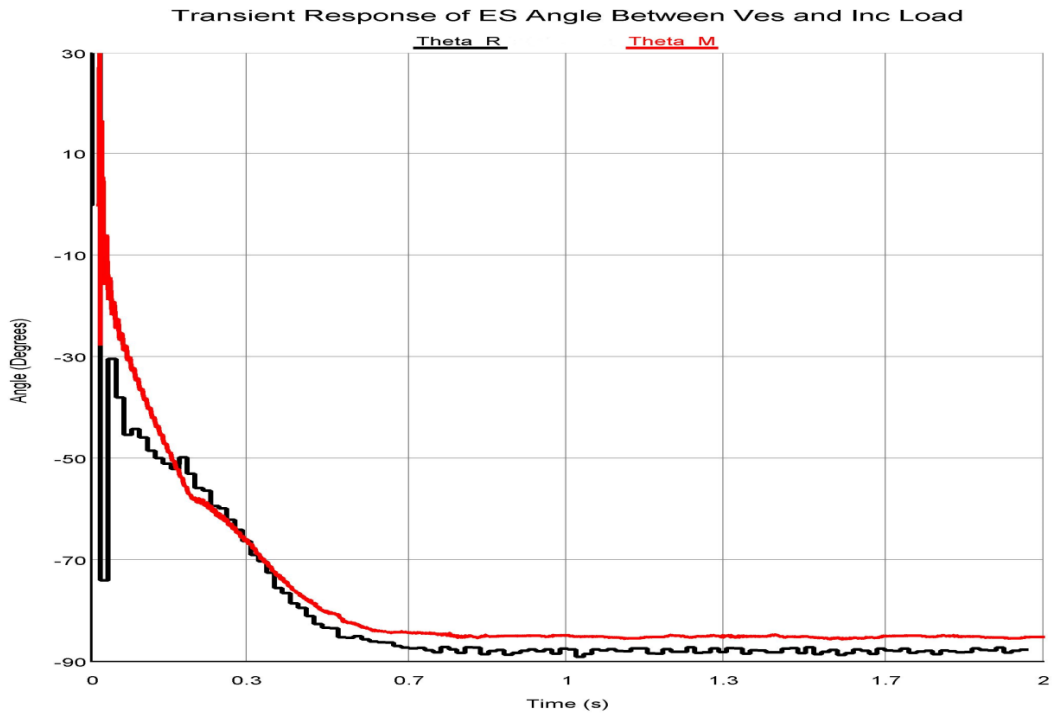

Figure 7-8 Comparison of ES angle difference between Ves and Inc response in sudden change capacitive mode

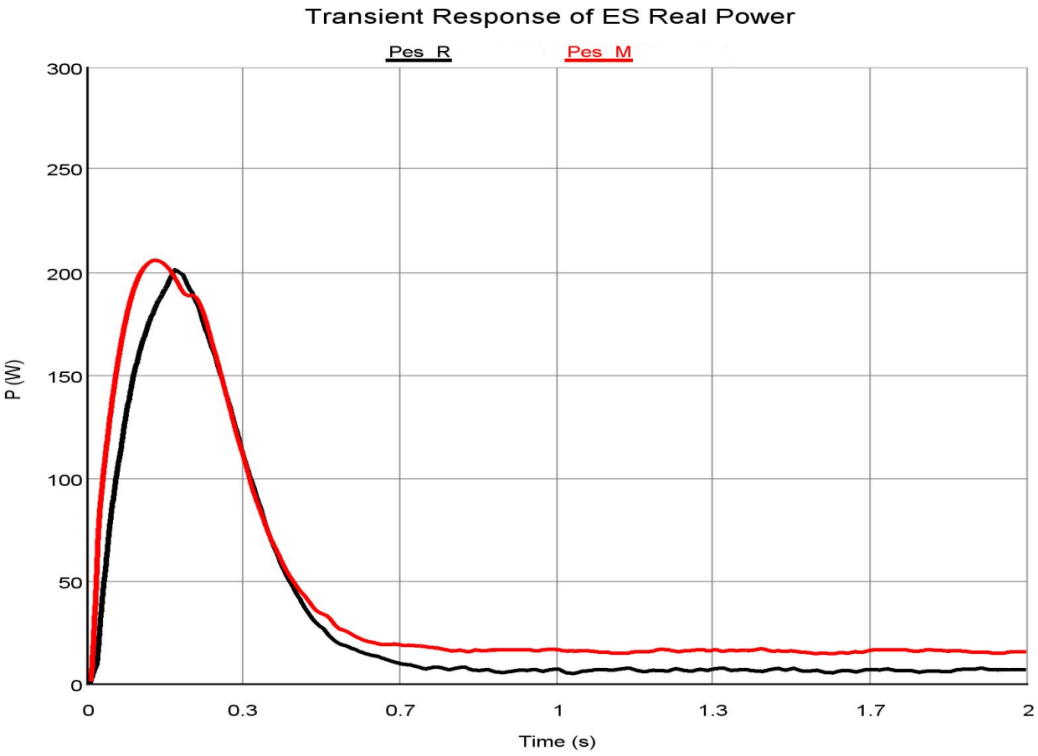

Figure 7-9 Comparison of ES active power response in sudden change capacitive mode

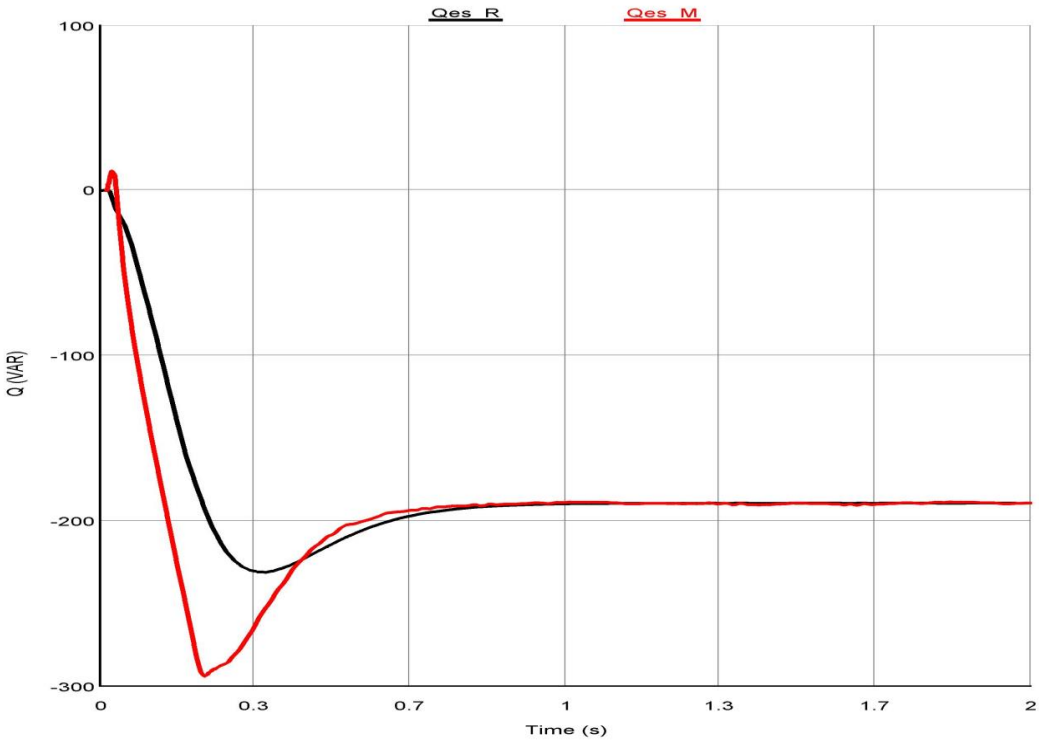

Figure 7-10 Comparison of ES reactive power response in sudden change capacitive mode

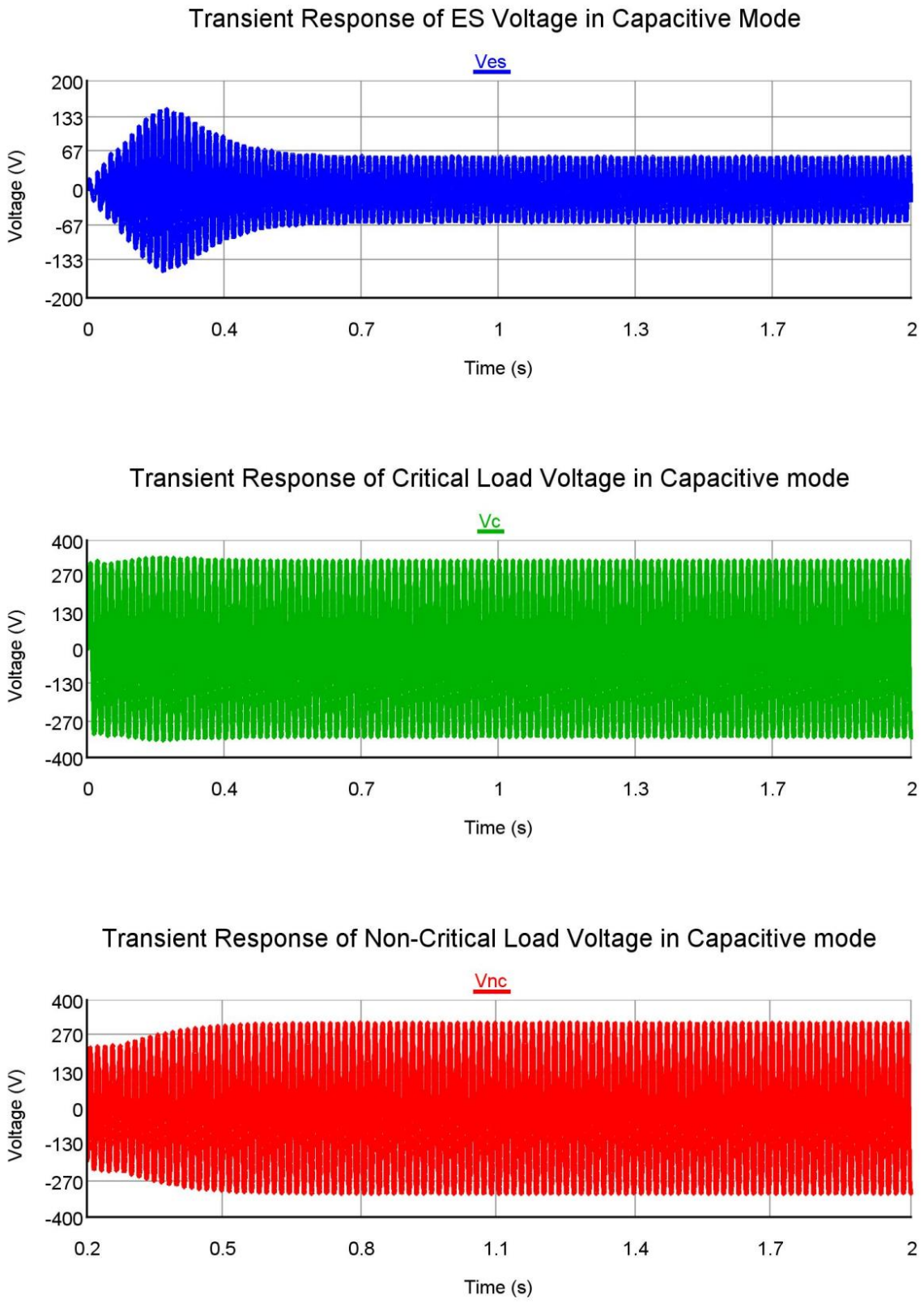

Figure 7-11 ES, critical and non-critical time varying voltage responses in sudden change capacitive mode

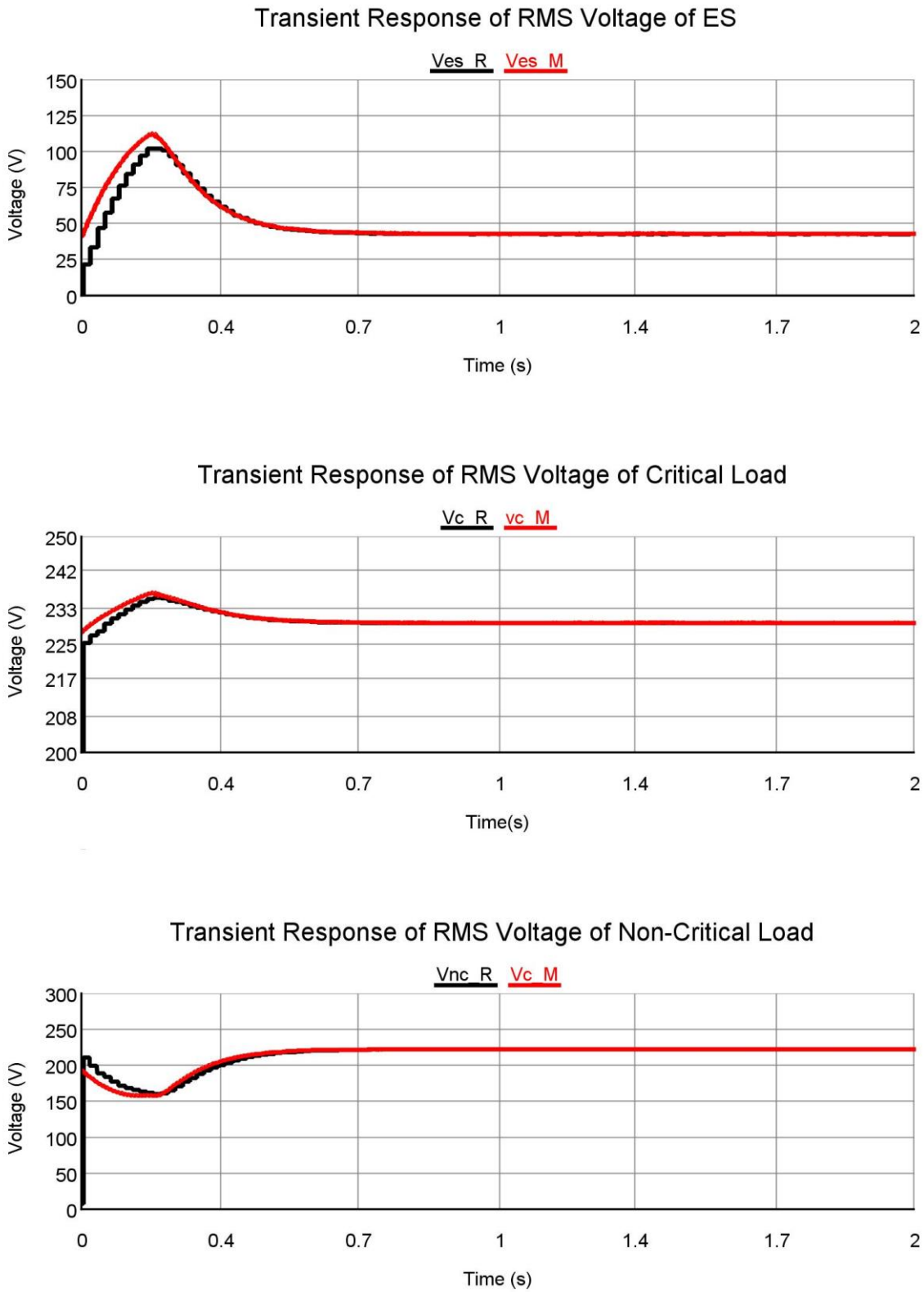

Figure 7-12 ES, critical and non-critical rms voltage responses in sudden change capacitive mode

7.2 Multi Disturbances

Multiple disturbances have been carried out for 7.5s to investigate the performance of the electric spring. As seen in Figure 7-13 to Figure 7-15, the simulation is divided into three time periods. The first period is 1.5s when the ES and current source are deactivated. The second period is extended to 3s when the source current ($\boldsymbol{I_r}$) varies in the range of ($\mathbf{7.5, 0, 11}\ \boldsymbol{A}$ 1s each).

It is noted that the non-critical load voltage ($\boldsymbol{V_c, V_{nc}}$) and power ($\boldsymbol{P_c, P_{nc}}$) are identical. In the last time period, electric spring is enabled and current profile of the renewable energy source is repeated again for 3s. ES starts responding regarding current variation by injection a series voltage compensation. ES operates in different modes to regulate the fluctuated voltage.

The capability of the electric spring for voltage regulation are depicted in Figure 7-13 to Figure 7-15 respectively. Output power of renewable energy source ($\boldsymbol{P_r}$), real power consumption by critical and non-critical load ($\boldsymbol{P_c, P_{nc}}$) and the generated power by the grid connected ($\boldsymbol{P_g}$) are depicted in Figure 7-16 to Figure 7-18 respectively

The output current profile of renewable energy source is repeated again to show the responses of modulation index ($\boldsymbol{M}$), angle difference between electric spring voltage and the non-critical load current ($\boldsymbol{\theta}$) and the reactive power generation by the electric spring ($\boldsymbol{Q_{es}}$) in different modes as depicted in Figure 7-19 to Figure 7-21. M and R in figures refer to MATLAB and RTDS results respectively.

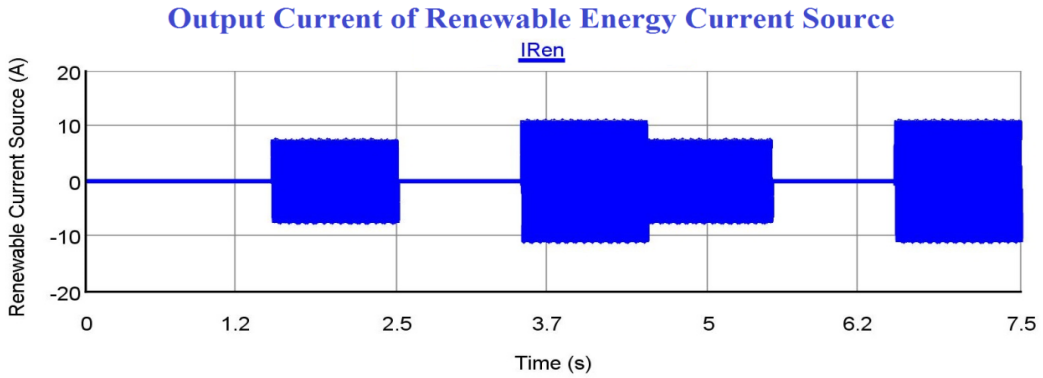

Figure 7-13 Intermittent renewable energy current source in different modes

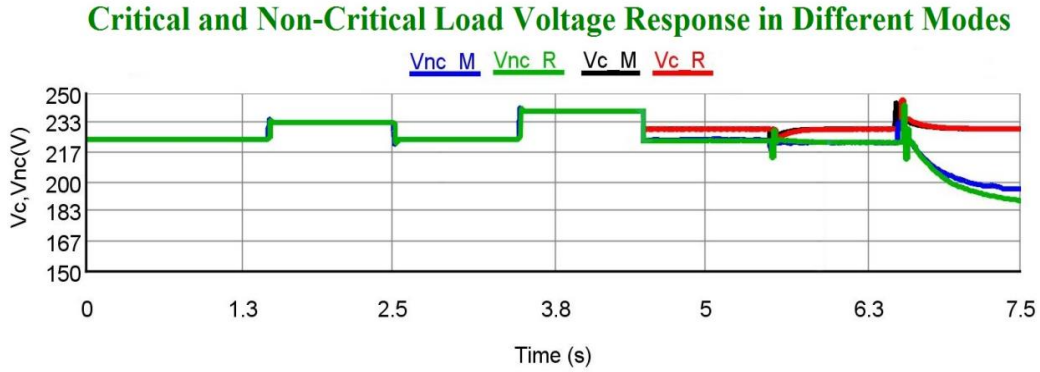

Figure 7-14 Comparison of critical and non-critical load voltage responses in different modes

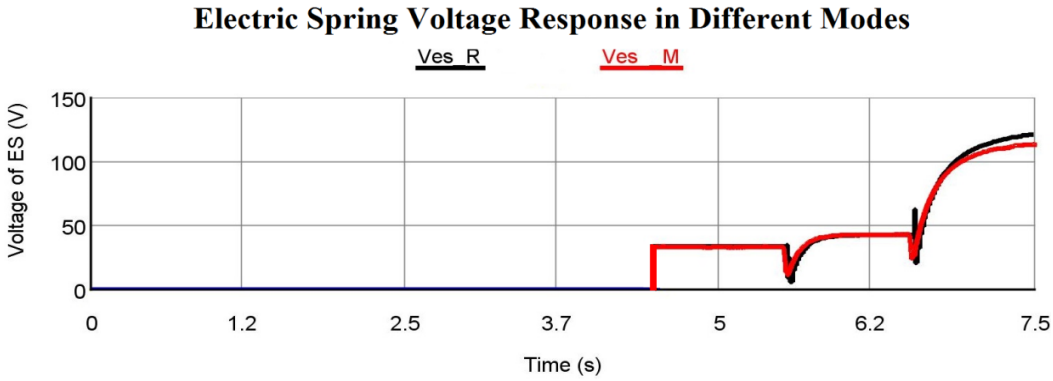

Figure 7-15 Comparison of ES voltage responses in different modes

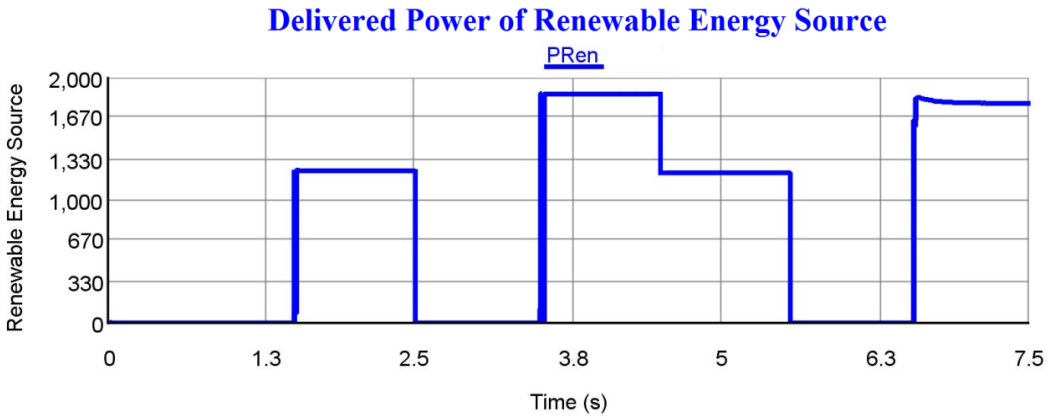

Figure 7-16 Generated reap power of renewable energy current source in different modes

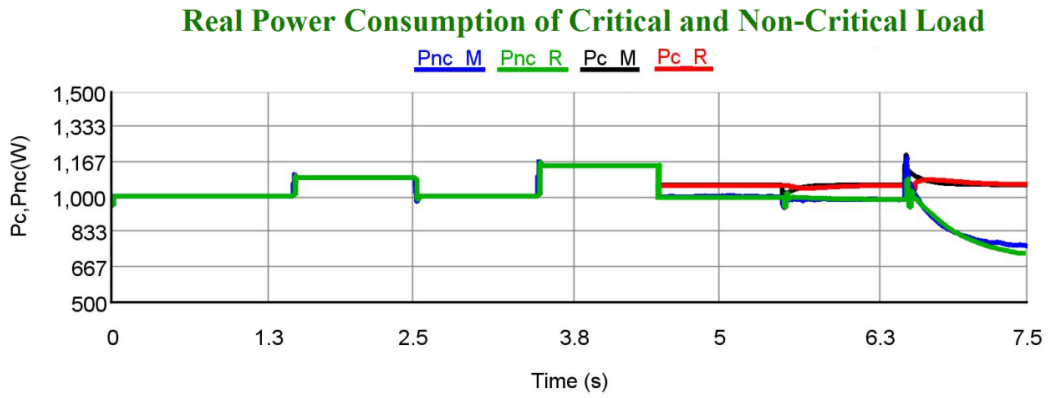

Figure 7-17 Comparison of real power consumption of critical and non-critical load in different modes

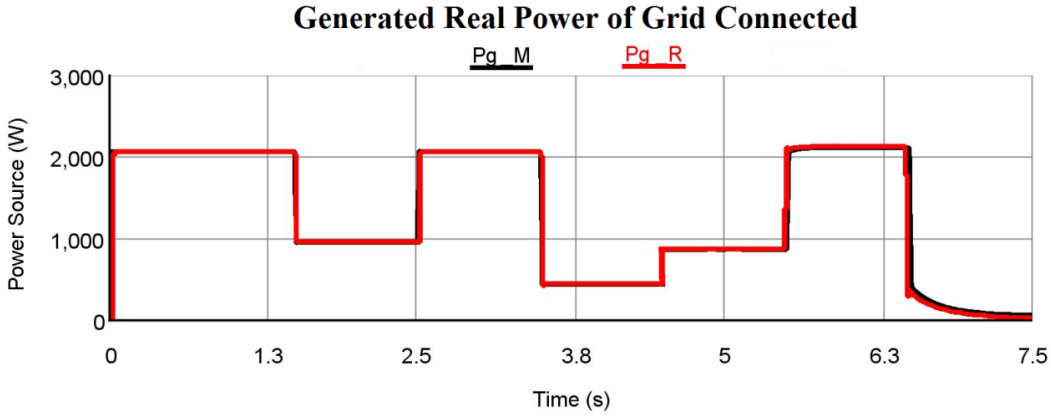

Figure 7-18 Comparison of generated real power of the grid source in different modes

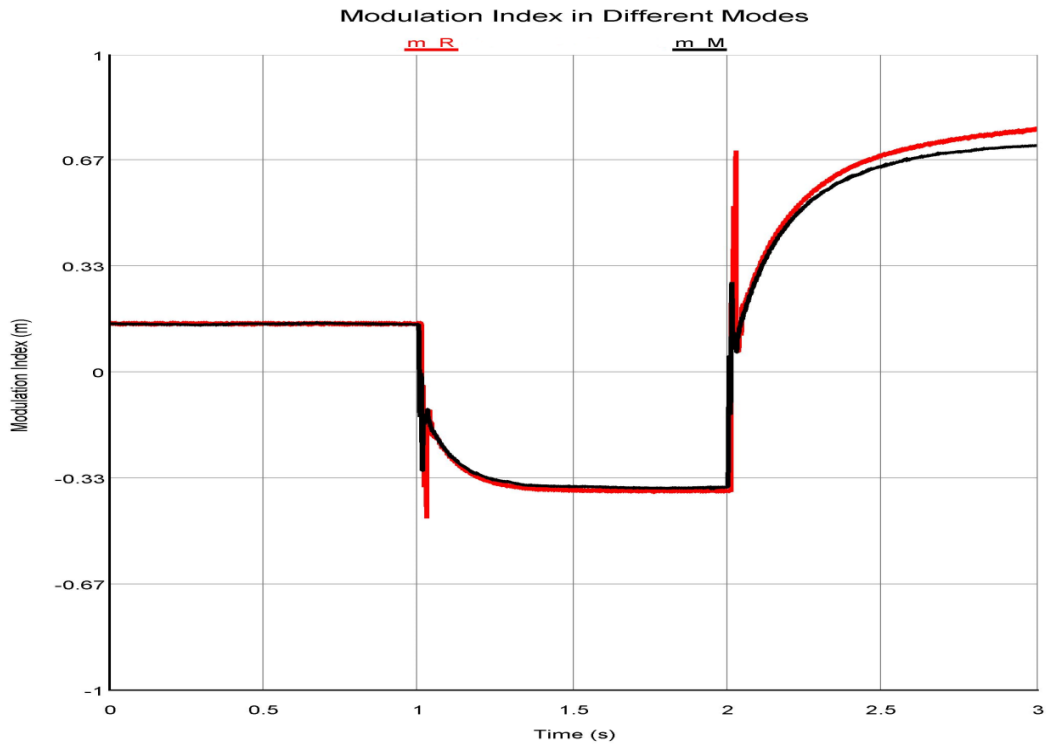

Figure 7-19 Comparison of modulation signal in different modes

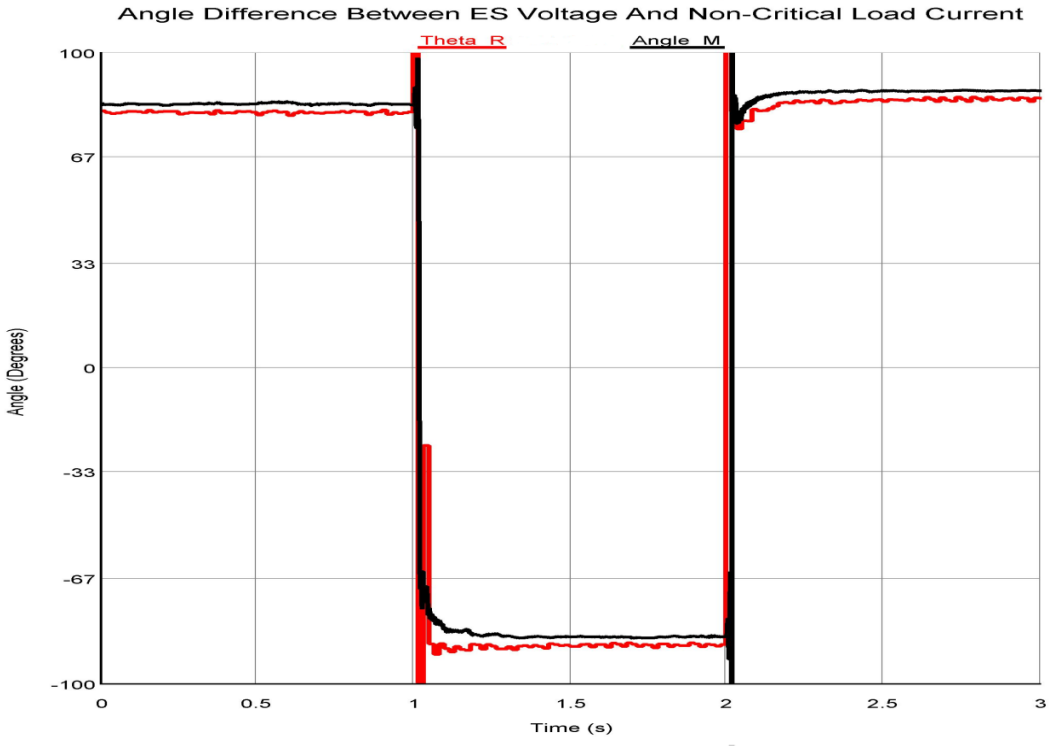

Figure 7-20 Comparison of angle difference between Ves and Inc in different modes

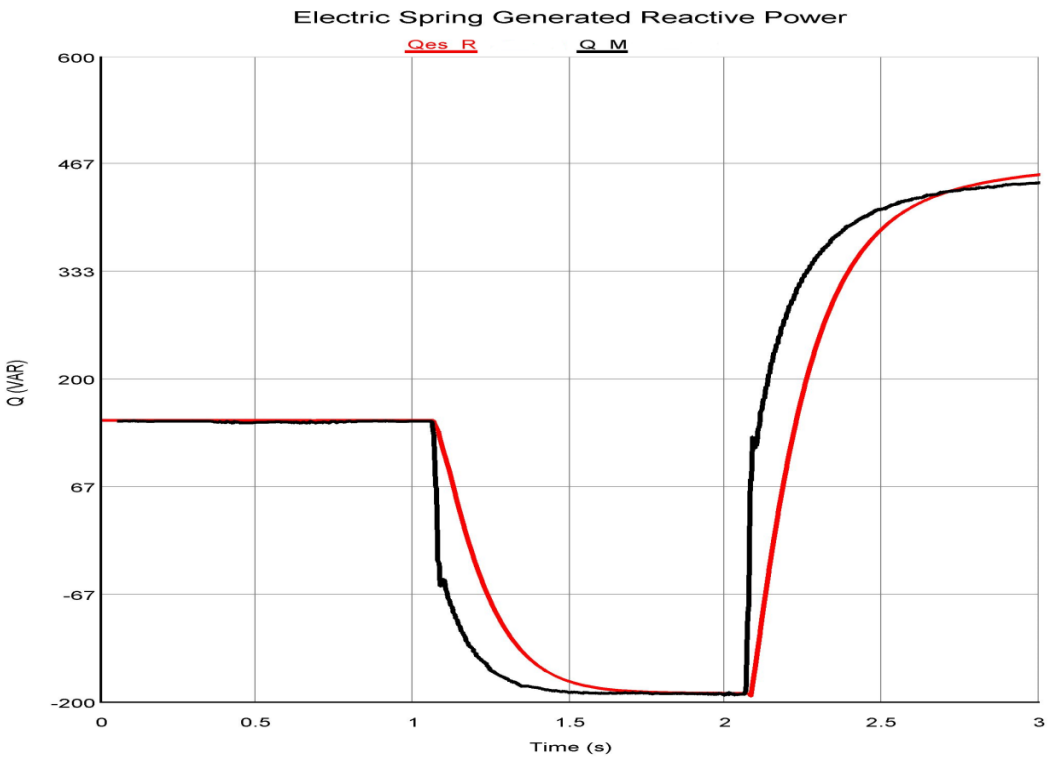

Figure 7-21 Comparison of ES generated reactive power in different modes

7.3 Critical Load Variation

In this case, power system is simulated for two time periods 1s each. The current source injects 10 A. In the second period, critical load is suddenly disturbed by switching on an inductive load $\mathbf{50 + 24\ \Omega}$ with o.9 PF. Therefore, ES will automatically adjust the terminal voltage to regulate the main voltage as seen in Figure 7-22 to Figure 7-24 respectively. M and R in figures refer to MATLAB and RTDS results respectively.

It is noted that the ES voltage is increased higher than the first period. The new inductive load consumes higher amount of reactive power. However, the voltage drop through the distribution feeders will be increased. Therefore, the modulation index of the ES is increased.

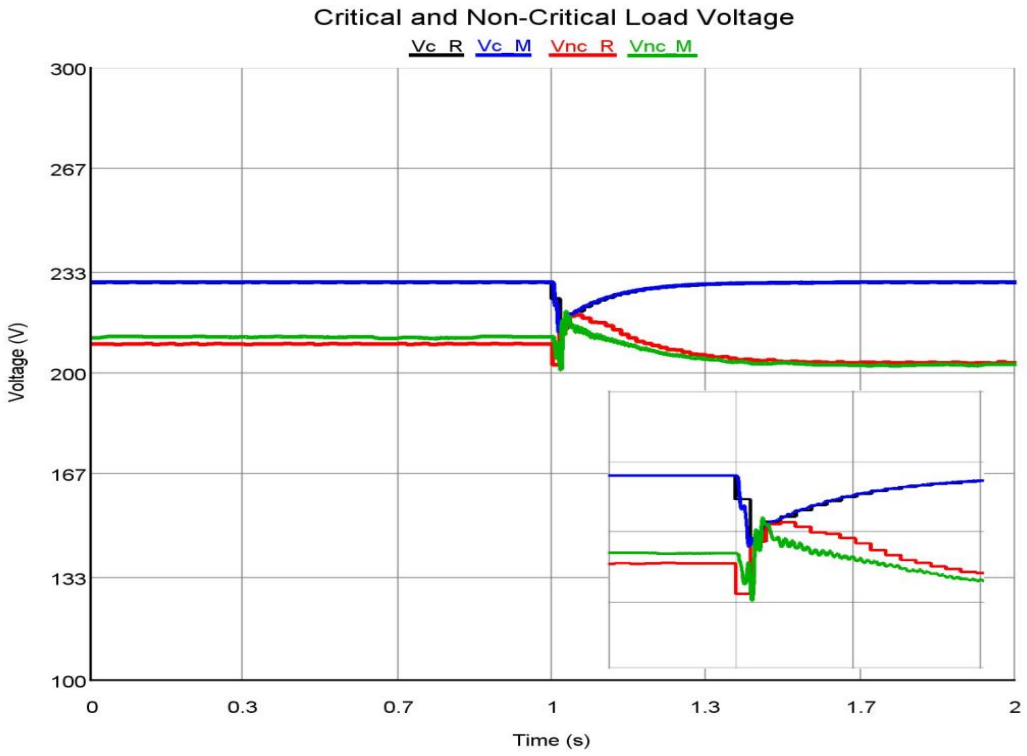

Figure 7-22 Comparison of critical and non-critical load voltage in case of critical load variation

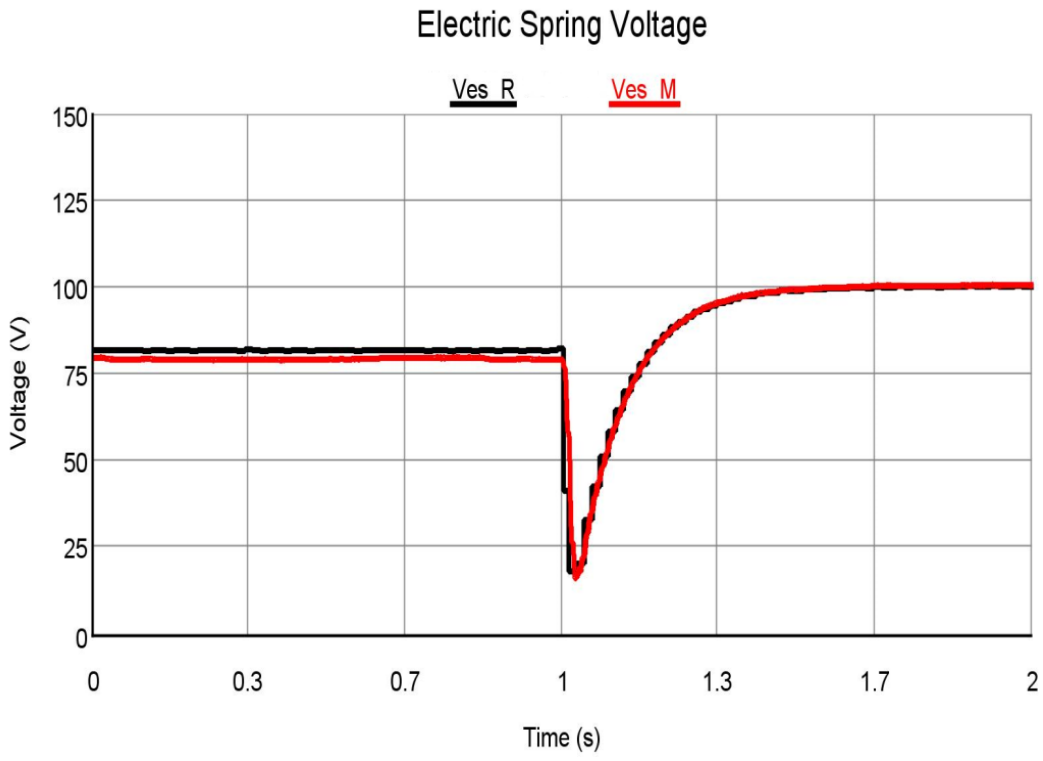

Figure 7-23 Comparison of ES voltage in case of critical load variation

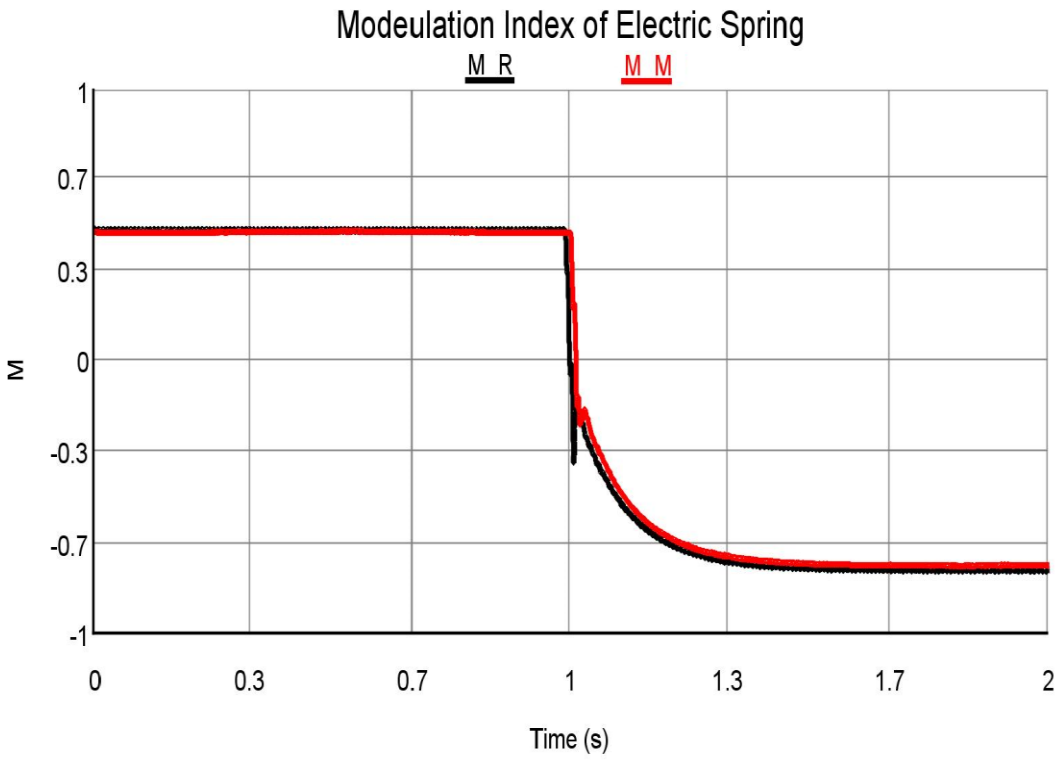

Figure 7-24 Comparison of modulation index signal in case of critical load variation

7.4 Resistive Critical and Non-Critical Load Variation

Simulation is carried out for 3s by varying the resistive critical and non-critical loads. System test simulation is performed for 3 time steps. Each time step is 1s. In the first time period, the critical and non-critical loads are kept constant and it equals 50 Ω each. In the second period, resistive loads are changed by inserting 75 Ω in parallel with non-critical load and 20 Ω in series with critical load. This leads to decrease the non-critical load resistance. On the other hand, the load resistance of critical load is increased. So, non-critical load current is increased and the capacity of ES is improved. Therefore, ES injects a lower voltage at its terminal. In the last time period, 20 Ω resistive load is inserted in series with the non-critical load and 75 Ω is inserted in parallel with the critical load. This leads to increase the non-critical load resistance. On the other hand, the

load resistance of critical load is decreased. This switching leads to limit the ES capacity by decreasing the non-critical load current. So, ES a higher voltage compensation as compared to the previous time step. See Figure 7-25 to Figure 7-27. M and R in figures refer to MATLAB and RTDS results respectively.

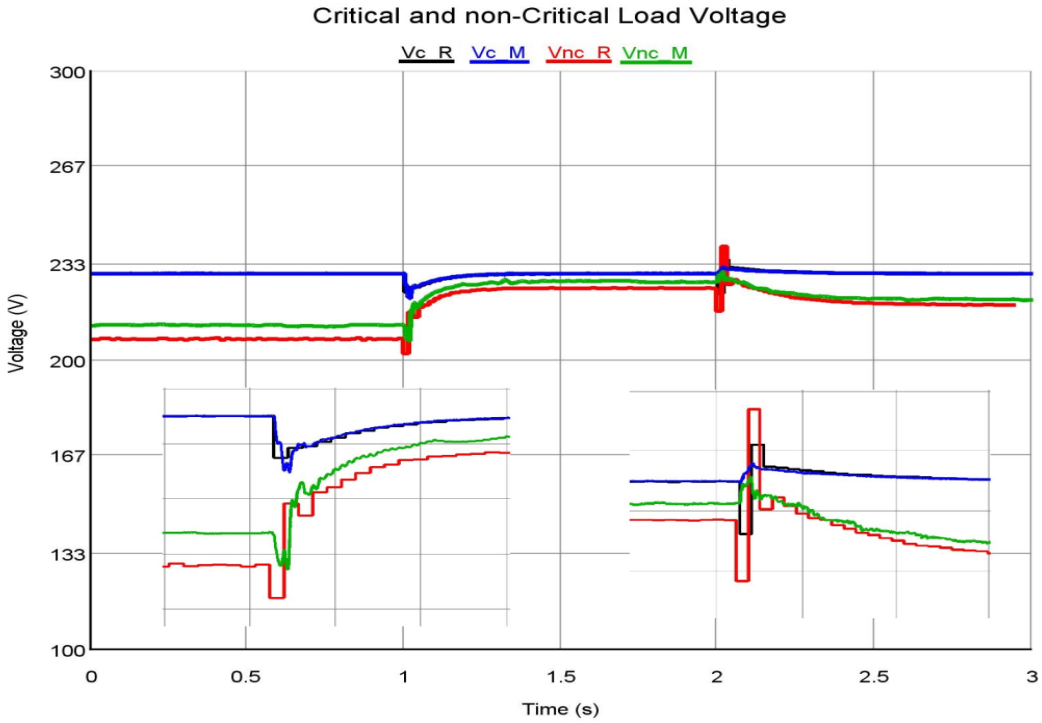

Figure 7-25 Comparison of critical and non-critical load voltages in case of resistive loads variation

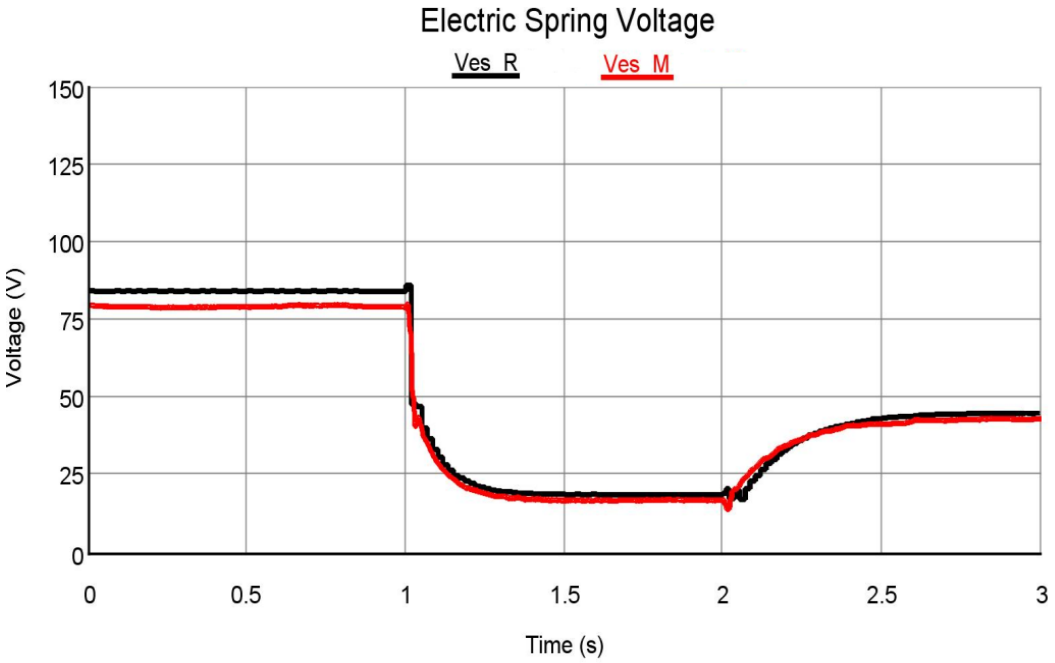

Figure 7-26 Comparison ES voltages in case of resistive loads variation

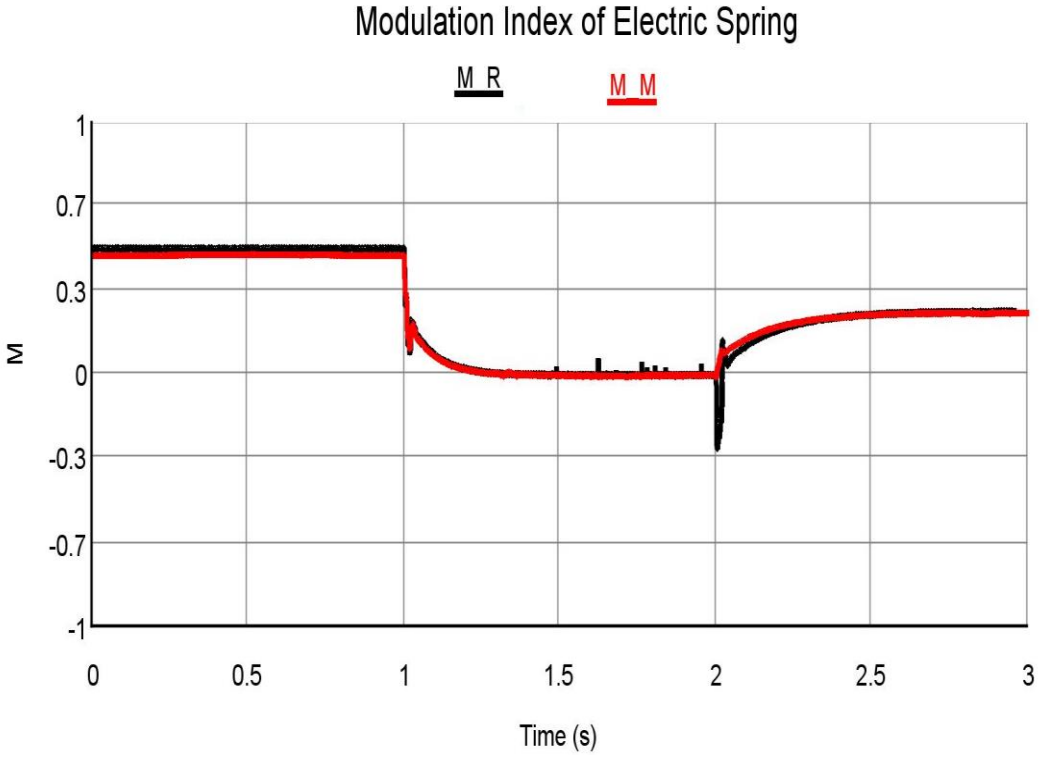

Figure 7-27 Comparison of modulation index signal in case of resistive loads variation

CHAPTER 8

CONCLUSION AND FUTURE WORK

8.1 Conclusion

In this thesis, a new control approach in the distribution system level is proposed as a new technique to demand side management in smart grid area. Electric spring has great potential in stabilizing the future smart grid by regulating the mains voltage despite the fluctuation of the output power of the intermittent renewable energy sources. Therefore, it can be integrated with home appliances allowing the load to follow the intermittent generation of renewable energy sources. Thus, this approach is unlike the previous idea that depends on generating enough energy to meet the requirements of the load demand either completely or partially.

The main achievements of this thesis work can be summarized as follows:

- ES switched model is proposed and implemented to verify the capability of ES to perform the DSM function successfully.
- Nonlinear time-domain based objective function is proposed and optimized using real coded genetic algorithm (RCGA). The optimal parameters of the ac and dc PI voltage controllers have been obtained. Simulation results under different sudden change modes, multiple disturbances and load variation operating conditions have been carried out. The results show the effectiveness of the electric spring as a new approach to demand side management.

- ES averaged model is considered. Derivations of mathematical expressions have been carried out for all components of the system i.e. distribution system, PLL and PI controllers.
- Control parameters of ES averaged model have been well optimized using particle swarm optimization technique (PSO). A non-linear time domain objective function is considered. Power system is optimized in two different cases, when critical and non-critical loads are resistive loads or when these loads are inductive. Runge-Kutta numerical analysis method was used to solve the system.
- Linearizing the power system consisting of distribution system and control.
- Identifying the operating limits of the electric spring after applying different kinds of disturbances and control signal. Limitations are studied when applying different levels of renewable current source variations, modulating signal variations with respect to multiple levels of applied voltages on the point of common coupling where loads are connected, and investigation of ES behavior with different values of power factor.
- ES with the proposed controller are implemented on MATLAB/SIMULINK platform. The corresponding results are compared with those results coming from the experimental setup using Real Time Digital Simulation (RTDS) with hardware in the loop dSPACE 1103 controller.

8.2 Future Work

Several ideas can be addressed as a future work for this thesis:

- ES can be modeled and verified when it is distributed in the smartgrid for one or aggregated loads.

- Integrating a PV system with the power system consisting of the ES to investigate the capability of the ES to mitigate the partial shading effect phenomenon as a new application of the ES.
- The performance of ES can be compared with other demand side management techniques like real time pricing (RTP) and its effects can be investigated accordingly.

APPENDIX

Power system is linearized as follows:

1. Power System Linearization

Linearizing resistive critical and non-critical loads, and power plant equations leads to Eq. (1)-Eq. (4)

$$\Delta \dot{V}_{es} = \left(\frac{1}{C_f}\right) * \Delta I_{inj} + \left(\frac{R_c}{C_f * (R_c + R_{nc})}\right) * \Delta I_d - \left(\frac{1}{(R_c + R_{nc}) * C_f}\right) * \Delta V_{es} \quad (1)$$

$$\Delta \dot{I}_{inj} = -\left(\frac{R_f}{L_f}\right) * \Delta I_{inj} + \left(\frac{m}{L_f}\right) * \Delta V_{dc} + \left(\frac{V_{dc}}{L_f}\right) * \Delta m - \left(\frac{1}{L_f}\right) * \Delta V_{es} \quad (2)$$

$$\Delta \dot{V}_{dc} = \left(\frac{2R_f}{C_{dc}} * \frac{\dot{I}_{inj}}{V_{dc}}\right) \Delta I_{inj} - \left(\frac{R_f}{C_{dc}} * \frac{I^2{}_{inj}}{V^2{}_{dc}}\right) \Delta V_{dc} \quad (3)$$

$$\Delta \dot{I}_d = \left(\frac{1}{L_s + L_d + L_g}\right)\left(-\left(R_g + R_s + R_d + \frac{R_c * R_{nc}}{R_c + R_{nc}}\right)\Delta I_d - \left(\frac{R_c}{R_c + R_{nc}}\right)\Delta V_{es} + \left(R_g + R_s\right)\Delta I_r + \left(L_g + L_s\right)\Delta \dot{I}_r + \Delta V_g\right) \quad (4)$$

2. Single Phase Phase Locked Loop Linearization (PLL)

Linearizing Phase locked loop (PLL) gives

$$\Delta \dot{q}_v = w * \Delta V_1 + V_1 * \Delta w \quad (5)$$

$$\Delta \dot{V}_1 = -w * \Delta q_v \pm w * \Delta V_1 + (I_{nc} - V_1 - q_v) * \Delta w + w * \Delta I_{nc} \quad (6)$$

$$\Delta\dot{w} = Ki * sin(\theta) * \Delta q_v + cos(\theta) * (K_i - K_p * w) * \Delta V_1 + [K_i * qv * cos(\theta) - K_i * V_1 * sin(\theta) - Inc * K_p * w * sin(\theta) + K_p * V_1 * w * sin(\theta)]\Delta\theta + K_p * cos(\theta) * (Inc - V_1)\Delta w + K_p * w * cos(\theta)\,\Delta\, I_{nc} \quad (7)$$

$$\Delta\dot{\theta} = \Delta w \quad (8)$$

To replace I_{nc} in term of state variables, the following Eq. (9)- Eq. (12) can be written

$$I_{nc} = I_{es} - I_{inj} \quad (9)$$

$$I_{nc} = C_f * \dot{V}_{es} - I_{inj} \quad (10)$$

$$\Delta I_{nc} = C_f * \Delta\dot{V}_{es} - \Delta I_{inj} \quad (11)$$

$$\Delta I_{nc} = \left(\frac{R_c}{R_c + R_{nc}}\right) * \Delta I_d - \left(\frac{1}{R_c + R_{nc}}\right) * \Delta V_{es} \quad (12)$$

Replacing I_{nc} in Eq. (6) and Eq. (7) by Eq. (12)

$$\Delta\dot{V}_1 = -w * \Delta q_v + -w * \Delta V_1 + \left(-V_1 - qv - \left(\frac{V_{es} - I_d * R_c}{R_c + Rnc}\right)\right) * \Delta w + \left(\frac{R_c * w}{R_c + R_{nc}}\right)\Delta I_d + \left(\frac{-w}{R_c + R_{nc}}\right)\Delta V_{es} \quad (13)$$

$$\Delta\dot{w} = Ki * sin(\theta) * \Delta q_v + cos(\theta) * (K_i - K_p * w) * \Delta V_1 + \left[\left(\frac{\left(K_p * w * \sin(\theta) * (V_{es} + R_c * V_1 + R_{nc} * V_1 - I_d * R_c)\right)}{(R_c + R_{nc})}\right) - K_i * (V_1 * \sin(\theta) - qv * \cos(\theta))\right]\Delta\theta + \left[K_p * cos(\theta) * (I_d - V_1) - \left(\frac{\left(K_p * \cos(\theta) * (V_{es} + I_d * R_{nc})\right)}{(R_c + R_{nc})}\right)\right]\Delta w + \left[\left(\frac{\left(K_p * R_c * w * \cos(\theta)\right)}{(R_c + R_{nc})}\right)\right]\Delta I_d + \left[\left(\frac{-\left(K_p * w * \cos(\theta)\right)}{(R_c + R_{nc})}\right)\right]\Delta V_{es} \quad (14)$$

3. Controller Linearization

The linearization have also been done for Controller as written in Eq. (15) - Eq. (17)

- DC Controller:

$$\Delta\dot{m}_1 = -\left[\frac{2 * I_{inj} * K_{pdc} * R_f * \sin(\theta)}{C_{dc} * V_{dc}}\right]\Delta I_{inj} + \left[\left(\frac{{I_{inj}}^2 * K_{pdc} * R_f * \sin(\theta)}{C_{dc} * {V_{dc}}^2}\right) - K_{idc} * \sin(\theta)\right]\Delta V_{dc} + \left[-\left(\frac{{I_{inj}}^2 * K_{pdc} * R_f * \cos(\theta)}{C_{dc} * V_{dc}}\right) + V_{dcref} * K_{idc} * \cos(\theta) - K_{idc} * V_{dc} * \cos(\theta)\right]\Delta\theta \quad (15)$$

- Full Controller:

$$\dot{m} = cos(theta) * ((3 * Kpac * Rc\text{^}4 * Rnc * ((Vg + Irdot * (L1 + Lg) + Ir * (R1 + Rg) - I2 * (R1 + R2 + Rg) - (Rc * (Ves + I_d * Rnc))/(Rc + Rnc))/(L1 + L2 + Lg) + (I_d * Rc - Ves + Iinj * Rc + Iinj * Rnc)/(Rnc * cf * (Rc + Rnc))) * (Ves + I2 * Rnc)\text{^}2)/(T * VcRMS * (Rc + Rnc)\text{^}4) - (Kpac * Rc\text{^}4 * (Ves + I_d * Rnc)\text{^}3 * (L1 + L2 + Lg + Rc * Rnc * cf))/(T * VcRMS * cf * (Rc + Rnc)\text{^}5 * (L1 + L2 + Lg))) \Delta V_{es}$$

$$+((Kpac * Rc\text{^}4 * cos(theta) * (Ves + I_d * Rnc)\text{^}3)/(T * VcRMS * cf * (Rc + Rnc)\text{^}4) - (2 * Iinj * Kpdc * Rf * sin(theta))/(Cdc * Vdc)) \Delta I_{inj}$$

$$+\left(-sin(theta) * \left(Kidc - \frac{Iinj^2 * Kpdc * Rf}{Cdc * Vdc^2}\right)\right) \Delta V_{dc}$$

$$+(cos(theta) * ((3 * Kpac * Rc\text{^}4 * Rnc\text{^}2 * ((Vg + Irdot * (L1 + Lg) + Ir * (R1 + Rg) - I_d * (R1 + R2 + Rg) - (Rc * (Ves + I_d * Rnc))/(Rc + Rnc))/(L1 + L2 + Lg) + (I2 * Rc - Ves + Iinj * Rc + Iinj * Rnc)/(Rnc * cf * (Rc + Rnc))) * (Ves + I2 * Rnc)\text{^}2)/(T * VcRMS * (Rc + Rnc)\text{^}4) - (Kpac * Rc\text{^}4 * Rnc * (Ves + I_d * Rnc)\text{^}3 * ((R1 * Rc + R2 * Rc + R1 * Rnc + R2 * Rnc + Rc * Rg + Rc * Rnc + Rg * Rnc)/((Rc + Rnc) * (L1 + L2 + Lg)) - Rc/(Rnc * cf * (Rc + Rnc))))/(T * VcRMS * (Rc + Rnc)\text{^}4))) \Delta I_{d2}$$

$$+(cos(theta) * (Kiac - (Kpac * Rc\text{^}4 * Rnc * ((Vg + Irdot * (L1 + Lg) + Ir * (R1 + Rg) - I_d * (R1 + R2 + Rg) - (Rc * (Ves + I_d * Rnc))/(Rc + Rnc))/(L1 + L2 + Lg) + (I2 * Rc - Ves + Iinj * Rc + Iinj * Rnc)/(Rnc * cf * (Rc + Rnc))) * (Ves + I_d * Rnc)\text{^}3)/(T * VcRMS\text{^}2 * (Rc + Rnc)\text{^}4))) \Delta VcRMS$$

$$+ \text{ (- sin(theta)} * (Kiac * VcRMS - Kiac * Vcref + (Kpac * Rc\text{^}4 * Rnc * ((Vg + Irdot * (L1 + Lg) + Ir * (R1 + Rg) - I_d * (R1 + R2 + Rg) - (Rc * (Ves + I_d * Rnc))/(Rc + Rnc))/(L1 + L2 + Lg) + (I_d * Rc - Ves + Iinj * Rc + Iinj * Rnc)/(Rnc * cf * (Rc + Rnc))) * (Ves + I2 * Rnc)\text{^}3)/(T * VcRMS * (Rc + Rnc)\text{^}4)) - (cos(theta) * (Kpdc * Rf * Iinj\text{^}2 + Cdc * Kidc * Vdc\text{^}2 - Cdc * Kidc * Vdcref * Vdc))/(Cdc * Vdc)) \Delta\theta$$

$$+ ((Kpac * cos(theta) * (R1 + Rg) * (I_d + Ves/Rnc)\text{^}3)/(T * VcRMS * (1/Rc + 1/Rnc)\text{^}4 * (L1 + L2 + Lg))) \Delta I_R$$

$$+ ((Kpac * cos(theta) * (I_d + Ves/Rnc)\text{^}3 * (L1 + Lg))/(T * VcRMS * (1/Rc + 1/Rnc)\text{^}4 * (L1 + L2 + Lg))) \Delta \dot{I}_r$$

$$+ ((Kpac * cos(theta) * (I2 + Ves/Rnc)\text{^}3)/(T * VcRMS * (1/Rc + 1/Rnc)\text{^}4 * (L1 + L2 + Lg))) \Delta V_g \quad (16)$$

$$* \dot{V}_{cRMS} = ((3 * Rc\text{^}4 * Rnc * ((Vg + Irdot * (L1 + Lg) + Ir * (R1 + Rg) - I2 * (R1 + R2 + Rg) - (Rc * (Ves + I_d * Rnc))/(Rc + Rnc))/(L1 + L2 + Lg) + (I_d * Rc - Ves + Iinj * Rc + Iinj * Rnc)/(Rnc * cf * (Rc + Rnc))) * (Ves + I_d * Rnc)\text{^}2)/(T * VcRMS * (Rc + Rnc)\text{^}4) - (Rc\text{^}4 * (Ves + I_d * Rnc)\text{^}3 * (L1 + L2 + Lg + Rc * Rnc * cf))/(T * VcRMS * cf * (Rc + Rnc)\text{^}5 * (L1 + L2 + Lg)))\Delta V_{es} + ((Rc\text{^}4 * (Ves + I_d * Rnc)\text{^}3)/(T * VcRMS * cf * (Rc + Rnc)\text{^}4))\ \Delta I_{inj} + ((3 * Rc\text{^}4 * Rnc\text{^}2 * ((Vg + Irdot * (L1 + Lg) + Ir * (R1 + Rg) - I_d * (R1 + R2 + Rg) - (Rc * (Ves + I_d * Rnc))/(Rc + Rnc))/(L1 + L2 + Lg) + (I_d * Rc - Ves + Iinj * Rc + Iinj * Rnc)/(Rnc * cf * (Rc + Rnc))) * (Ves + I_d * Rnc)\text{^}2)/(T * VcRMS * (Rc + Rnc)\text{^}4) - (Rc\text{^}4 * Rnc * (Ves + I_d * Rnc)\text{^}3 * ((R1 * Rc + R2 * Rc + R1 * Rnc + R2 * Rnc + Rc * Rg + Rc * Rnc + Rg * Rnc)/((Rc + Rnc) * (L1 + L2 + Lg)) - Rc/(Rnc * cf * (Rc + Rnc))))/(T * VcRMS * (Rc + Rnc)\text{^}4))\Delta I_2$$

$$+ \quad -(Rc\text{^}4 * Rnc * ((Vg + Irdot * (L1 + Lg) + Ir * (R1 + Rg) - I_d * (R1 + R2 + Rg) - (Rc * (Ves + I_d * Rnc))/(Rc + Rnc))/(L1 + L2 + Lg) + (I_d * Rc - Ves + Iinj * Rc + Iinj * Rnc)/(Rnc * cf * (Rc + Rnc))) * (Ves + I_d * Rnc)\text{^}3)/(T * VcRMS\text{^}2 * (Rc + Rnc)\text{^}4)\Delta VcRMS$$

$$+ \quad (((R1 + Rg) * (I_d + Ves/Rnc)\text{^}3)/(T * VcRMS * (1/Rc + 1/Rnc)\text{^}4 * (L1 + I_d + Lg)))\Delta IR$$

$$+((I_d + Ves/Rnc)\text{^}3 * (L1 + Lg))/(T * VcRMS * (1/Rc + 1/Rnc)\text{^}4 * (L1 + L2 + Lg))\Delta \dot{I}R$$

$$+((I_d + Ves/Rnc)\text{^}3/(T * VcRMS * (1/Rc + 1/Rnc)\text{^}4 * (L1 + L2 + Lg)))\Delta Vg$$

(17)

It can be concluded that the Eigen value approach for this type of controller is not suitable for an optimization technique because the complexity comes from the RMS block. It is clearly shown how much complexity the system is.

References

[1] T. Longenthiran, D. Srinivasan, and T. Z. Shun, "Demand Side Management in Smart Grid Using Heuristic Optimization, " IEEE Transaction on Smart Grid, vol. 3, no. 3, pp 1244-1252, sep. 2012.

[2] Q. Li, and M. Zhou, "The future-oriented grid-smart grid, "J. Comput., vol. 6, no. 1, pp. 98–105, 2011.

[3] J. Lu, D. Xie, and Q Ai, "Research on Smart Grid in China, " IEEE T&D Asia, pp 1-4, 2009.

[4] D. G. Hart, "Using AMI to Realize the Smart Grid, " IEEE Power and Energy Society General Meeting – Conversion and Delivery of Electrical Energy in 21st Century, pp. 1-2, 2008.

[5] S. Massoud Amin, and B.F. Wollenberg, "Toward a Smart Grid: power delivery for the 21st century, " IEEE Power and Energy Magazine, vol. 3, no. 5, pp. 34-41, Sept.-Oct. 2005.

[6] F. Xi , M. Satyajayant, X. Guoliang, and Y. Dejun, "Smart Grid – The New and Improved Power Grid: A Survey, " IEEE, Communications Surveys & Tutorials, vol. 14, no. 4, pp 944-980, 2012.

[7] S. Rahman, and Rinaldy, "An efficient load model for analyzing demand side management impacts, " IEEE Transactions on Power Systems, vol. 8, no. 3, pp 1219-1226, 1993.

[8] M.J. Edvinsson, and M.O. Nilsson, "Integrating Load Management with Supply-side Operation, " IEEE Trans. On Power Systems, vol. 2, no. 3, Aug. 1987.

[9] C.W. Gellings, and W.M. Smith, "Integrating Demand Side Management into Utility Planning", Proceedings of IEEE, vol. 77, no. 6, June 1989.

[10] E. Hirst, and C. Goldman, "Key issues in Integrated Resource, Planning for Electric Utilities, " IEEE Trans. on Power Systems, vol. 5, November 1990.

[11] M. Pedrasa, T. D. Spooner, and I. F. MacGill, "Scheduling of demand side resources using binary particle swarm optimization," IEEE Trans. Power Syst., vol. 24, no. 3 , pp.1173–1181, 2009.

[12] G. M. Masters, Renewable and Efficient Electric Power Systems, Hoboken, NJ: Wiley, 2004, pp. 291.

[13] A. I. Cohen, and C. C. Wang, "An optimization method for load management scheduling," IEEE Trans. Power Syst., vol. 3, no. 2, pp. 612-618, May 1988.

[14] C. D. Vournas, "Interruptible load as a competitor to local generation, for preserving voltage security," in Proc. 2001 IEEE Power Enf. Soc. Winter Meeting, vol. 1,pp. 236-240.

[15] S. H. Huang, C. Gonzales-Perez, J. Dumas, and W. J. Lee, "Grid security, through load reduction in the ERCOT market," in Proc. 2007 IEEE Industry Applications Conf., New Orleans, LA, pp. 1082–1086.

[16] C. D. Vournas, "Interruptible load as a competitor to local generation for preserving voltage security," in Proc. IEEE Power Eng. Soc. Winter Meeting, vol. 1, pp. 236–240, 2001.

[17] S. H. Huang, C. Gonzales-Perez, J. Dumas, and W. J. Lee, "Grid security through load reduction in the ERCOT market," IEEE Industry Applications Conf., New Orleans, LA, pp. 1082–1086, 2007.

[18] S. Majumdar, D. Chattopadhyay, and J. Parikh, "Interruptible load management using optimal power flow analysis," IEEE Trans. Power Syst., vol. 11, no. 2, pp. 715–720, May 1996.

[19] J. Bai, H. B. Gooi, L. M. Xia, G. Strbac, and B. Venkatesh, "A probabilistic reserve market incorporating interruptible load," IEEE Trans. Power Syst., vol. 21, no. 3, pp. 1079–1087, Aug. 2006.

[20] L. M. Xia, H. B. Gooi, and J. Bai, "Probabilistic spinning reserves with interruptible loads," IEEE Power Eng. Soc. General Meeting, vol. 1, pp. 146–152, 2004.

[21] K. Y. Huang, "Demand subscription services—An iterative dynamic programming for the substation suffering from capacity shortage," IEEE Trans. Power Syst., vol. 18, no. 2, pp. 947–953, May 2003.

[22] J. Wang, X. Wang, and X. Ding, "The forward contract model of interruptible, load in power market," presented at the IEEE/PES Power Engineering Society Transmission and Distribution Conf. & Exhibition: Asia and Pacific, Dalian, China, Aug. 2005.

[23] K.-Y. Huang, H.-C. Chin, and Y.-C. Huang, "A model reference adaptive control strategy for interruptible load management," IEEE Trans. Power Syst., vol. 19, no. 1, pp. 683–689, Feb. 2004.

[24] M. Fan-Lin , and Z. Xiao-Jun, "An Optimal Real-Time Pricing for Demand-Side Management: A Stackelberg Game and Genetic Algorithm Approach, " pp. 1703-1710, 2014.

[25] L. Gelazanskas, and K.A.A. Gamage , "Neural Network Based Real-Time Pricing in Demand Side Management for Future Smart Grid, " International Conference on Power Electronics, Machines and Drives, pp. 1-5, 2014.

[26] Jin Xiao, Jae Yoon Chung, Jian Li, R. Boutaba , and J.W. -K. Hong, "Near Optimal Demand-Side Energy Management Under Real-Time Demand – Response, " Conference on Network and Service Management (CNSM), pp. 527-532, 2010.

[27] P. Finn, C. Fitzpatrick, and M. Leahy, "Increased penetration of wind generated electricity using real time pricing & demand side management, " International Symposium on Sustainable Systems and Technology, pp. 1-6, 2009.

[28] U. D. of Energy, "Benefits of demand response in electricity markets and recommendations for achieving them: A report to the united states congress pursuant to section 1253 of the energy policy act of 2005,"U.S. Department of Energy, Tech. Rep., February 2006.

[29] S. K. Corentin Evens, "Pricing models and mechanisms for the promotion of demand side integration," VTT Technical Research Centre of Finland, Tech. Rep. VTT-R-06388-09, 2009.

[30] Chenye Wu , H. Mohsenian-Rad, Jianwei Huang , and A. Y. Wang, "Demand side management for Wind Power Integration in microgrid using dynamic potential game theory, " pp. 1199-1204, 2011.

[31] Z. Zhu, J. Tang , S. Lambotharan, W.H. Chin, and Z. Fan, "An integer linear programming and game theory based optimization for demand-side management in smart grid, " IEEE GLOBECOM Workshops, pp. 1205-1210, 2011.

[32] Hung Khanh Nguyen , J.B Song, and Zhu Han, "Demand side management to reduce Peak-to-Average Ratio using game theory in smart grid, " IEEE Computer Communications Workshops, pp. 91-96, 2012.

[33] A.-H. Mohsenian-Rad, V.W.S. Wong , J. Jatskevich, R. Schober , and A. Leon-Garcia, " Autonomous Demand-Side Management Based on Game-Theoretic Energy Consumption Scheduling for the Future Smart Grid, " IEEE Transaction on Smart Grid, vol. 1, no. 3, pp. 320-331, 2010.

[34] W. Saad , Zhu Han, H.V. Poor , and T. Basar , "Game-Theoretic Methods for the Smart Grid: An Overview of Microgrid Systems, Demand-Side Management, and Smart Grid Communications, " IEEE Signal Processing Magazine, vol. 29, no. 5, pp. 86-105, 2012.

[35] Peng Yang, Gongguo Tang, and A. Nehorai, "A game theoretic approach for optimal time-of-use electricity pricing," IEEE Trans. Power Syst., vol. 28, pp. 884–892, 2013.

[36] D. Fudenberg and J. Tirole, Game Theory. Cambridge, MA: The MIT Press, 1991

[37] A.-H. Mohsenian-Rad and A. Leon-Garcia, "Optimal residential load control with price prediction in real-time electricity pricing environment," IEEE Trans. Smart Grid, vol. 1, pp. 120–133, 2010.

[38] C. Chen, S. Kishore, and L. V. Snyder, "An innovative RTP-based residential power scheduling scheme for smart grids," in Proc. ICASSP, Prague, Czech Republic, pp. 5956–5959, May 2011.

[39] R. Hartway, S. Price, and C. K. Woo, "Smart meter, customer choice and profitable time-of-use rate option," Energy, vol. 24, pp. 895–903, 1999.

[40] P. Samadi, A.-H. Mohsenian-Rad, R. Schober, V. W. Wong, and J. Jatskevich, "Optimal real-time pricing algorithm based on utility maximization for smart grid," in Proc. Int. Conf. Smart Grid Communications, Gaithersburg,MD, pp. 415–420, Oct. 2010.

[41] E. Çelebi and J. D. Fuller, "A model for efficient consumer pricing schemes in electricity markets," IEEE Trans. Power Syst., vol. 22, no.1, pp. 60–67, Feb. 2007.

[42] Quantum Consulting Inc. and Summit Blue Consulting, LLC Working Group 2 Measurement and Evaluation Committee and Southern California Edison Company, Demand response program evaluation—Final report Apr. 2005.

[43] A. H. Mohsenian-Rad and A. Leon-Garcia, "Optimal residential load control with price prediction in real-time electricity pricing environments," IEEE Trans. Smart Grid, vol.1, no. 2, pp. 120–133, Sep. 2010.

[44] Wei-Yu Chiu, Hongjian Sun, and H.V. Poor, " Demand side energy storage system management in smart grid ," Smart Grid Communications, pp. 73–78, 2012.

[45] H. K. Nguyen, J. B. Song, and Z. Han, "Demand side management to reduce peak-to average ratio using game theory in smart grid, " in Proc. iEEE into Conference on Computer Communications Workshops, Orlando, FL, USA, pp. 91-96, Mar. 2012.

[46] P.M. Van de Ven , N. Hegde, L. Massoulie , and T. Salonidis, "Optimal Control of End-User Energy Storage, " IEEE Trans. Smart grid, vol. 4, pp. 789–797, June. 2013.

[47] R. Urgaonkar,B. Urgaonkar, M. Neely, and A. Sivasubramanian, "Optimal power cost management using stored energy in data centers," in Proc. ACM SIGMETRICS, San Jose, CA, USA, Jun. 7–11, Oct. 2010, pp. 221–232, Oct. 2010.

[48] Y. Guo, Z. Ding, Y. Fang, and D. Wu, "Cutting down electricity cost in internet data centers by using energy storage," in Proc. IEEE GLOBECOM, Houston, TX, USA, Dec. 5–9, 2011.

[49] K. Ahlert and C. Van Dinther, "Sensitivity analysis of the economic benefits from electricity storage at the end consumer level," in Proc. IEEE Bucharest Power Tech Conf., Bucharest, Romania, Jun. 28–Jul. 2, 2009.

[50] W.Hu, Z. Chen, and B.Bak-Jensen, "Optimal operation strategy of battery energy storage system to real-time electricity price in Denmark," in Proc. IEEE Power Energy Soc. Gen. Meet., Minneapolis, MN, Jul. 25–29, 2010.

[51] S. Y. R. Hui, C. K. Lee, and F. F. Wu, "Electric springs—a new smart grid technology," IEEE Trans. Smart Grid, vol. 3, no. 3, pp. 1552–1561, Sep. 2012.

[52] N.R. Chaudhuri, C.K. Lee, B. Chaudhuri, and S.Y.R. Hui, "Dynamic Model of Electric Spring, " IEEE Transactions on Smart Grid, vol. 5, no. 5, pp. 2450-2458, 2014.

[53] C.K. Lee , S.C. Tan , F.F. Wu , S.Y.R. Hui , and B. Chaudhuri , "Use of Hooke's law for stabilizing future smart grid — The electric spring concept," Energy Conversion Congress and Exposition (ECCE), pp. 5253-5257, 2013.

[54] Chi Kwan Lee, Kai Lok Cheng, and Wai Man Ng, "Load characterization of electric spring," Energy Conversion Congress and Exposition (ECCE), pp. 4665 – 4670, 2013.

[55] S. C. Tan, C. K. Lee, and S. Y. R. Hui, "General steady-state analysis and control principle of electric springs with active and reactive power compensations," IEEE Trans. Power Electron., vol. 28, no. 8, pp. 3958–3969, Aug. 2013.

[56] C.K. Lee, N. Chaudhuri, B. Chaudhuri and S.Y.R. Hui, "Droop Control of Electric Springs for Distributed Stability Support of Smart Grid", IEEE Transactions on Smart Grid, vol. 4,pp. 1558-1566, Sep. 2013.

[57] C. K. Lee and S. Y. R. Hui, "Reduction of energy storage requirements for smart grid using electric springs," IEEE Trans. Smart Grid, vol.4, pp. 1282-1288, Sep. 2013.

[58] Chi Kwan Lee, B. Chaudhuri , and Shu Yuen Hui, "Hardware and Control Implementation of ElectricSprings for Stabilizing Future Smart Grid With Intermittent Renewable Energy Sources," IEEE Transactions. Smart Grid, vol.1, pp. 18-27, March. 2013.

[59] P. Kanjiya, and V. Khadkikar, " Enhancing power quality and stability of future smart grid with intermittent renewable energy sources using electric springs," Renewable Energy Research and Applications (ICRERA) , pp. 918 - 922, 2013

[60] Yan Shuo , Siew-Chong Tan , C.K. Lee, and S.Y.R. Hui, "Electric spring for power quality improvement, " Applied Power Electronics Conference and Exposition (APEC),Twenty-Ninth Annual IEEE, pp. 2140-2147, 2014.

[61] X. Luo, Z. Akhtar, C.K. Lee, B. Chaudhuri, S.-C. Tan, and S.Y.R. Hui, "Distributed Voltage Control with Electric Springs: Comparison with STATCOM, " IEEE Transactions on Smart Grid, vol. PP, no. 99, 2014.

[62] S. Yan, S.-C Tan, C.-K. Lee, B. Chaudhuri, and S.Y.R. Hui, "Electric Springs for Reducing Power Imbalance in Three-Phase Power Systems, " IEEE Transactions on Power Electronics, vol. PP, no. 99, 2014.

[63] A. Roshan, R. Burgos, A.C. Baisden, F. Wang, and D. Boroyevich, "A D-Q Frame Controller for a Full Bridge Single PhaseInverter Used in Small Distributed Power Generation Systems, " Applied Power Electronics Conference, Twenty Second Annual IEEE, pp. 641-647, 2007.

[64] D.N Zmood, and D.G Holmes, “Stationary frame current regulation of PWM inverters with zero steady-state error” IEEE Transactions on Power Electronics, vol. 18, issue 3, pp.814 - 822, May 2003.

[65] M.J Ryan, W.E Brumsickle, and R.D Lorenz, “Control topology options for single-phase UPS inverters”, IEEE Transactions on Industry Applications, vol. 33, issue 2, pp. 493 - 501, March-April 1997.

[66] Y. Y. Tzou, R. S. Ou, S. L. Jung, and M. Y. Chnag, “ High-performance programmable AC power source with low harmonic distortion using DSP-based repetitive control technique”, IEEE Transaction on Power Electronics, vol. 12, pp. 715-725, July 1997.

[67] W. Herrmann, W. Wiesner, and W. Vaassen, “Hot spot investigations on PV modules-new concepts for a test standard and consequences for module design with respect to bypass diodes,” in Conference Record of the Twenty Sixth IEEE Photovoltaic Specialists Conference - 1997, pp. 1129–1132, 1997.

[68] H. Kawamura, K. Naka, N. Yonekura, S. Yamanaka, H. Kawamura, H. Ohno, and K. Naito, “Simulation of I–V characteristics of a PV module with shaded PV cells,” Solar Energy Materials and Solar Cells, vol. 75, no. 3–4, pp. 613–621, Feb. 2003.

[69] H. Patel and V. Agarwal, “MATLAB-Based Modeling to Study the Effects of Partial Shading on PV Array Characteristics,” IEEE Transactions on Energy Conversion, vol. 23, no. 1, pp. 302–310, Mar. 2008.

[70] H. Patel and V. Agarwal, “Maximum Power Point Tracking Scheme for PV Systems Operating Under Partially Shaded Conditions,” IEEE Transactions on Industrial Electronics, vol. 55, no. 4, pp. 1689–1698, Apr. 2008.

[71] M.A. Abido, Y.L. Abdel-magid, “Optimal multiobjective design of robust power system stabilizing using genetic algorithms”, IEEE Transactions on Power Systems, vol. 18, issue 3, pp. 1125-1132, 2003.

[72] M.A. Hassan, M.A. Abido, “Optimal design of Microgrid in Autonomous and Grid Connected Modes Using Particle Swarm Optimization”, IEEE Transactions on Power Eletronics, vol. 26, issue 3, pp. 755-769, 2011.

Vitae

Name	:Emad Fuad Naim Areed
Nationality	:Palestinian / Jordanian
Date of Birth	:7/3/1987
Email	:emadfuadareed@hotmail.com
Address	:KFUPM Housing
Academic Background	:Electrical Engineering / Power Engineering

Thesis Outcomes

1. E.F. Areed and M.A. Abido, " Design and Dynamic Analysis of Electric Spring for Voltage Regulation in Smart Grid," (under preparation)
2. E.F. Areed and M.A. Abido, " RTDS Implementation of Electric Spring for Distribution Voltage Regulation" (under preparation)
3. E.F. Areed and M.A. Abido, " Electric Spring as a Novel Approach to Demand Side Management in Smart Grid: A Review" (under preparation)
4. E.F. Areed and M.A. Abido, "Analysis of Electric Spring Performance and Limitations for Voltage Regulation," (under preparation)